A Visibility and Safety Assessment of Urban Intersection Sight Distance using mobile LiDAR Data

by

Omar Kilani

A thesis submitted in partial fulfillment of the requirements for the degree of

Master of Science

in

Transportation Engineering

Department of Civil and Environmental Engineering
University of Alberta

Abstract

This thesis focuses on intersection sight distance design, which is an extremely critical element in urban road design. Research has shown that providing adequate sight distance contributes to safe operation at intersections. Conversely, a restricted sight distance impacts drivers' fields of vision and reduces their ability to complete certain maneuvers smoothly and safely. The existence of obstacles within the intersection sight triangle limits drivers' visual fields and blocks their ability to see and react to vehicles on the crossing road. These obstacles could be buildings, structures, trees, bushes, or any roadside object. However, locating these obstacles through site visits is generally not an efficient way to address such issues since this is a tedious process, labor-intensive, and exposes the workforce to high safety risks. It requires surveying equipment and, in some cases, road closures. Also, to simply identify obstacles does not account for the different types of modes traveling through the intersection and could lead to inaccurate outcomes.

Several researchers have attempted to study the sight distance and identify the obstructions at intersections; however, previous work in this area is very scarce and involves a manual process, especially at urban intersections. Therefore, the first part of this thesis focuses on developing a fully automated method using mobile LiDAR point cloud to extract the information about the road objects that impact drivers' vision by conducting a visibility assessment. This part includes (a) detecting the obstacles to estimate the blockage percentage and a visualization of the obstruction from a driver's perspective, (b) conducting a sensitivity analysis to study the impact of different voxel size on visibility assessments, and (c) investigate the impacts of operating speeds on drivers' fields of vision and intersection visibility.

The second part of this research conducts a safety-based assessment, using the LiDAR dataset to study the relationship between the collisions and the visibility information extracted at the urban

intersections. Understanding the root cause of a visibility problem is crucial for improving safety at intersections and achieving the goals of Vision Zero. The collision analysis was performed using the Empirical Bayesian technique to identify intersections that exhibited an over-representation of specific collision patterns caused by visibility problems. The results show that intersections with limited available sight distances due to road obstacles exhibited an increased risk of collisions. This would significantly help road safety agencies prioritize and rank the hazardous intersections for potential treatment and select cost-effective countermeasures.

Dedicated to my dear parents

my beloved wife

my sweet children

ACKNOWLEDGMENT

Foremost, all praise is due to Allah, the Almighty, for giving me the strength to complete this work.

I would like to express my sincere gratitude to my supervisor Dr. Karim El Basyouny, for giving me the opportunity to pursue graduate studies; for his continuous support, guidance, and encouragement throughout the research and master's journey. I am thankful to my examination committee, Dr. Tae J. Kwon, Dr. Ahmed Bouferguene, and Dr. Mustafa Gul (Chair), for their time to review my work and for their advice.

I am grateful to my professors at the University of Alberta and Jordan University of Science and Technology for the knowledge and the advice they offered me.

In addition, I would like to thank all my friends and colleagues for their help and support.

Lastly, and in the first place, I would like to extend my deepest gratitude to my parents for their unconditional support, endless love, care, prayers, motivation, and inspiration. I am thankful to my dear sister and brothers for their support. With all my love, words cannot describe how grateful I am for my wife for her unending love, prayers, and encouragement, and for that, I am forever grateful.

TABLE OF CONTENTS

LIST OF TABLES

LIST OF FIGURES

LIST OF ABBREVIATIONS

LiDAR	Light Detection and Ranging
FHWA	Federal Highway Administration
ASD	Available Sight Distance
ROW	Right of Way
MLS	Mobile Lidar Scan
AASHTO	American Association of State Highway and Transportation Officials
PRT	Perception–Reaction Time
DTM	Digital Terrain Model
DSM	Digital Surface Model
DEM	Digital Elevation Model
GIS	Geographic Information System
ALS	Aerial Lidar Scan
MMS	Mobile Mapping System
TAC	Transport Association of Canada
AT	Alberta Transportation
EB	Empirical Bayes
BB	Beta-Binomial
ODOT	Oregon Department of Transportation
AADT	Average Annual Daily Traffic
LOS	Line of Sight
HDS	Highway Design Software
GPS	Global Positioning System
GNSS	Global Navigation Satellite System
TIN	Triangulated Irregular Network
RMSE	Root Mean Square Error Mean Absolute Error

MAE	Mean Absolute Error
RTM	Regression to The Mean
NB	Negative Binomial
AV	Autonomous Vehicle
CoE	City of Edmonton
TOF	Time of Flight
GLM	Generalized Linear Model
MLE	Maximum Likelihood Estimation

1 INTRODUCTION

1.1 Background

1.1.1 Urban Intersections a Safety Challenges

Intersections are hazardous due to high conflict potential, resulting in high collision frequency and fatal collisions [1]. The Federal Highway Administration (FHWA) has reported that 2.4 million collisions occur at intersections each year, which accounts for about 40% of all collisions and 21.5% of traffic fatalities [2]. In 2017, crashes at intersections made up 58.2% of the total collisions and resulted in 70.6% of total injuries and 48.1% of Edmonton's fatalities [3]. Hence, the improvement of intersections requires a better understanding of the collision causes in order to develop or select effective countermeasures.

Among the many causes for collisions at intersections are traffic control measures, traffic operation, the driver's behavior, and design. One of the most common leading causes of urban intersection collisions includes failing to yield to the right of way (ROW) and restricted visibility in the driver's visual field. When a driver fails to observe the yield or stop sign or observe oncoming traffic from the major road due to visibility issues from the intersection, it may increase their collision risk. Even when no traffic sign exists (i.e., uncontrolled intersection), the driver requires adequate distance to observe conflicting vehicles and must have a clear sight area; otherwise, a collision may occur.

The vision is a critical element to a driver's ability to react in a road environment. Having a superior view is essential to observe the road features and objects so that drivers can drive safely. Hence, it is vital to understand the driver's visual field and extract the object that blocks the drivers' visibility within the sight triangle by estimating the blockage percentage. To illustrate this concept, Figure 1 shows a vehicle approaching an intersection and the area visible to the driver.

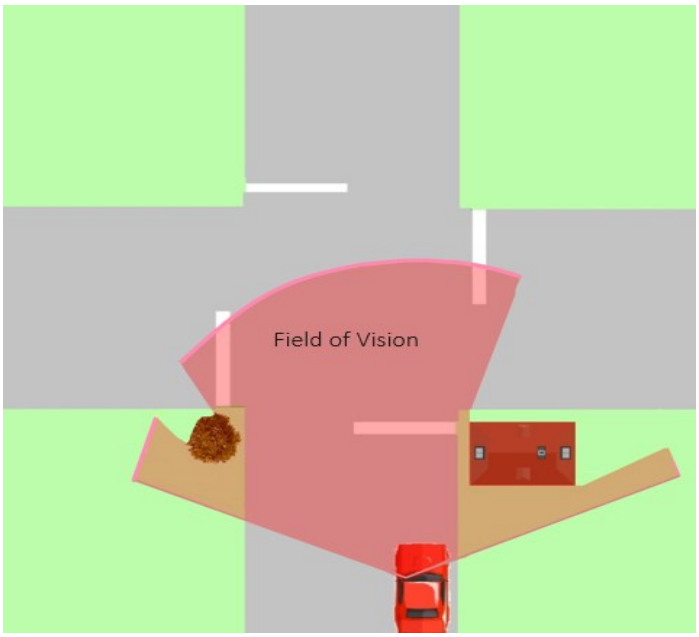

Figure 1 Driver's Field of Vision

Many studies have explored the impact of traffic and geometric road characteristics on intersection collisions [4-7]. However, little attention has been devoted to studying the impact of sight distance and its influence on drivers' ability to observe potential conflicting vehicles in an urban environment or road objects that restrict the available sight distance. A review of intersection safety and sight limitations indicates that intersections with poor visibility, due to restricted available visible distance, experience higher than normal collision rates [8].

The intersection sight triangle has been regarded as an integral element in road design. It provides the driver with a clear area near an intersection to safely complete a departing maneuver [9-11]. However, the mere fact of the sight triangle providing a designated sight distance does not offer a realistic representation of the driver's visual field at a given position on the vehicle's driving path. Moreover, theoretical intersection sight distance is based on certain assumptions which do not account for safety performance and objects in the 3D environment. Furthermore, design standards and guidelines assume the driver behavior is deterministic and do not account for all human limitations, both crucial—and distinct—components in road safety that significantly impact the visual field. Instead, they focus primarily on road and vehicle characteristics.

Previous studies show that elderly drivers are more likely to be involved in an intersection collision where limited sight distance exists. In fact, collisions involving elderly drivers had a higher probability of occurrence when the intersection was stop-controlled [12]. Gargoum, et al. [13]

indicated that elderly drivers, who often have limited cognitive abilities, were more likely to be involved in collisions where appropriate sight distance was not provided. The AAA organization, serving approximately 59 million drivers in the US and Canada, reports that the useful field of vision becomes smaller with age and that this impact on drivers' vision may constitute a safety risk [14].

In addition, the visual field of the driver moving on the road is affected by speed when decelerating near an intersection to observe oncoming vehicles. A moving vehicle approaching an intersection has a dynamic visual field based on its driving speed and location, affecting the driver's sensitivity and focus on the road ahead. In other words, a driver moving at high speed has a smaller field of vision, which substantially impacts what the driver sees. Thus, speed is a critical element in intersection visibility assessments [15]. Driving at low speed increases the field of vision and allows significantly more time to react in the event of unexpected situations [16]. Thus, a simulation of the drivers' viewpoint and visual field—taking into consideration parameters such as the horizontal viewing angle, the driver's eye height, mode of transportation, and speed to provide a realistic visualization—is essential for the accurate assessment of visibility. The most important step is to generate a highly accurate virtual environment of the urban intersection to represent the real-world situation; this would significantly help in assessing visibility at the intersection from different perspectives. These can be created using remote sensing technology and Mobile LiDAR Scan (MLS) to explore the field of view. The safety of an intersection can also be improved by examining the historical crash records, understanding the relationship between inadequate visibility and collision occurrence, and conducting a safety analysis to prioritize collision-prone intersections for potential interventions.

The next section explains the design criteria for intersection sight distance based on current design guidelines. It highlights the potential transformation that could be achieved by evaluating intersection safety—through simulated and automated assessments—to enhance the design and visibility of the existing road infrastructure by utilizing remote-sensing technology.

1.1.2 Intersection Sight Distance Design

One of the most important road design elements in an urban environment is adequate sight distance at intersections. As defined by the American Association of State Highway and Transportation Officials (AASHTO), sight distance is the minimum distance required by a driver to be able to

effectively observe conflicting vehicles and complete certain maneuvers [9]. It is fundamental to intersection operation and safety that vehicles approaching an intersection should have clear visibility. The standards laid out in the majority of design guidelines are based on specific measures to meet the minimum requirements for the intersection's sight distance [10, 11]. These measures provide an area along the intersection leg, resulting in a triangle area known as the sight triangle. Previous studies have shown the influence of this geometric feature on road safety and its impact on traffic operation [17, 18].

Sight distance is a critical design element associated with visibility and central to the inherent safety of intersections. The intersection sight distance is laid down in the road design guide, based on the extreme values of components, including speed, deceleration rate, perception–reaction time (PRT), and acceptance gap time. Although such distances are sufficient to ensure that drivers have a clear vision of conflicting vehicles, such minimum distances cannot always be achieved in densely built-up urban areas, and, consequently, safety problems arise at intersections. In other words, maintain a large area clear from vegetation, buildings, or any road feature is challenging in the urban environment. Furthermore, road conditions may change during the design life cycle due to maintenance work or the installation of overhead utilities, significantly restricting the sight distance available at the intersection.

To assess if the sight distance at an intersection meets current guidelines, and the sight triangle is clear from obstructions in the urban environment, a sight distance assessment must be conducted. However, it may be ineffective to use conventional field-assessment techniques that are time-consuming, require an extensive workforce, based on certain assumptions, and of varying accuracy, as it may not be possible to observe all objects impacting a driver's visibility when using different transportation modes where the driver's height differs. Furthermore, previous work has shown that design, terrain information [19, 20], and the Digital Terrain Model (DTM) [21, 22] do not accurately represent obstructions and overhanging objects that physically impact the driver's vision by limiting the available sight distance.

Many researchers have focused on assessing road design elements using geospatial data in order to overcome the errors resulting from field procedures. Few studies have attempted to explore intersection visibility and sight distance by creating and importing Digital Elevation Models (DEMs) and extracting obstacles using Geographic Information System (GIS) tools. Although

some studies were thriving and relatively accurate, the research involved manual work, site visits, and considerable time to process data due to software limitations and, sometimes, a failure to capture cantilever objects. For instance, visibility analysis could result in errors when detecting obstructions at intersections with many large trees. In addition, the majority of previous studies focused on using Aerial LiDAR Scans (ALS) and the Mobile Mapping System (MMS), which has a lower point density than the MLS, which could be ineffective in extraction procedure and performing the assessment and provide overestimated information about the available sight distance.

Remote sensing has been widely used in transportation applications to mitigate the limitations found in conventional techniques. Light Detection and Ranging (LiDAR) technology has attracted significant attention for its ability to produce a visibility-related analysis that can precisely represent real-world situations in the form of a point cloud. The MLS produces a high level of accuracy that represents all aspects of the road and surrounding environment, and thus, closer alignment with the road scanned [23]. It has significant potential in transforming traditional processes to enable the precise, automated sight-distance assessment and captures road infrastructure, vegetation, and existing buildings with a high level of 3D detail, as shown in Figure 2. It facilitates sight distance assessment by extracting intersection information and detecting obstacles within the driver's field of vision without the need for field visits or any interruption to the traffic operation.

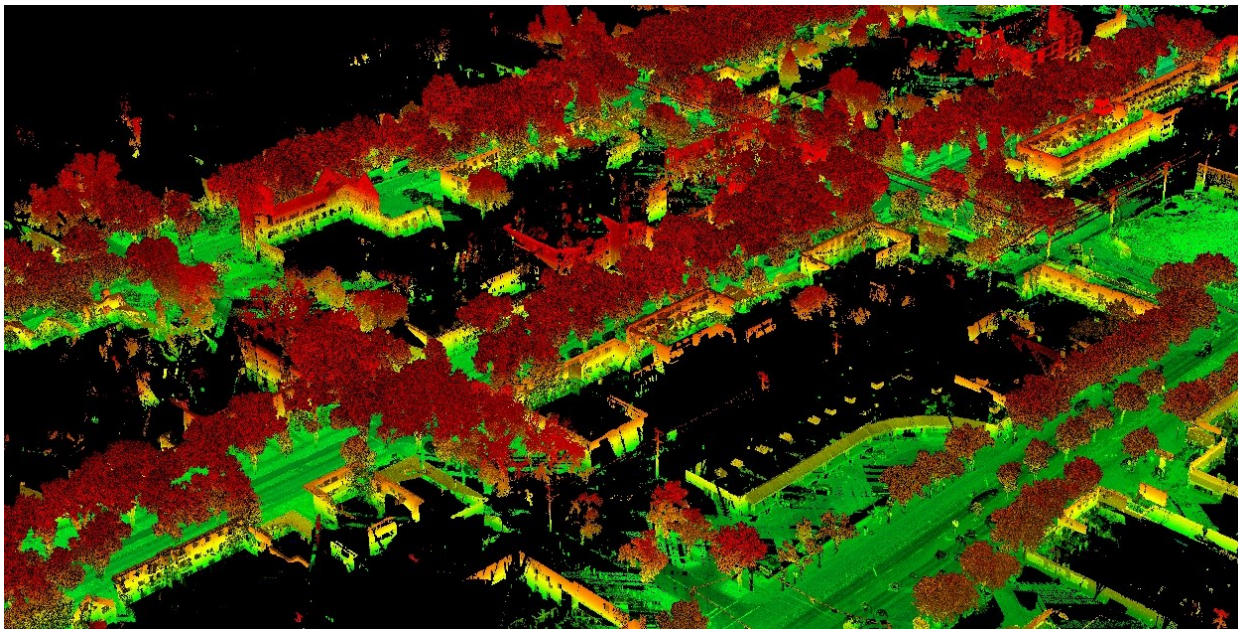

Figure 2 LiDAR Point Cloud in Edmonton, Alberta

This thesis proposes a unique method to mitigate previous research limitations and fill the existing literature gap by utilizing Mobile LiDAR data. The method develops a fully automated, novel algorithm that extracts obstacles blocking the visibility to observe conflicting vehicles by simulating the driver's visual field, represented by the sightlines cast by virtual rays—and accounting for human limitations. The intersection sight distance algorithm works by defining the driver's location based on the intersection control sign and detecting the objects blocking visibility from the driver's perspective. The observer point is defined on the vehicle trajectory along the driving lane, parallel to the roadway at equal intervals. The visual field is then generated considering the driver's peripheral view to exploring the objects represented by the LiDAR point cloud in 3D. Once this is achieved, a visibility analysis is conducted to compute the blockage rate by recording the distances for each sightline traveled and comparing it with the angular sight triangle area. The outputs provide insights into visibility at the intersection that are useful in conducting collision analysis and safety-based assessments to identify hazardous intersections through considering particular collision patterns resulting from visibility problems at intersections. This information could significantly help to rank intersections, prioritize improvements, and select cost-effective countermeasures to improve road safety.

1.2 Problem Statement

Poor road design is regarded as one of the main contributory factors to road collisions. Intersection sight distance is an essential element in road design; however, sight distance at urban intersections and its impact on road safety have not been investigated to the extent that they deserve. A 3D method for assessing current intersection visibility and performance in delivering a reliable sight triangle clear from obstruction is still lacking. A thorough investigation of the relationship between historical collision records and existing urban intersection sight distance design is required, with an analysis of reliable data to implement safety improvements.

The research on the impact of inadequate sight distance on safety at urban intersections is extremely scarce and provides an unreliable outcome. In addition, it does not consider the speed of the vehicle approaching the intersection and the impact this has on the driver's dynamic field of vision when performing certain maneuvers. A simulation of the driver's viewpoint considering transportation mode provides a necessary 3D representation of the real-life situation. The most effective way to achieve this is through a LiDAR-based analysis that facilitates a broad-scale assessment of the existing road design by using MLS. The MLS collects high-resolution data that can be utilized to extract valuable visual information about the intersection infrastructure and landscape in 3D from the driver's perspective.

1.3 Objectives

This thesis aims to evaluate sight distance at urban intersections by assessing visibility in the sight triangle, which is the area defined by the design guidelines. The analysis is performed using an automated assessment, extracting the vehicle trajectory, simulating the driver's visual field, and then detect the obstacle object to estimate the blockage percentage and available visible distance. Bayesian analysis is then performed on the information extracted to conduct safety-based assessments, aiming to improve road safety and cater to driver needs. This overarching goal of the thesis is achieved in two major parts.

1.3.1 Part I Automated Visibility-Based Assessment

This part proposes a method that can be used to effectively assess, in 3D, the intersection sight distance and visibility of an urban intersection with yield or stop signs at the minor intersection. It also develops a novel algorithm that facilitates fully automated extraction of the objects in the sight

triangle area. In addition, it focuses on visibility assessment by simulating the driver's eye and analyzing the driver's sightlines in an urban intersection using high-resolution MLS to estimate the rate of blockage at the intersection. This includes the following objectives:

- Review the available techniques and applications for defining urban intersection sight distance and sight triangles.
- Develop an algorithm that processes the MLS data and obtains accurate information that accounts for all road obstructions.
- Simulate the driver's visual field and perform visibility analysis within the intersection sight triangle.
- Conduct sensitivity analysis to assess the robustness of the developed algorithm.

1.3.2 Part II Safety-Based Assessment

The next objective is to investigate how the information obtained from *Part one* can be used to conduct a safety-based assessment. For this, ten years of historical collision records were analyzed. The Empirical Bayes (EB) technique is used to evaluate intersection safety to identify the collision-prone intersections and study their relationship with blockage percentage.

The following are the specific objectives:

- Identify intersections that exhibit an overrepresentation of specific collision pattern that is associated with poor visibility.
- Examine the relationship between intersections with poor visibility and collision occurrence.

The proposed methods have been applied to the Strathcona area of Edmonton, Alberta, Canada, where the majority of roads are classed as local roads or collectors controlled by two-way stop or yield signs.

1.4 Thesis Structure

The thesis is divided into two main parts: Automated visibility-based assessment and Safety-based assessment used for the intersection sight distance. In the first part, the visibility analysis has been performed for most of the intersections across the study area. Such assessment provides information about the rate of blockage for each intersection. Then, in the second part, a collision

analysis is conducted to locate the hazards intersections based on the visibility assessment outcome. This thesis is divided into five main chapters. Details for each chapter covered are described as follow:

- ***Chapter 1*** explains the intersection problems and challenges and highlights the need for the visibility assessment to achieve a safer urban environment.
- ***Chapter 2*** provides a comprehensive literature review of studies that used remote sensing data to assess and estimate the available sight distance. The review includes different methodologies and techniques that have been developed to assess ASD and extract the obstruction and main limitations.
- ***Chapter 3*** presents details about the LiDAR data collection and scanning system used in this research. It also highlights the benefits of the LiDAR technology and its contribution to transportation engineering and road safety. This chapter describes the method used to extract/assess the information from the LiDAR data for the visibility assessment and the impact of the voxel size and speed on the assessment. Furthermore, it includes the data acquired to conduct the collision analysis and proposes a possible technique to identify the hazardous intersections because of the visibility problems.
- ***Chapter 4*** summarizes and discusses the results of the visibility and safety assessment. It shows the estimated blockage percentage for intersections from the driver's perspective. Then, it compares the blockage percentage between the stop and yield sign using a different mode of transportation. The impact of the point cloud's voxel size on the accuracy and quality of information obtained from the LiDAR is also presented. It illustrates the speed effect on the drivers' vision. Finally, the collision-prone intersections using the empirical Bayes technique are presented.
- ***Chapter 5*** concludes the thesis with a summary of its main contributions. It also points out the limitations and avenues through which future research could broaden the work presented in this research.

2 LITERATURE REVIEW

2.1 Background

The intersection sight distance assessment is performed to ensure that drivers have a clear area that is free from any obstruction. It can be evaluated through field assessment, graphical methods, or design software. The design software creates DTMs to conduct sight distance analysis, which does not represent all the road features and objects. In recent decades, the researcher shifted to using the GIS tools to estimate the available sight distance and conduct visibility analysis. These tools helped in generating the Digital Surface Model (DSM) to ease the sight distance estimation that accounts for objects which were not considered in the DTM using a different source of data (i.e., aerial images, LiDAR images, or DTM) [22, 23]. Although several studies have been proposed using GIS for sight distance evaluation, the manual procedure required for the assessment, especially when implementing it on a large scale, makes it impractical.

With the advancement in remote sensing technology, there was a growing interest in utilizing the LiDAR in transportation applications. The use of the LiDAR and, in particular, road safety was an appealing alternative for transportation researchers due to improvements in processing times and optimizing the computational costs [21]. Despite the significant potential of LiDAR, a few research studies utilized this technology to extract information about the intersection obstacle and estimate the blockage percentage.

This chapter includes a thorough review of previous studies that attempted to assess sight distance and estimate the available visible distance. The challenges and gaps associated with each extraction procedure that exists in the literature are highlighted.

2.2 Design Guidelines

The design guide standard is an essential aspect for those who design, build and maintain road infrastructure. It is common for the available sight distance to be less than the minimum distance required by design standards. Before proceeding with the design deviation, further evaluation, engineering judgment, and quantitative analysis are required [11]. According to the TAC guidelines, this process is known as the design exception process, including cost estimation, risk evaluation, and mitigation measures [11].

Municipalities or jurisdictions follow a thorough process to set a mitigation plan to account for these design deviations. For instance, the Oregon Department of Transportation (ODOT) explains that when the intersection sight distance measurement is less than the guidelines standards, mitigation measures and actions should be considered to determine if the deviation may be approved [24]. While some of these measures are proposed to increase the available sight distance, others might reduce the required intersection sight distance. In order to have adequate sight distance at the intersection, it may be necessary to take multiple actions and mitigation strategies to ensure that. The actions that ODOT adopted are listed in order as follows

(a) Remove the sight distance obstructions (i.e., signs, vegetation, utility apparatus, embankments).
(b) Use the intersection sight distance measurement taken 10 feet from the edge of the traveled way when the posted speed limit is 35 mph or less.
(c) Evaluating the design speed and study whether if lowering the speed would be appropriate or not.

Other geometric and traffic aspects could be considered in the mitigation process, such as studying the left turn and Average Annual Daily Traffic (AADT), relocating or regrading the driveway, and stopping sight distance [24]. Even though the recommended mitigation process might work in some cases, it still needs an in-depth assessment.

In addition, adopting field-based assessment is impractical as it may result in an error and inconsistency in sight distance along the intersection. The LiDAR-based assessment is a robust and feasible approach to evaluating sight distance performance and assessing intersection visibility. Such an approach will not only evaluate the deviation of the design from the standard guides but also allows the transportation agencies to assess the design elements throughout the design service life.

2.3 Standards for Intersection Sight Distance

The AASHTO Green Book highlighted that intersections' conflict visibility could be significantly reduced by designing the intersection with adequate sight distance. Harwood, et al. [25] developed a methodology to determine the adequate sight triangles for a safe intersection that was later adopted by the AASHTO and become a policy. A minimum unobstructed length for the line of

sight between the driver entering the intersection and the vehicle approaching from the right and left was defined. The adequate sight distance requires a specified defined area known as "Intersection Sight Triangles" that should be clear from obstruction along with the intersection approach. The triangle legs defined by AASHTO that is dependent on design speed and type of intersection traffic sign [9]. Two types of intersection sight triangles are considered in the design – approach sight triangles and departure sight triangles, as shown in Figure 3.

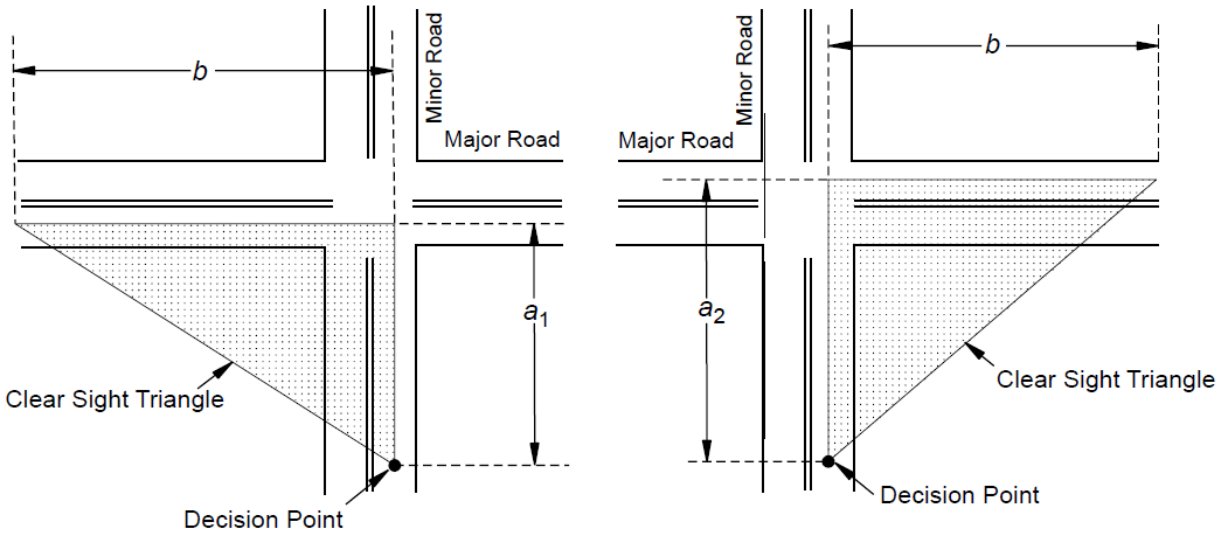

Approach Sight Triangles (Uncontrolled or Yield-Controlled)

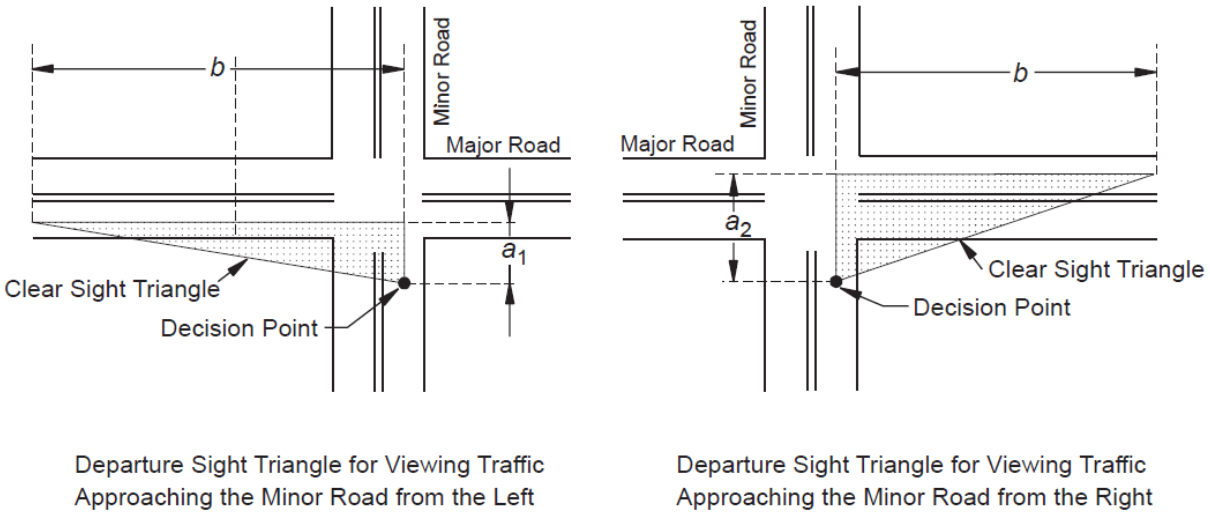

Figure 3 Intersection Sight Triangles [9]

The sight distance is the length that the driver needs to clearly recognize path objects and react appropriately to avoid a collision. It is essential for the drivers entering an intersection to have clear visibility of the on-coming traffic and surrounding environment [9].

When the intersection is uncontrolled or controlled by a yield sign, the decision point is the location when the driver begins to brake and slow down on the minor road to observe the conflicting vehicle in the major road. AASHTO defines a_1 as distance in from major road along the minor road to the left, while a_2 is the same distance but to the right, and it may include the width of the median on major if exists. Distance b is defined as the length of the sight triangle leg along the major road. However, for the stop-controlled intersection, the short leg of the sight triangles depends on the stop sign location and stop line marking on the road surface that may vary accordingly to the intersection conditions. The front length of the vehicle from the driver's location also contributes to defining the short legs [9].

In the condition when the intersection has a stop sign at the minor road, there are three situations to be considered for the departure sight triangle: left turn, right turn, and a crossing maneuver. When the driver tends to carry out left or right turn maneuver, the distance measurement of the sight triangle leg a on the minor road is defined in the AASHTO 4.4m - 5.4m from the road's edge. This is the location of the decision point that represents the driver's eye on the minor road. This figure came from field investigation as the front of the passenger car's position would stop 2m

from the major road's edge and might be less. Also, the distance of the driver's eye to the front vehicle is nearly always considered 2.4 m for the current US passenger car. The AASHTO recommends that in some situations, the distance is up to 5.4 m, which would provide a large sight triangle. For computing the *b* distance on the major road, it is essential to provide a sufficient gap time for a vehicle in the intersecting road to accelerate from a stop and complete a right, left turn, or crossing maneuver from the minor road without impacting the traffic operation in the major road. The gap time values are independent of the design speed in the major road and determined on the basis of the intersection sight distance determinations. Field studies have shown that the drivers would decelerate and reduce their speed when a vehicle turns from a minor road onto a major road. The gap time values are shown in Table 1.

Table 1 Time Gap (Stop Control) [9]

Maneuver Direction	Design Vehicle	Time Gap
Left	Passenger car	7.5
	Single-unit truck	9.5
	Combination truck	11.5
Right	Passenger car	6.5
	Single-unit truck	8.5
	Combination truck	10.5
Crossing	Passenger car	6.5
	Single-unit truck	8.5
	Combination truck	10.5

The intersection sight distance in the major road is determined as follows, shown in Table 2

Table 2 Intersection Sight Distance (ISD)[9]

US Customary	Metric
$ISD = 1.47\, v_{major}\, t_g$	$ISD = 0.278\, v_{major}\, t_g$
ISD = intersection sight distance (length of the leg of sight triangle along the major road) (ft)	*ISD* = intersection sight distance (length of the leg of sight triangle along the major road) (m)
V_{major} = design speed of major road (mph)	V_{major} = design speed of major road (km/h)
t_g = time gap for a minor road vehicle to enter the major road (s)	t_g = time gap for a minor road vehicle to enter the major road (s)

For the yield-controlled intersections and apart from the sign control of the intersection and design speed, two situations are considered to measure the distance of clear sight distance, which are crossing maneuver of the major road and right-and-left turn maneuver. The focus of this thesis for

the left turn maneuver where the length of the sight triangle leg a_1 along the minor road to accommodate the right turn without stopping is defined to be 25m. The distance a_2 for left turns is equal to a_1 plus the width of the major roadway. This distance was set based on certain assumptions, which consider that the turning speed is 16 km/h. For the yield-controlled intersection, distance *b* along the major road is similar. However, the time gap should be increased by 0.5 s, as shown in Table 3. The driver requires 3.5s from the decision point to the intersection. This represents the additional travel time required at the yield-controlled intersection, whereas the same time is not needed at a stop-controlled intersection. However, the time of acceleration after entering the major road is 3 s more for the stop sign than the yield sign since when turning; the acceleration starts from 10 km/h rather than from stop condition [9]. The 0.5 s increase in travel time for vehicle turning from intersecting road where the sign is yield is the between the 3.5 s increase in travel time and the 3 s reduction in travel time [9].

Table 3 Gap Time (Yield Control)[9]

Design Vehicle	Time Gap (t_g)(s)
Passenger car	8.0
Single-unit truck	10.0
Combination truck	12.0

All gap time values apply to a two-lane roadway with minor approach grades of 3 percent or less and no median. These values should be adjusted when the site situation does not comply with these specific conditions. Additional time should be considered when medians and multilane roadways exist accordingly to the design vehicle.

The intersections with yield control approaches require greater sight distance than approaches controlled by a stop sign. When the available sight distance for the yield-controlled intersection is not sufficient, consideration of stop sign instead of yield sign should be used instead. Moreover, AASHTO recommends installing a regulatory sign at the intersection of the major road to control the speed and reduce it for the approaching vehicles [9].

2.4 Sight Distance Assessment Types

2.4.1 Design & Terrain Data

There have been many efforts to conduct the sight distance analysis during the design phase, Hassan, et al. [20] attempted to estimate the sight distance along the horizontal alignment according to the analytical process. The method developed a computer program to perform the analysis and assess the no-passing zones on two-lane highways. The proposed method also provided accurate results and found feasible in terms of time and error; however, the study focused only on assessing the continuous lateral obstruction design phase to replace the graphical techniques.

Lovell David [26] proposed a method to calculate the sight distance along roadway alignment in an automated way by representing the roadway's centerlines using parametric curves. These curves were used to evaluate the sight distance in the 2D plane. The study focused on replacing the geographical method with an automatic calculation that computes the horizontal projections and lateral clearance. The methodology did not consider the road topography and terrain and is limited to horizontal alignment, which was then enhanced to account for more complicated conditions [27].

Ismail and Sayed [19] estimated the sight distance by developing a flexible approach based on a parametric representation of roadside and highway features in 3D. The study aimed to develop an algorithm to find the location of obstruction that links the driver line of sight tangential to any road surface. The sight distance was examined on various geometric elements, and the results were analyzed of different alignment configurations. The authors did not represent any implicit approximation of the roadway surface; however, they assessed the influence of various alignment on stopping sight distance in both 2D and 3D on a horizontal curve and found a relationship between the two models when comparing the outcome.

Kim and Lovell [28] assessed the 3D sight distance by developing an algorithm to estimate the maximum available sight distance using the structural mechanics of thin plate spline interpolation and computational geometry to represent the DEM and generate a road surface. The sight distance analysis was calculated in the same resolution in which the geometric data were specified by

determining the shortest line that does not block any objects. The methodology has been tested on sample alignment data, and the authors compare it with traditional 2-dimensional procedures.

Jha, et al. [29] developed a 3D design technique to assess the sight distance at the planning stage by overcoming the inconsistency in design that resulted from separate processing of the traditional two-stage process of horizontal and vertical alignment, which cannot detect the drivers' response until the complete construction of the road. The authors used the 3D design methodology to reflect the design process to estimate the available sight distance into three developed surfaces. The authors indicate the method needs to be tested in real-world projects.

These methods solely used the information of roadway design characteristics and geometric attributes in addition to the terrain topographic information to perform the sight distance analysis. These techniques developed without considering the road objects such as buildings, trees, and, depending on analyzing the geometrical road elements and assuming constant road characteristics.

2.4.2 Geographic Information System (GIS)

In the last decade, researchers tend to utilize GIS technology to assess sight distance from DEM. The development of GIS provided advanced tools such as Line of Sight (LOS) and viewshed to compute the available sight distance and find the road obstacles in the roadway. These assessments were carried out in accordance with available GIS elevation models considering the terrain and the surface characteristics. The outcome is then used for evaluation purposes with other data sources like the geometrical attributes of the roadway and roadside.

The viewshed and LOS tools provided by commercial ArcGIS have been used significantly in this area to compute the available sight distance. According to certain parameters and assumptions, the viewshed tool generates ray lines that reflect the driver's field of view. Then, extract the available sight distance by estimating the intersection area included in the viewshed polygon. However, in LOS, Polylines is created that represents the path points of the road trajectory to extract the last visible point.

The DEM derived from LiDAR was created in various studies on urban and rural roadways. The GIS has contributed to the LiDAR technology's evolution to model the surface by collecting the elevation data. The first model was the DTM that represents the bare ground surface, but this kind of model ignores the road features in the landscape. However, sight distance assessment requires

taking into consideration the potential blockage and visual obstruction within the roadways and roadsides. To fill this gap, the DSM was proposed to compromise and account for the landscape features above the terrain surface to account for this limitation.

2.4.2.1 Digital Terrain Model (DTM)

Previous work shows that many efforts were invested in assessing the sight distance. This is to make sure that the standards are satisfied throughout the service life of roadways. Available sight distance is often evaluated through site inspections, field measurements, or highway design software (HDS). The DTM was utilized by the HDS, considering the roadway design elements to perform the ASD calculation. Other studies used GIS to run the ASD analysis.

Nehate and Rys [30] used Global Positioning System (GPS) data to develop an algorithm to assess the available sight distance in a highway profile. The surface was created by estimating the cubic B-splines using the GPS data to represent the highway surface and sight obstruction. The available sight distance is detected by finding the intersection between the element representing the highway and sight obstruction and sightlines. Despite the average accuracy in detecting the sight obstruction, the authors pointed out that the analysis outcome might be inaccurate. The authors indicate that this is because of using the second-order smoothness curves, which do not consider the road bumps.

Castro, et al. [22] used ArcGIS to develop a method that evaluates the existing highway's available sight distance. The first step of this method starts by creating a DTM raster to calculate the viewshed with observer input. The viewsheds area was represented on the raster of visible cells, which means that it is visible to the observer. These visible areas are vectorized to produce polygons and intersect with a vehicle trajectory to obtain the available sight distance and then compare it with the result value given by highway design software (Trivium). This analysis was found to be slow and labor-intensive in the large section. There were also various locations where the viewshed analysis provides longer sight distances than the design software, which means that it can detect the vertical curves obstruction better.

With technological advancement, the application of remote sensing in transportation engineering is incorporated in assessing sight distance. Many researchers tend to use LiDAR data to conduct sight distance assessments and form DTM or DSM using GIS. Castro, et al. [31] developed a

model that extracts the sight distance by generating a DTM surface from the aerial LiDAR data. By using the ArcGIS features, the method assessed multiple target points' visibility to estimate the available sight distance and by comparing the outcome of Castro, et al. [22] using Kolmogorov–Smirnov, and Mann–Whitney–Wilcoxon tests that do not show any significant difference. However, the authors claim that the data processing time is much faster than in Castro, et al. [31].

In another study using airborne LiDAR where the vehicle trajectory line was collected by the Global Navigation Satellite System(GNSS), Castro, et al. [32] studied the impact of the successive station spacing within the vehicle path on the result of the sight distance analysis and the influence of the resolution of DTM combined with several stations and spacing distances along the roadway. The outcome showed that the DTM resolution has a greater impact on the quality of the results than the spacing between the calculated points. They also found that the spaces between the stations rise significantly when the DTM resolution increases.

2.4.2.2 Digital Surface Model (DSM)

Khattak, et al. [21] utilized the LiDAR elevation data to extract the intersection geometry and detect potential obstructions on driver sightlines. The LOS analysis was performed at the intersection within the sightline at six intersections on the IA-1 corridor in Iowa. Field validation using videotaping was reported to verify the obstruction detected by the LOS analysis. The validation shows that 66 lines of sight were found blocked during the LOS visibility analysis, of which 62 (89.8%) were confirmed in the validation process. The authors highlighted the effectiveness of LiDAR elevation data in obstruction extraction, which was successful in identifying the potential visibility issues at intersections. However, the authors stated that the spacing between the sightlines could affect the extraction quality.

In a different study, Khattak Aemal and Shamayleh [33] used the aerial LiDAR collected along Iowa Highway 1, which is also known as Solon Bypass, to assess the highway stopping and passing sight distances and assess the study feasibility. Using the ArcGIS, the triangulated irregular network (TIN) surface was created by processing the LiDAR data. The surface was examined visually to find potential locations with sight obstruction issues to the stopping and passing sight distance. The authors then investigate the same locations using the LOS tool in ArcView to see the sight distance obstacles and found 10 locations with visibility issues. The method was validated and found feasible to use the LiDAR to create a surface model for the sight distance assessment.

Tsai, et al. [34] assessed the ASD on intersections using LiDAR data by proposing a method to manually detect obstructions within the line of sight. The method used GPS points to represent the roadway centerlines on major corridors and intersecting roads. The sight triangles' dimensions were estimated based on the speed limit of intersection approaches and the type of traffic control. LiDAR data were used to generate DSM to carry out sight distance analysis. A market LiDAR software was utilized to get a raster grid, and by overlaying the triangle area enclosed onto the DSM, visible and nonvisible pixels were identified. LiDAR-based assessment results were compared with the conventional site survey, which detected 92% and 65% of obstruction, respectively. This shows the effectiveness of LiDAR data to identify intersection sight distance obstructions.

Bassani, et al. [35] performed sight distance analysis using mobile mapping systems. Road segment's photogrammetric images were collected and converted the point clouds to DSM. Then using ArcGIS tools, the ASD was calculated using LOS between observer and target points. The study used the "add XY coordinate" command to define the obstruction points of sightlines. The results for tested road segments provided a successful detection of obstructions. However, the authors recommended utilizing an automated approach for 3D ASD analysis.

Gargoum, et al. [36] proposed an algorithm to assess the stopping and passing sight distance using mobile LiDAR point cloud data in two different highway segments. The LiDAR data was used to generate a DSM raster to identify the observer and target points. Then, a LOS is constructed that connects the observer and target points by using the ArcGIS tool to assess the visibility of the target and the terrain along the LOS. The method identifies the obstructions by detecting the intersection between the LOS and surface model where the objects have a higher elevation than the LOS and where the target is not visible. The available sight distance is then estimated from the GIS outputs using Microsoft VB.

Bassani, et al. [37] performed the sight distance analysis using a mobile mapping system. The photogrammetric image was acquired along the road segment and converted into a point cloud. Once the DSM model is created, the available sight distance can be extracted using the GIS tool. The outcome demonstrates accurate results for scale 1:500 and 1:1000 through low-cost photogrammetry systems, which allowed the authors to identify the objects along the roadside, which compared with the conventional sight distance regional maps (1:10000-25000) and found a

significant improvement in object identification. However, the authors pointed out the need for more work to automate the extraction of the available sight distance into 3D models.

2.4.2.3 Comparing DTM and DSM

The influence of features, elevation models, and other inputs on the sight distance is crucial. Understanding the result and interpreting the outcome is fundamental to illustrate the deficiencies in the sight distance and discuss the impact of roadside obstruction on analysis using different DEMs.

de Santos-Berbel, et al. [38] studied the influence of DEMs on sight distance and analyzed the result of three DEMs classes to estimate the available sight distance by highlighting the strengths and weaknesses of each class. The outcome explains that using DTM is reliable when no road objects like trees or cantilevered elements restrict the sight distance are above the roadway. On the other side, the DSMs are more realistic and suitable to extract the available sight distance. When the DSM is derived from airborne LiDAR, the interpretation of output data is easy and requires less processing time, but the sight distance analysis is entangled by the impossibility of representing the scene surface because of the limitation of Delaunay triangulation. The third class is DSM obtained from MMS, which generates a model by reproducing the roadway more realistically. However, the sensitivity of this technology created a problem in preprocessing the point cloud. The authors highlighted that these models require in-depth analysis to distinguish whether the reason for inadequate sight distance is the road geometry and landform or contrary due to roadside items.

Castro, et al. [23] studied the accuracy and difference when detecting sight distance information between the DTM and DSM surfaces using the mobile and aerial LiDAR. The outputs for these models were tested using Kolmogorov–Smirnov, and Mann–Whitney–Wilcoxon to assess the difference in sight distance. The outcome explains that the difference between the models means that DMSs can detect more obstruction than DTMs as the DSMs have shorter sight distances than DTMs. DTM approach was found inaccurate since the sight obstruction like trees, buildings, walls, and traffic signs cannot be modeled in DTM. In real life, various 3D objects have a significant impact on available sight distance. Therefore, considering these elements is essential to carry out an accurate analysis that simulates the actual driver environment leading to appropriate assessment of sight distance. The results also illustrate that the mobile DSMs are denser, which means higher

resolution when compare to the aerial and mobile DEMs. Thus, a more accurate representation of the environment.

Malpica, et al. [39] proposed a method that demonstrates the potential and versatility of GIS in extracting the sight distance in a horizontal curve. The study considered the driver's eye height, other target object height, vehicle trajectory, and elevation model as input data. The focus was on the resolution of the DEM to detect the sight distance on the highway. Two different elevation models DTM and DSM were created. The authors compared the sight distance using these models to illustrate the influence of roadside objects using the DTM and DSM. The method plots the graphs that permit obstruction detection, which limit the driver's visibility. When using the DTM model, the minimum available sight distance is 55m, whereas the corresponding to the DSM is 15m. The difference in these distances demonstrates the impact of vegetation of the roadsides employing DEM choice, which means that some portion can be seen when using DTM whereas cannot be seen with DSM.

2.4.3 LiDAR Point Cloud Model

Recently, The LiDAR data has been utilized to extract the road feature and geometric characteristics of the roadways, which have great potential to provide a high level of accurate information with the support of programming software for data processing. For instance, Jung, et al. [40] developed an algorithm to assess the intersection sight distance using high-resolution Mobile LiDAR data. In this study, the ground points were separated and used to determine the ground level. The methodology converted the point cloud data into 2D grids and gridded on a horizontal plane representing the road and surrounding objects to perform the LOS analysis. Obstructions within the field of view of the driver are detected and then evaluated in the 3D space. The method examines the distance between the grid cell that is representing an obstacle to the constructed LOS. The study compared the results from the algorithm with conventional field measurements considering several parameters efficient. The authors indicated that the method is not applicable when the ground is more rigorous

Ma, et al. [41] used the airborne and terrestrial LiDAR data to propose an algorithm to estimate the 3D sight distance for stopping maneuvers in a highway with complex roadside obstacles. The method was supported by MATLAB that combines the modified Delaunay triangulation and cylindrical perspective to generate a vehicle trajectory along the highway with 1-meter average

spacing discrete points to simulate the driver's view and generate sight distance. The result showed that when comparing the sight distance produced by the new and conventional methods, there was a difference in estimating the distance when only DTM was used. The authors indicated that the method might be limited when the vehicle path and project information are not available. Also, the processing time was not satisfactory when processing high-density MLS data.

Shalkamy, et al. [42] developed an algorithm using mobile LiDAR to assess the available sight distance on a large scale. The first step of the algorithm was to define the observer and target points' locations within the vehicle trajectory. Then, reduce the data volume by converting the point cloud data into a 3D voxel. After that, it computes the available sight distance by mapping the observers and targets onto the grid of voxels. The visibility analysis is conducted by detecting the voxel that obstructs the vector links the observer and target points. The authors stated that the result results in extracting the available sight distance were accurate, and the sight limitations were mainly due to the vertical crest curves and pavement surface.

In a very recent study, Gargoum and Karsten [43] proposed a LiDAR-based method to assess the sight distance along a highway. The method includes discretizing the point cloud into a voxel and constructs sightlines between the observer and target point to extract and categorize the obstruction and feature available within the road alignment and roadside. The method was tested in Alberta, Canada, in four road segments and successfully quantified the highway's available sight distance. The authors stated that the method is valuable for transportation agencies to improve road safety. However, the method can not differentiate between the horizontal and vertical alignment along the road segment.

2.5 Voxel-based LiDAR Extraction

Many studies have been widely used DEMs to represent the LiDAR data. The surface-based analysis by creating a surface model from LiDAR points was an appealing method in previous researches due to its simplicity. It also has a vast volume of software and hardware available to support them. On the other hand, the voxel-based method has been scarcely used as it needs more to develop in LiDAR data processing. The surface-based model also provides relatively accurate information about the scene; however, it may be impractical when assessing the sight distance at an intersection using a high density of point clouds where a high level of accuracy is important to account for all objects where no compromise on safety.

In recent years, the voxel-based method has been used in remote sensing applications, including transportation engineering. Voxelization was a substantial process in previous research methods to extract road design features and objects to enhance road safety. There are many advantages of using voxel to represent the LiDAR point cloud over the DEMs to model the virtual 3D scene, which overcome the issues of overlapping surfaces and account for a complex situation and provides high-quality information that assists in promoting road safety. The research that used voxelization in transportation engineering illustrates outstanding results, which other available techniques do not provide the same range of accuracy. It is also valuable in applications where the variation in objects under the canopy is an interest that may be blockage by the object's surface [44].

Pyysalo [45] conducted a viewshed analysis using voxel-based models. The author aimed to compare different voxel models to explore the variation in the size of the visible area among these models and visualize the result using a number of cartographic means. The analysis includes constructing LOS between two locations and examining all voxels in the model. The result explains that the shape for the 3D environment was sustained and maintained a continuous ground surface without exploring the performance of different voxel size and their impact on the analysis.

Hagstrom [44] explored the advantage of voxel models by applying various outstanding issues in remote sensing such as LiDAR quality metrics, LOS mapping, and multi-model fusion. The models were validated and examined, which compared with new methods. The result shows that the voxel-based method could extract information that is not available in other existing methods. The author also stated that the impact of the voxel size parameter was not implemented due to time constraints and the complexity of the situation. However, the authors studied the impact of hitting and transmission pulses voxel size by estimating the Root Mean Square Error (RMSE) and Mean Absolute Error (MAE) to evaluate the tendency toward higher transmission values of smaller voxels.

Cabo, et al. [46] developed a voxel-based method to extract the pole-like object from MLS. Each layer of the 3D grid was segmented and analyzed individually. The voxel size was the most critical parameter for the algorithm configuration, and the right selection impacts the reliability of the result and the speed of data processing. The result shows that a set of segments associated with a

Z coordinate of a candidate part of a pole. The method was tested and found an average of the correctness of 83.3% and completeness of 92.3%.

The voxel-based method is a useful technique in extracting obstacles in sight distance and visibility assessments, which provide a robust solution when the DEMs conflict with realistic 3D geometry. Recent studies in this area used the voxel-based method, which highlighted the importance of voxelization in the assessment to detect the obstruction and quantity of the available sight distance along the road segment to improve the road safety by comparing it with recommended distance in the guidelines [42, 43]. Both studies used 20cm voxel size in the assessment; without explaining the impact of using smaller or larger voxel size on the result and information extracted.

In transportation engineering, the relationship between the voxel size and extraction of road features and objects was often unaddressed and has not been explored in previous studies, requiring more attention to choose the ideal voxel size in the trade-off between the gap and resolution. This leaves the researchers and analysts in a dilemma as no information about ideal voxel size when extracting information from LiDAR. In order words, they remain vague about the efficiency and accuracy of the information, especially when using them in a critical discipline such as road safety. In this thesis, the impact of the voxel size parameter is assessed to evaluate the extraction performance in the intersection visibility assessment application.

2.6 Speed and Visual Field Relationship

Driving is a complex activity, and the performance of the driver's visual field is critical. It is essential to study the relationship between moving vehicles and the field of vision to improve the driver's visibility and road safety. A driver's field of view increase as speed decreases. At lower speed, the driver has adequate time to see and react to potential hazards, conflict vehicles, and view objects in the surrounding environment [16]. Speed is especially lethal for vulnerable users such as pedestrians and cyclists, and the risk of death or serious injury increase as a driver's field of view is reduced [16]. Speeding significantly increases the likelihood of death as a result of a severe collision. In fact, exploring the effect of speed on the driver's field of vision and its relationship with the visual field is crucial. The studies on this area are minimal as it requires a lot of experimental investigations.

Jo, et al. [47] investigated the influence of speed on driver's visual attention. The experimental investigation assessment aims to study the effect of speed by understanding the maximum field of vision that can balance against the maximum amount of information a driver can manage. As the driver's speed increases, there is a certain limit that the driver can handle to process the visual information, which needs a driving experience to handle the situation due to visual information processing limitation.

Bhise [48] found the relationship between occlusion time as a function of vehicle speed. The study shows the occlusion time in an empty road at daylight is more when compared with road environment driving on winding curvy road at night and was more demanding. It illustrates the time limit at a certain speed that should be considered in a different driving scenario for a good visual display.

Yuan, et al. [49] applied the Hidden Markov model-based framework to estimate the driver's eye's-off road in three road scenarios; an urban road, rural road, and motorway, where the speed limit is 60km/h, 90km/h, and 120km/h, respectively. Using the duration in a driving simulator and sequences of glance location, the urban road found to be the more demanding, followed by the rural and the motorway, which is the least demanding. The occlusion duration recorded was 0 s, 1s, and 2s, respectively. The results could contribute to improving the safety of drivers by improving the driver's field of vision.

U.S. Department of Transportation - Federal Highway Administration [15] provided guidelines for the visual impact assessment of highway projects. It highlights that the viewshed of a traveler moving along a roadway is affected by the driving speed. To illustrate, the vehicle movement impacts the viewer sensitivity of drivers. Thus, the faster a driver moves, the smaller the area of the field of view in which they are focusing their attention. For instance, when a vehicle drives at 40km/h, the viewing angle is approximately 100 degree, which drops to narrow to 40 degrees when the driving speed at 100km/h, which substantially reduce the deriver's vision.

In fact, the design guide does not consider the vehicle speed at a minor road when approaching the intersection and only considers the deceleration rate that is based on assuming that the speed at the turning point is 16km/hr when the vehicle tends to carry out certain maneuver and specifies constant gap time acceptance that varies according to the vehicle type. Both parameters are constant regardless of the road design speed of the minor road. Moreover, the focus when

designing the sight triangle is on the speed of the major road and the gap time acceptance, which is based on certain assumptions. In this thesis, the impact of a vehicle's speed approaching an intersection is considered in the visibility assessment, simulating the driver's visual field at various observer points along the vehicle trajectory.

2.7 Safety Analysis

Network screening is a vital process in the safety management process, which defines the safety problem. It investigates the network to prioritize and rank sites to reduce the number of collisions and severity and select cost-effective countermeasures. The collision at a specific site is a random variable and fluctuates over an unknown mean. The randomness nature of collision data does not accurately reflect its characteristic in the long term. This can be explained when a location experiencing a high frequency of collision during a short duration may have a low collision proportion during this specific duration [50].

The regression to the mean (RTM) is a statistical phenomenon that suggests that due to the random nature of the collision, locations with a high collision frequency than the normal in a specific time are likely to experience fewer numbers in the subsequent period, even though no changes were made. One of the methods to account for the RTM is to use the empirical Bayes approach [50, 51]. The EB technique considers the number of collisions at any location as a random variable [52]. the EB combines two crucial clues to refine the estimate of expected collision frequency (a) regional historical collision records for a group of sites with similar entities and (b) site-specific historical collision records at the entity of interest. The EB approach provides a criterion by which this clue information can be combined to minimize the RTM artifact.

In recent decades, the development of collision modeling has been substantially researched. At an early stage, the Poisson distribution was typically used to model collision. Eventually, this distribution was found to be inadequate due to its failure to account for over-dispersion. Thus, the Poisson-gamma hierarchy was suggested as a suitable alternative instead [53]. In the Poisson-gamma distribution, it is assumed that the mean is gamma distributed that the conjugate distribution gives rise to the Negative Binomial (NB) distribution [54]. The NB distribution is a commonly used statistical model and is well-suited when analyzing the frequency of collisions with high sample mean and high sample size. When analyzing collision proportions, the BB statistical model has been proposed, which is capable of modeling extra variability due to the

overdispersion that is inherent in the collision data. Previous studies explain that NB provides instability for data characterized with low sample mean[55]. In this thesis, the BB model is used in the safety assessment and is relied on to examine the relationship between the visibility assessment outcome and the occurrence of specific types of collisions.

2.8 Impacts of Sight Distance on Road Safety

Collision risk encompasses an unavoidable liability to the traffic operation. The risk measures in the transportation system include exposure, probability, and consequences. The exposure can be measured as the overall times when the road users are in a potentially hazardous situation. The probability expects the chances that the system failure is formed under certain conditions, and the consequences quantify the severity of the potential failures [56].

Studies have been conducted to assess the safety of roadways aiming to study and quantify the sight distance of roadways exerts on traffic safety. Sufficient and real collision data should be acquired to perform safety analysis [57]. Sight distance, which is one of the most critical elements in road design, has an impact on traffic safety. Babkov [58] highlighted that the sight distance limitation in the former Soviet Union was one of the collisions contributing factors and accounted for around 10% of total collisions. In China, inadequate sight distance was found to be a major cause of collisions [59].

The main aim of the road design is to ensure having high safety standards. This can be achieved by providing sufficient sight distance, which is clear from potential obstruction. Thus, the influence of sight distance on safety has been addressed in various studies. Olson, et al. [60] made a comparison in the occurrence of collisions on sections that met or did not meet the stopping sight distance standards on vertical crest alignment in Michigan. The result showed that where the sight distance sites are adequate, there are significantly fewer collisions. Sparks [61] studied the correlation between the collision rate and available sight distance in the US, and the result illustrates a negative correlation. Urbanik II, et al. [62] performed statistical safety analysis to address the impact of restricted available sight distance and vertical alignment in Texas. Although the authors did not find any relationship between the collision frequency and available sight distance on two-lane crest vertical roadway, intersections within the restricted sight distance sections on the vertical crest curves reported a statistically significant increase in collision rates.

Coburn [63] stated that fatalities and injuries decreased by 65% when the visibility has been improved on curves in the United Kingdom (UK) roads.

Fambro, et al. [64] addressed the influence of sight distance on the vertical crest curve. The authors indicated that the sight distance limitation was not a safety issue. The deficiency, when compared to the standard available sight distance, was found relatively marginal and did not affect the collision rate. Conversely, when the sight distance is not adequate, it was found to affect the collision risk. The study did not provide any statistical analysis of the results. Fitzpatrick, et al. [65] studied the relationship between the stopping sight distance and safety to examine whether the limited sight distance on a vertical crest curve contributed to an increase in collisions. The research found that the collision rate in the two-lane rural highway with sight distance limitation is similar to all other rural two-lane highway collision rates. Hence, the authors concluded that the sight distance does not necessarily appear to be a safety problem.

This disparity in terms of the impact of sight distance on safety is intriguing. Previous studies showed that there are several different methods to estimate the available sight distance. However, they did not elaborate on whether the road features and objects that impact the driver's visibility were considered and taken into account when a safety analysis was conducted.

2.9 Summary

Although the research in intersection sight distance is scarce, the last decade shows a growing interest in this area. Previous research used different methods and data such as design and terrain data, GPS data, GIS platform, and LiDAR to examine the visibility of the intersection and estimate the available sight distance. However, most of the methods involved manual works to simplify the road geometry, which could be labor-intensive.

At the early stage, the sight distance analysis begins with design and terrain data. Then, the researchers started to develop design software to perform a sight distance analysis by exploring the obstacle objects in space and integrating the GIS tools to create a road surface model. Other studies also used the ALS to generate the DEMs and take advantage of the LOS and viewshed tools to estimate the available sight distance and compare it whether with the existing design or with the minimum distance as defined in the AASHTO. Moreover, some studies were not

concerned with the extraction of overhanging objects, particularly those analyzing the geospatial data using the DTMs, which were found to provide inaccurate results.

LiDAR remote sensing technology shows a great interest in applications that targets sight distance detection and visibility assessment. In fact, despite the high level of accuracy and quality of information that the Mobile LiDAR provides, most of the previous work attempted to perform the visibility assessment from ALS data by creating DEMs using GIS technology. The quality of the results depends on the digital models generated to represent the road geometric features and terrain and neglecting road safety. Some researchers found that performing visibility analysis on road segments and intersections might be unreliable using GIS functions [23, 38, 41]. The review also demonstrates the need for more work to take real advantage of the LiDAR to improve safety performance in intersections and fully utilizing it in sight distance assessment.

The available methodologies for assessing the driver's 3D visibility suffer from different limitations. The main and common limitation is neglecting the available cantilever objects when analyzing the data by creating DEMs, resulting in one-sided estimates and consequently biasing the visibility assessments [22, 30-32, 66]. Moreover, the produced DEMs have a low resolution, which is a challenge to estimate the available sight distance accurately. The studies do not account for drivers' motion along the driving lane when assessing the sight distance. It also does not consider the driving speed when decelerating at an intersection to complete certain maneuver that reflects the available visual field or provide an image of obstruction from a driver perspective.

One more common issue in sight distance assessment is that most studies used the LiDAR technology, which deployed the ALS to conduct the visibility analysis. A major drawback of using ALS data is its low point density compared to mobile LiDAR data. In other words, the aerial LiDAR data may not represent all the obstacles in the point cloud accurately. As a result, it impacts the level of accuracy when performing the sight distance analysis. On the other hand, aerial LiDAR data processing time is relatively higher since the data size is controllable, whereas mobile scans have a longer processing time [21, 23, 31, 33, 34].

In this thesis, a fully automated algorithm to estimate the blockage percentage for urban intersections is proposed. Then, a safety assessment to identify hazardous intersection is performed. In addition, the relationship between the collisions due to visibility problems and the

rate of blockage are investigated. Finally, a sensitivity analysis to study the impact of the voxel size on the extraction quality and the impact of speed on the driver's visual field is conducted.

3 METHODOLOGY

This chapter provides details about the LiDAR data collection process, the laser scanner device used to scan the study area, detailed description of the proposed algorithm used to process the LiDAR data. In addition, it describes the historical collision data and the empirical Bayes techniques used in safety assessment to identify the hazardous intersection and its link to intersections with poor visibility.

3.1 Light Detection and Ranging (LiDAR)

LiDAR stands for Light Detection and Ranging, an optical remote sensing technology that uses the time between transmitting and receiving laser signals to determine the distance (or range) [67]. These laser lights collect information about the surrounding environment. There are two types of wave lasers: pulsed and continuous. The pulsed laser is usually used for a very short duration. Based on the amplitude of received signals, the range can be detected. In contrast, continuous-wave uses the difference in phase between the transmitted and received signals to detect the ranges and find coordinates of scanned points [68].

One significant benefit of LiDAR is that the data can be collected in the daytime or at night time, as long as there is no distortion between the objects and laser systems such as rain, snow, or smoke [67]. Another main advantage of LiDAR is that it collects the data into three-dimensional (3D) coordinates of the objects. This means it measures the geographic environment in 3D and does not have the problem of geometric distortion [67]. The most powerful feature of LiDAR is the capability for the laser energy to penetrate through canopy gaps, which measures different elevations within the same direction of the laser rays. This characteristic helps researchers to generate continuous Digital Terrain Models under the dense canopy. Also, the LiDAR point cloud collected, for instance, can be used to extract multiple features on an entire highway since each point has different attributes.

LiDAR is an active remote sensing method that can be used in a ground-based platform, airborne and spaceborne. Airborne LiDAR can be used with Airborne Laser Scanning, Airborne Laser Swath Mapping, or Laser Radar. Ground-based LiDAR is often called Terrestrial Laser Scanning, which can be either Stationary Terrestrial Laser Scanning from a fixed vantage point on the surface of the earth and Mobile Terrestrial Laser Scanning (MLS) from a moving vehicle. The variety of

details and attributes through MLS and high point density, as illustrated in Figure 4, making it desirable in transportation applications [69]. MLS is capable of scanning the road environment to generate accurate models while traveling at high speeds. This would not impact the traffic operation on roadways and collect the data in reduced time.

There are several scanning methods, and the use of these methods depends on the application type. A suitable method can be used according to the density of points required. For instance, when studying the road features to locate the objects that block the driver's sightlines or vertical faces, like buildings' edges or faces, a high point density on such surfaces is required, and thus MLS is the best method [69]. However, the airborne method collects lower point density, which is appropriate for collecting information on building and pavement surfaces. Since the airborne LiDAR has a wider field of view, the drawback is that it has a lower point cloud density [70]. Airborne LiDAR can be used in different transportation engineering applications such as environment-based assessment, mapping, selection of road alignment, and feasibility studies [71].

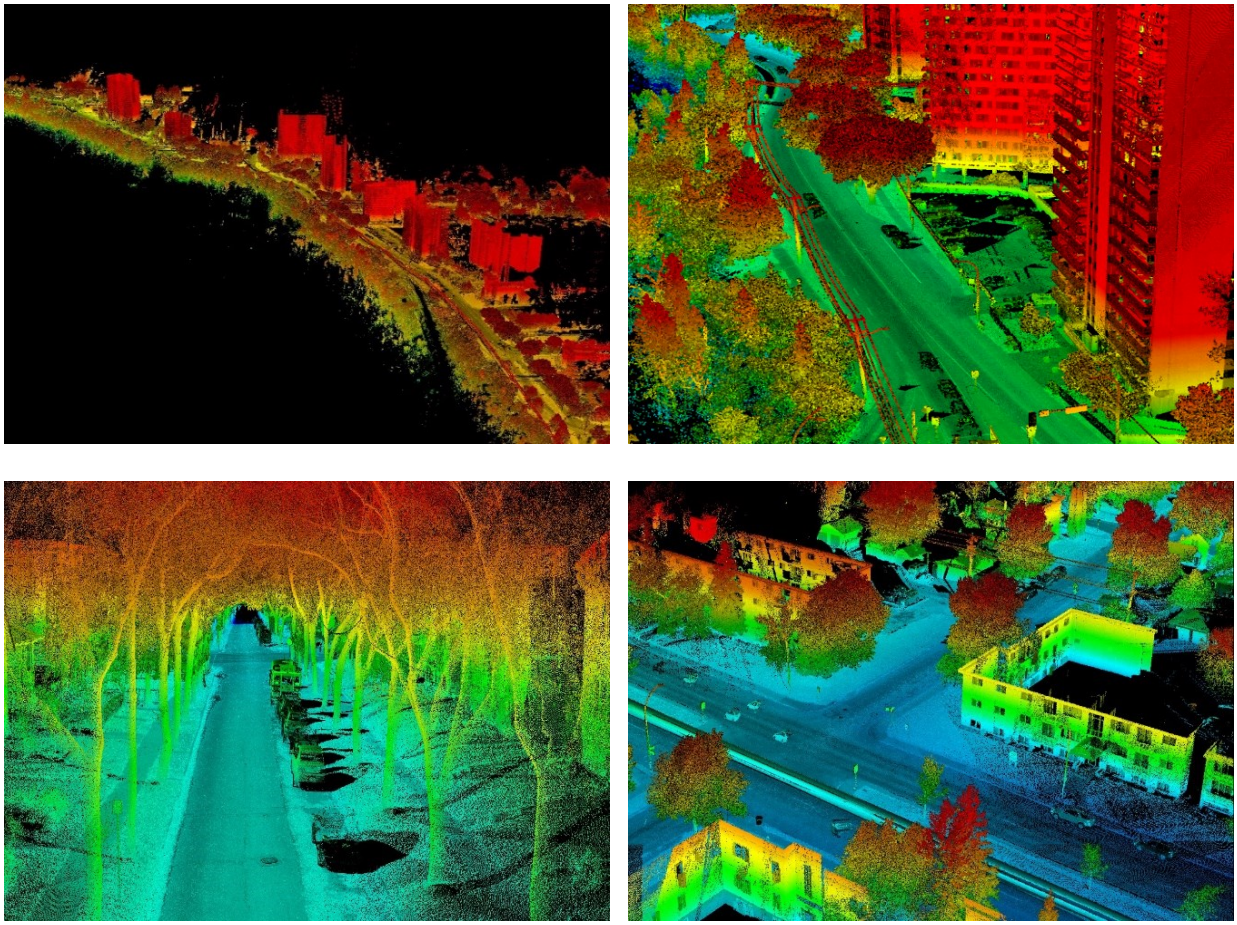

Figure 4 Lidar Point Cloud Sample Collected in Strathcona, Edmonton, Alberta

In 2013, research carried out by National Highway Cooperate Research Program (NCHRP) studied the potential application of LiDAR in Transportation Engineering [72]. The research found that different topics, such as enhanced traffic safety, are possible using MLS. Unfortunately, extracting the information from LiDAR data to facilitate such research has been extremely scarce.

3.2 LiDAR-Based Assessment in Transportation Engineering

With the advancement in remote sensing technology, reductions in cost, and the widespread data collection capabilities, many agencies started considering using LiDAR to assess various road design elements [73]. LiDAR technology nowadays plays an essential role in multiple transportation-related applications, including road safety analysis, asset management, maintenance, and planning. The interest in utilizing the LiDAR in transportation applications has a significant impact on improving traffic safety. The laser scanner device continually transmits light beams at surrounding landscape objects to capture accurate positional coordinates. Also, the reflected beam has specific characteristics that are useful in obtaining road information that can be processed for transportation infrastructure assessment.

Mobile LiDAR can scan the road environment to generate accurate models without impacting roadways' traffic operation and collect the data in a reduced time, which is very useful in urban areas. It permits precise and massive geospatial data collection of a roadway and roadsides. The information retrieved can be used in visibility assessment by processing these data using computer tools and advanced techniques. The outputs and results enable a realistic analysis of intersection sight triangle conditions.

Many researchers invested in using LiDAR in transportation engineering applications. Adopting the LiDAR as a reliable surveying option is based on developing useful applications that promote information extraction from LiDAR data in a competent way [74]. The focus was on the inventory of traffic sign extraction [75-84], while other studies developed algorithms to detect the pavement surface, road edges, lane marking, and deterioration measures (e.g., rutting and cracking) using different extraction techniques [85-92]. In regard to the elements related to geometric design, some studies explored the road elements and characteristics such as horizontal curves and vertical curves [87, 93-95]. However, research on intersection sight distance assessment and visibility analysis using mobile LiDAR data is minimal. Although some studies are available, they suffer from numerous limitations, such as not relying on MLS, which might impact the quality of extracted

information. It also involves significant manual data processing, which is a time-consuming process and not feasible for large-scale assessments [96].

3.3 Data Description and Collection

3.3.1 LiDAR Data

To assess the intersections' visibility using the LiDAR datasets, the first step is to scan the intersections at the area of interest using a mobile LiDAR scanning system. For this thesis, the Strathcona neighborhood in Edmonton, Alberta, was scanned. A third-party service provider collected the LiDAR data for the City of Edmonton (CoE) using a proprietary multifunction pavement surface profiling vehicle. The vehicle was equipped with RIEGL's VUX-1HA laser scanning system with IMU (Inertial Measurement Unit) and GNSS shown in Figure 5. The GNSS and IMU sensors are integrated with the scanning system to provide accurate positional details while LiDAR scanning vehicles travel along the roadway collecting the data. The GNSS system is the source of information related to the position (Latitude, longitude), speed, and laser scanning system time. Simultaneously, the IMU sensor records the scanning vehicle's altitude information during the roadway data collection phase. The microcomputer unit, accelerometers module, and gyroscopes.

A total of 54 surveys were conducted and saved in 54 LAS files with a total volume of 154 GB, as shown in Figure 6. Figure 7 shows a part of the Strathcona area captured from google earth. In addition, the integrated cameras allow the acquisition of imagery simultaneous with the captured LiDAR data. The image data in the form of panoramic images and ROW images were collected. Panoramic images were collected using a high-resolution Ladybug®3 spherical digital video camera system with six 2 MP cameras that enable the system to collect videos from more than 80% of the full 360° sphere [97]. ROW images are collected using a Point Grey Grasshopper camera system as a series of video-log images. The videos are geo-referenced and use the camera's coordinate system. As shown in Figure 8, samples of the video log show the driving vehicle's perspective within the vehicle's driving lane, including data collection date, name of the roadway, kilometer marker, latitude, and longitude coordinates embedded at the top of the image. The extraction of road features and objects in this thesis developed solely using LiDAR point cloud for intersection sight distance assessment and visibility analysis. However, the video log was vital as

it provides real-time supplementary information and visualization about the intersection scene (i.e., signs, posted speed, geometric characteristics, and obstacles.)

Figure 5 RIEGL VUX-1HA Mobile Laser Scanner

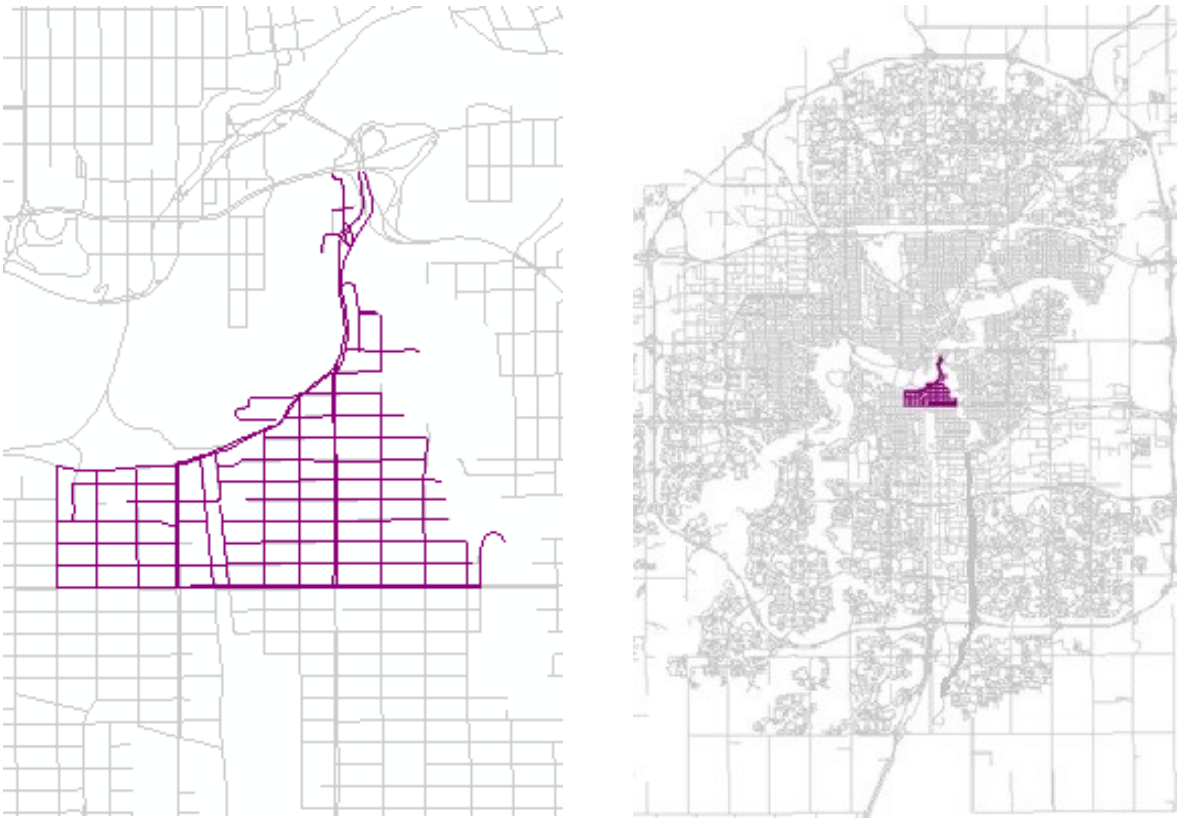

(a) Strathcona (b) Edmonton City

Figure 6 GIS Map of the Scanned Area

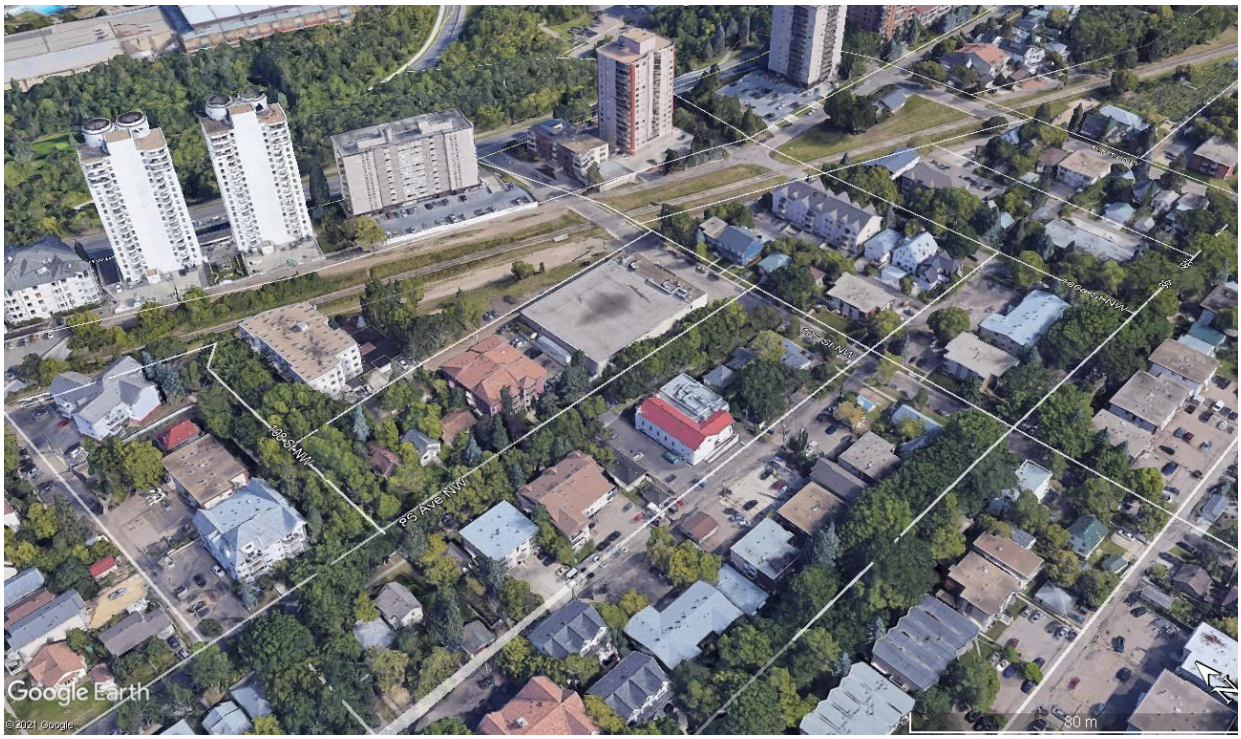

Figure 7 View of the Intersections in Strathcona (Google Earth)

Figure 8 Video-Log Sample of Saskatchewan Drive in Edmonton, Alberta

RIEGL VUX-1HA is a high accuracy kinematic LiDAR with high performance, a non-contact profile measuring system, and a fast-line scanning mechanism. These features allow a full 360-degree field of view beam detection at very high speed. RIEGL VUX-1HA is a scanner mobile mapping system that can perform a scanning rate of 1,000,000 measurements per second, with scan speed up to 250 scan lines/ second, 1000 kHz effective measurement rate, and 5mm accuracy for outstanding performance in a mobile application. Several features are recorded for each point in the scan, as shown in Table 4, which includes dense point clouds consisting of geographic, temporal, and additional attributes. It can collect the data at a typical road posted speed and dense point acquisition [97]. When scanning road features, the point cloud density depends on the speed and range of the scanning vehicle collecting the data. This is not a concern in an urban area as the posted speed is low and allow to collect high-density point. It is worth noting that RIEGL VUX-1HA can perform LiDAR scans on any vehicle and mountable in any orientation and under limited space conditions according to the interest survey area.

Table 4 Recorded Point Features and Their Definitions [98]

Point Feature	Definition
Intensity	Intensity is a measure of the return strength of the laser pulse reflected off a point.
GPS time	Records the time the laser pulse was generated
Return Number	One emitted laser pulse can return to the lidar sensor as one or several returns, depending on reflecting objects.
Number of Returns	The total number of returns for a given pulse
Scan Direction Flag	The direction of the scanner mirror at the time of pulse output.
Edge of Flight Line	Points are classified based on a value of 0 or 1. Points at the edge of the flight line will be given a value of 1, and all other points will be given a value of 0.
Scan Angle Rank	The scan angle of the laser pulse when generated from the scanner.
Point Source ID	Number of scanners emitting the reflected laser pulse.
TT Chainage M(cm)	Calculated chainage along the survey path for every point
TT Trans Offset M (cm)	Calculated offset from the survey path for every point. Negatives are along the passenger side, and positive values are along the driver's side.
TT Long Offset M (cm)	Calculated longitudinal offset from the survey for every point.
TT Vert Offset M (cm)	Calculated vertical offset from the sensor for every point. Positive values indicate the height of the sensor, and negative values indicate below.

When the individual point collected using the LiDAR scanner, they collectively represent a point cloud, the surrounding infrastructure objects, as shown in Figure 9. These point clouds aggregate the collected point using a specific laser scanning system when the light beam hits the objects within the surrounding environment and then reflected and returns to the scanner with specific attributes, based on the characteristics of reflected light beams and the position of the scanning system. Also, the intensity of object points reflected is stored in the scanning system according to the light beam's amount of energy. The point cloud intensity figure is a measure that provides information about the strength of a projected laser pulse that is calculated based on the pulse wavelength.

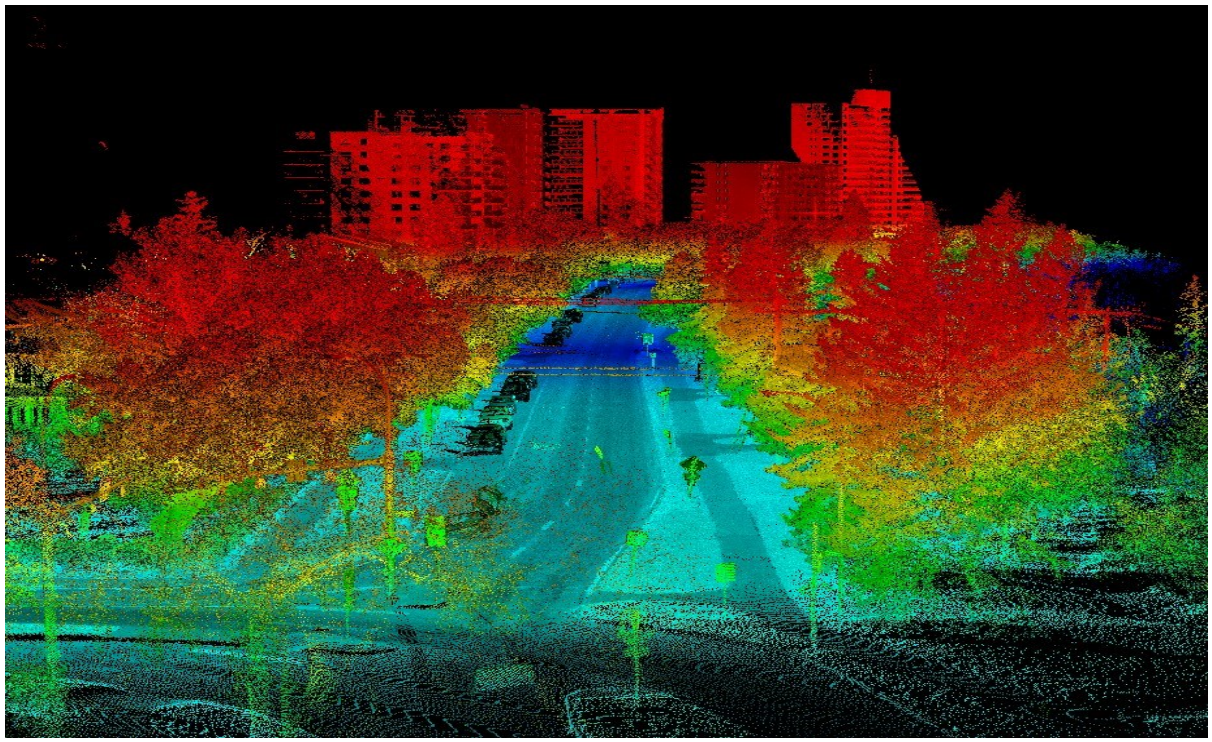

Figure 9 Sample of LiDAR data using RIEGL VUX-1HA

The mechanism used in the data collection depends on whether the laser scanning system is moving or not, which is Time of Flight (TOF) or Phase-Based Scanners [99]. The RIEGL VUX-1HA uses the reflection time to compute the position. The laser beam pulse's time duration takes to hit the target object and return to the scanner is measured. Since the laser light speed is known, the range between the scanner position and target point of the scanned object is computed using the TOF principle, as shown in the below eq (1)

$$d = \frac{\Delta t \times c}{2} \tag{1}$$

where d denotes the distance from the LiDAR scanner to the target point of the scanned object. Δt is the time difference between the emitted time of the beam and the time of the acquisition, and c is the light speed. The time must be divided by 2, as the laser beam travels the measured distance twice. However, in the phase-based scanner mechanism, distance is measured according to the reflected beam wavelength change.

3.3.2 Collision Data

This thesis focuses on Strathcona, which encloses the CoE, Canada's fifth-largest municipality and the sixth-largest census metropolitan area in Canada [100]. Strathcona is located in

Edmonton's center and has high collision potentials, including several schools and playground zones, making it an ideal study location. Ten years of historical collision records were acquired from the CoE, covering the period from 2009 to 2019, and collisions occurring at intersections were analyzed to evaluate the safety of these intersections in terms of visibility and intersection sight distance.

The collision data analysis started by identifying collisions at the intersections within the study area based on the data available, including collision cause, collision severity, party at fault, environment conditions, maneuver, and direction. The proportion of collisions involving specific collision patterns resulting from poor intersection visibility was determined for all intersections, as this is the most critical parameter in identifying collision-prone locations and developing a collision model. Since the analysis aimed to study the safety of the intersection in terms of obstructions within the sight triangle, stop sign and yield sign violations were considered in computing the collision proportions. The collision data show that collisions associated with poor visibility problems at the intersection are the second leading cause of collisions.

3.4 Automated Visibility-Based Assessment

3.4.1 Background

In this research, the proposed algorithm is used to assess the intersection sight distance by estimating the blockage percentage and investigate the available visible distance of the driver's viewing angles. Then, extract the vehicle trajectory, and discretize the point cloud into voxels in 3D. The voxel size and observer height need to be defined in this step. After that, the user needs to define the desired observer point, which depends on the intersection control sign and then, inputs the driver's viewing angle for the visibility assessment. By extending the ray cast sightlines that represent the simulated visual field, the algorithm can recognize the occupied voxels that represent the obstacle. These extracted points are then exported into a LAS file to produce an obstruction image from the driver's perspective. Figure 10 depicts the proposed method, and the following section explains each step in detail.

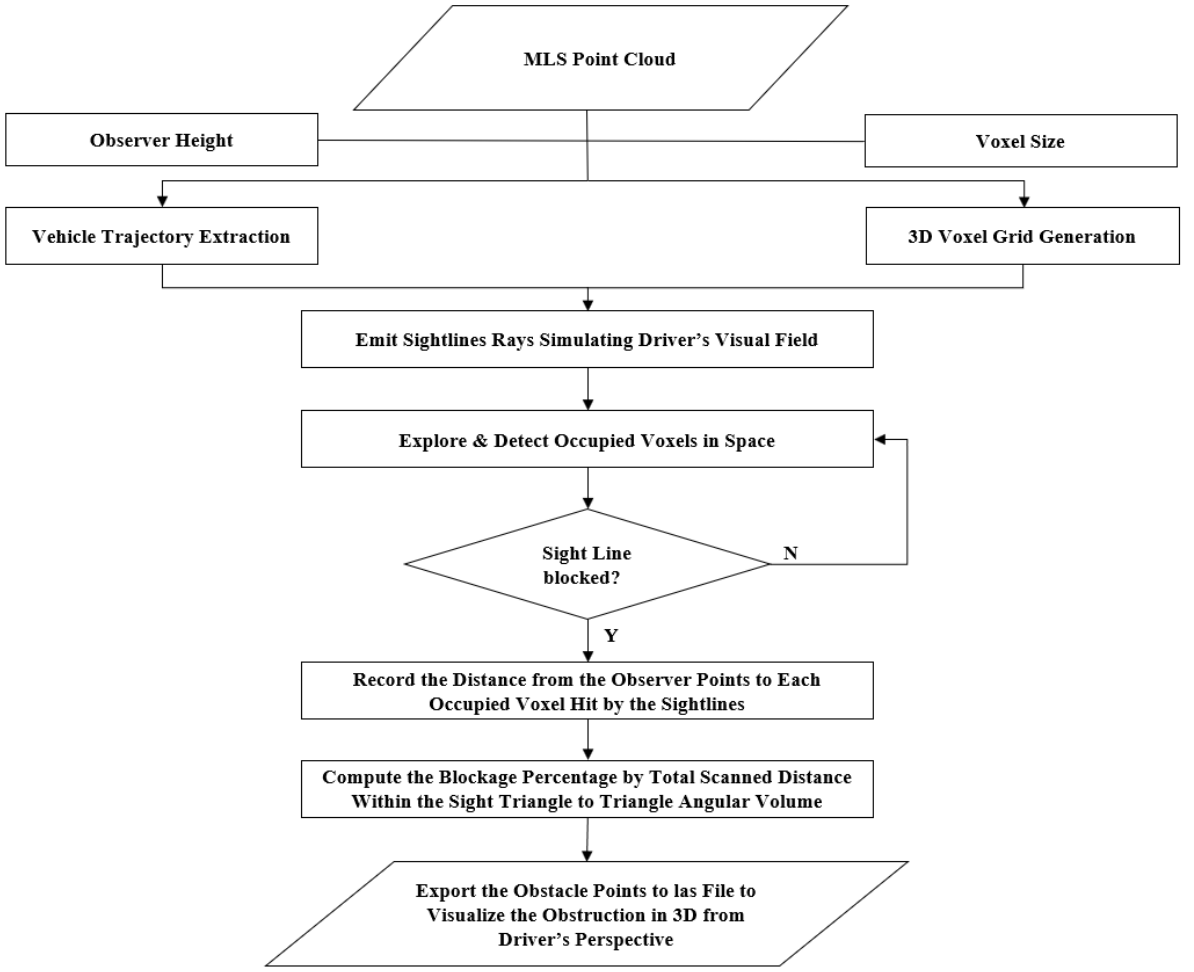

Figure 10 Proposed method flow chart

3.4.2 Point Cloud Segmentation

Before processing the LiDAR data, it requires preparing the LAS file for each intersection to reduce the number of point clouds and be more efficient in processing the data. It also includes removing unwanted and noise points that might impact the extraction of quality of information. The GPS time scalar field must be removed at the approach where the vehicle trajectory is not required to trace the sets of observer points that represent the trajectory at the desired approach only.

3.4.3 Extraction of Vehicle Trajectory

The first step of the algorithm is to extract the trajectory line of the vehicle collected from the LiDAR point cloud. The extraction process starts by defining the trajectory points along the

roadway that is parallel to the vehicle driving lane. These points are known as the position vectors, which are points used to trace the trajectory aligned with the road centerline. This path consists of a set of points filtered according to the scanning angle, which has zero value, and perpendicular to the scanner's road ground, and parallel to the roadway driving axis. It is right under the scanning system on the pavement surface of the roadway toward the gravity direction. It is also known as the Nadir plane in the literature, which is opposite to the Zenith.

To produce a straight line representing the vehicle trajectory at a constant interval, the interpolation technique is used to make the relevant point with a similar path straight by smoothing the Zenith points to produce an approximate car trajectory and interpolate points along the smoothed car trajectory. It is essential to define the vehicle's path for approaching an intersection to define the observer point that simulates the driver's eye location under investigation. The accuracy of location is important to assess the driver's visibility to spot conflicting vehicles.

Although these points provide accurate information about the vehicle path, the movement of the scanner around the yaw axis to the left and right of its direction of motion may come up with some point variation. To have a high level of accurate projection of position vectors, representing the vehicle path, the moving average method is used to locate the position with a reasonable approximation. This step is important in the extraction process to get the extracted line with no deviation. Since the scanning system used consists of two scanners to collect the point cloud, the average position of the time interval can be identified by estimating both average points for each scanner time interval segment. Then, take the mid-point of both scanners' average points at the observer's point. To illustrate, the position vector (P_a) is estimated according to the set of consecutive position vectors as follows

$$P_a = \frac{\sum_{i=1}^{n} P_i}{n} \qquad (i = 1 \; to \; n) \tag{2}$$

The location of the average position P_a is defined as the position vectors, which is the projection of the endpoint of each trajectory vector.

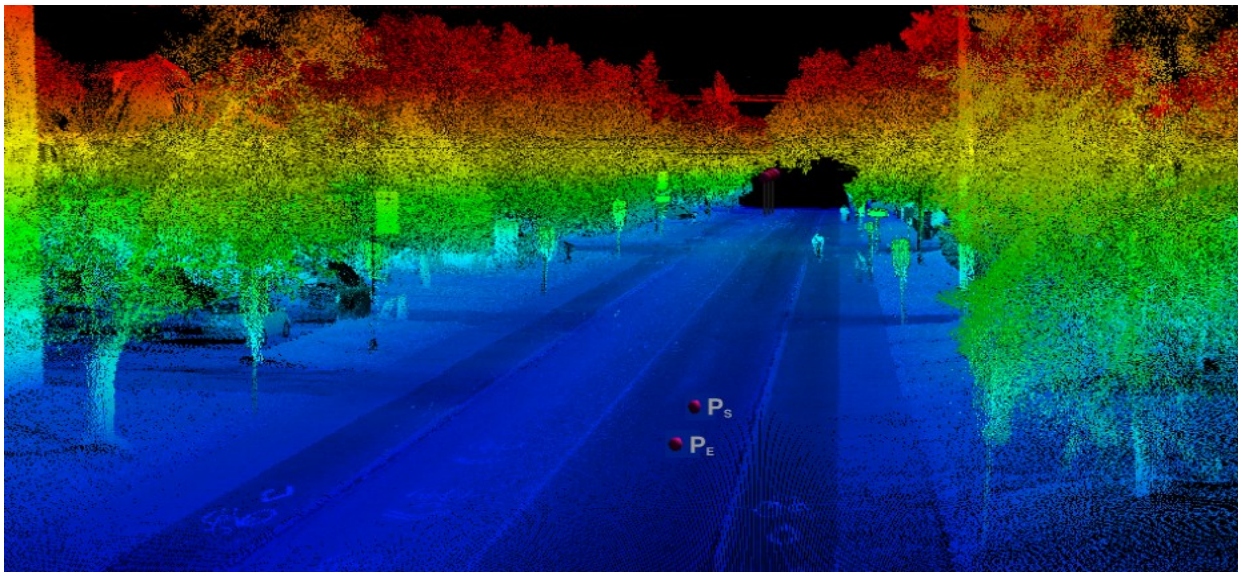

Figure 11 Points Representing Trajectory Vector

To estimate the trajectory vector, let P_S is defined as a point representing the start point of the trajectory vector, and P_E is defined as a point representing the endpoint of the trajectory vector. T is defined as the trajectory vector of two consecutive position vectors. The T can be defined as follows

$$T = \begin{bmatrix} x_E \\ y_E \\ z_E \end{bmatrix} - \begin{bmatrix} x_S \\ y_S \\ z_S \end{bmatrix} = \begin{bmatrix} x_E & - & x_S \\ y_E & - & y_S \\ z_E & - & z_S \end{bmatrix} \quad (3)$$

The algorithm allows the user to input the interval depending on the intersection location and characteristics. For instance, when extracting a trajectory for an intersection with a stop control sign, it is recommended to use 1m to accurately define the observer point to simulate the driver's location. In the stop control sign, the location of the vehicle is very close to the intersection, and thus, the need for accurate identification of observer points is vital for visibility analysis. However, in the yield control sign, since the distance is three times more than the stop control sign, it is recommended that the interval is between 2-3-meter intervals. In any case, it is the user's choice to select the suitable interval that represents the trajectory vector length; however, it should not be too long to get a highly accurate result. It is worth noting that the approach where the traffic sign exists must have an active GPS time for extraction of the trajectory, which records the time the laser pulse was generated during the data collection and scanning process.

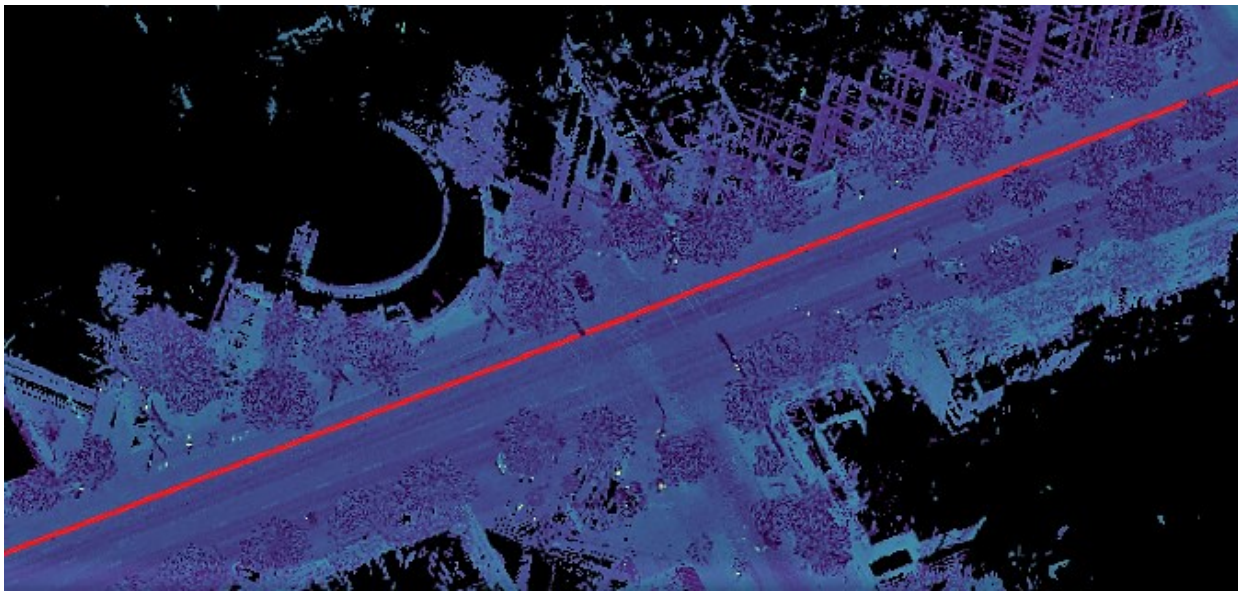

Figure 12 Vehicle Trajectory

The observer height is a crucial parameter to simulate the driver's eye and, thus, the appropriate elevation of analysis. Since the different modes of transportation have different observer heights, the driver observer height must be considered. It is worth noting that the vehicle trajectory extraction is a preprocessing step where the observer height needs to be defined based on the type of transportation mode.

To account for the orientation of the roadway and to extract the trajectory point position with no distortion, a rotation vector function (T_{zRot}) is formulated. This function will turn all points on *xy*-plan and around the *z*-axis to transform it into the zero origins coordinate system origin regardless of road orientation.

$$T_{zRot} = \begin{bmatrix} cos\,\theta & -\,sin\,\theta & 0 \\ sin\,\theta & cos\,\theta & 0 \\ 0 & 0 & 1 \end{bmatrix} T \tag{4}$$

where, θ is the rotation angle of the trajectory vector.

The next step is to determine the normal vector of the *xy*-plane. The normal vector (n_i) for each trajectory can be derived by the following:

$$n_i = [t_y \quad -t_x \quad t_z] \tag{5}$$

where, t_y, $-t_x$, and t_z are the trajectory vector *T* components in the 3-D axis.

Then, the angle ($\emptyset_z$) is calculated where the ($\emptyset_z$) is the rotation toward the *xy*-plane to rotate the vector (T_{zRot})

$$\emptyset_z = \frac{sin^{-1}(n_i . T_{zRot})}{\|n_i\|^2 \|T_{zRot}\|^2} \quad (6)$$

The normal *n* is the vector of the *xy*-plane. The new *z*-coordinate is a vector with the rotation to the *xy*-plane is as follow:

$$T_{zRot(xy)} = [Z_R(1) \quad Z_R(2) \quad z] \quad (7)$$

This rotation process will ensure that no misrepresentation of the position vector when generating the ray cast line to extract the obstacle objects at the intersection no matter the direction of the points on the roadway.

3.4.4 Voxelization of LiDAR Point Cloud

LiDAR data is collected by using different types of scanning systems. The MLS system is used for this research, which has a high density of point clouds. Dealing with large 3D datasets requires significant processing time, and computational cost is extremely expensive, which is impractical[101]. Thus, reducing the dataset volume is essential for the visibility assessment application using the programming tools. In this thesis, the voxelization process was used to convert the point cloud into a 3D grid in space to reduce the dataset volume without impacting or compromising the information [102-104]. This step also ensures that discretizing the LiDAR points cloud to a voxel is faster and more applicable in real-time applications that could be easily processed when comparing it to the points cloud. This process also represents the LiDAR point cloud as a set of volumetric elements, which is also a known spatial grid (i.e., voxels). The voxel geometry is defined by length, width, and height. The spatial location of the voxel in the space corresponds to a 3D grid system indexed by column (*i*), row (*j*), and layer (*k*), as shown in Figure 13.

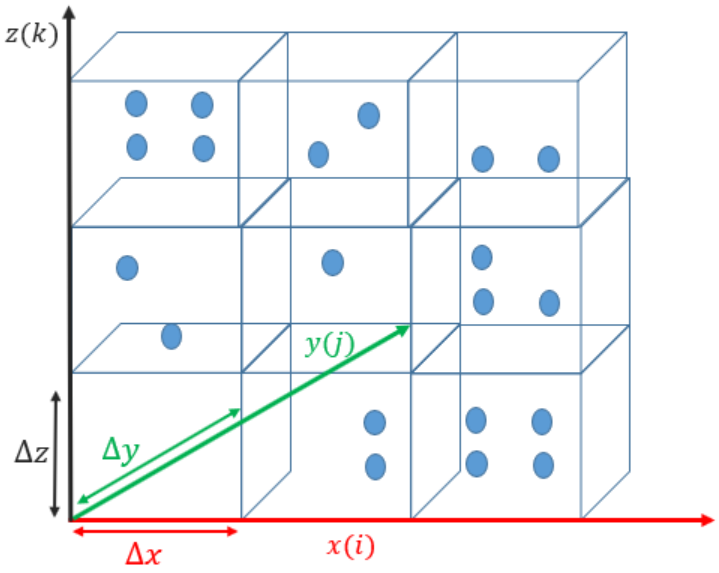

Figure 13 Voxel for point cloud in space

Each voxel in the 3D grid has a unique code known as feature ID. These voxels have their characteristics and are based on the point cloud geometrical information. Clustered point clouds are grouped into millions of tri-dimensional grids with topological relation, significantly improving the algorithm performance [105]. When points correspond to the coded voxel, the value assigned to each voxel ID represents the number of point clouds falling into that voxel. The algorithm defines the voxel when it contains point clouds irrespective of the number of points as an occupied voxel, otherwise non-occupied voxel. When the sightline hits the occupied voxel, the sightline stops exploring other occupied voxels at that viewing angle as the occupied voxel representing a road obstacle from the driver's perspective. However, voxels do not have any point cloud, it is defined as a non-occupied voxel, and they are considered visible by the virtual sightlines in the visual field assessment.

Each point cloud group is assigned to predefined voxel IDs in space to form a high level of road feature representation. To explain the process mathematically, let assume ***A*** *(x, y, z)* be a certain point in space within voxel ***B*** (*i, j, k*), which denotes a voxel parallel to *x*,*y*, and *z*-axis. Let the origin of the voxel in the 3D grid be x_0 y_0, and z_0, which are the minimum coordinate in the *xy*-plane of all point cloud in the space, where z_o is the minimum point which is perpendicular to the *xy*-plane. If the voxel dimension is *Δx, Δy Δz,* point ***A,*** which is in voxel ***B*** (*i, j, k*) is computed as follows:

$$i = \frac{int\ (x - x_0)}{\Delta x} \tag{8}$$

$$j = \frac{int(y - y_0)}{\Delta y} \tag{9}$$

$$k = \frac{int\ (z - z_0)}{\Delta z} \tag{10}$$

The voxel size is vital in retaining the feature object information of the point cloud [42]. The number of voxels in space depends on the voxel dimension. Small grids provide a high level of presenting the road features since it accommodates the small objects; however, it may not be feasible due to the high computational cost and time associated with the data processing. Despite that, the voxel size selection can be altered by the user; it is recommended to choose the voxel parameters that match the scanning system characteristics and the type of application [106]. In the visibility assessment, the voxel size used is 20cm, which represents the point cloud and laser scan lines approximately in an adjacent voxel.

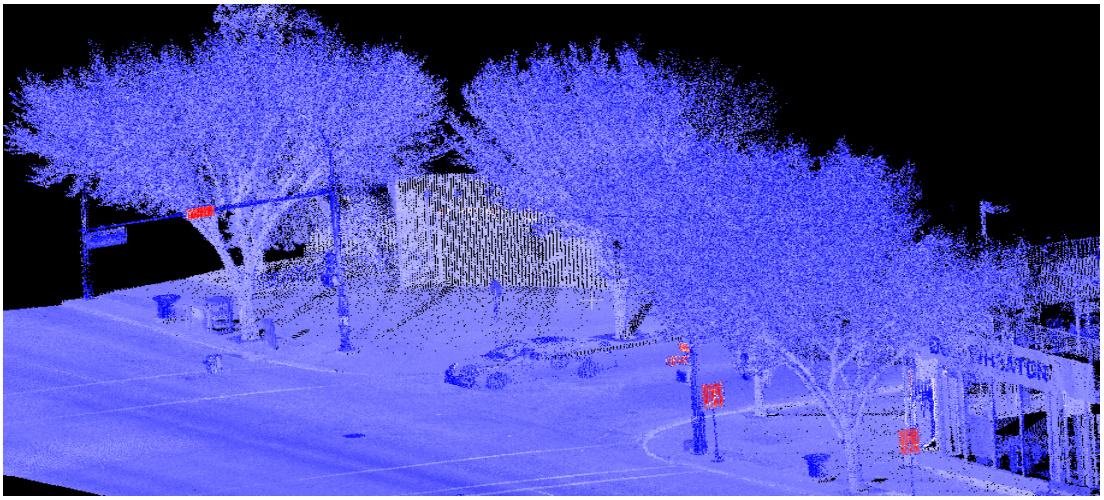

Figure 14 LiDAR Point Cloud

Although the variation in the voxel size is expected to influence the information extracted from the LiDAR dataset, the extent to which voxel changes could impact the extraction is unknown. Thus, the sensitivity assessment of the impact of the voxel size on the extraction quality is essential for developing an algorithm to extract information from LiDAR. Choosing the ideal voxel size is challenging and depends on the type of application used to extract the information, and it shows how the feature under investigation is sensitive to the voxel size. In order to capture the impacts of a voxel in estimating the available sight distance, different voxel sizes were drawn (0.1m, 0.15m,

and 0.2m), as shown in Figure 15 (a) to (c) shows an intersection after voxelization for different voxel sizes.

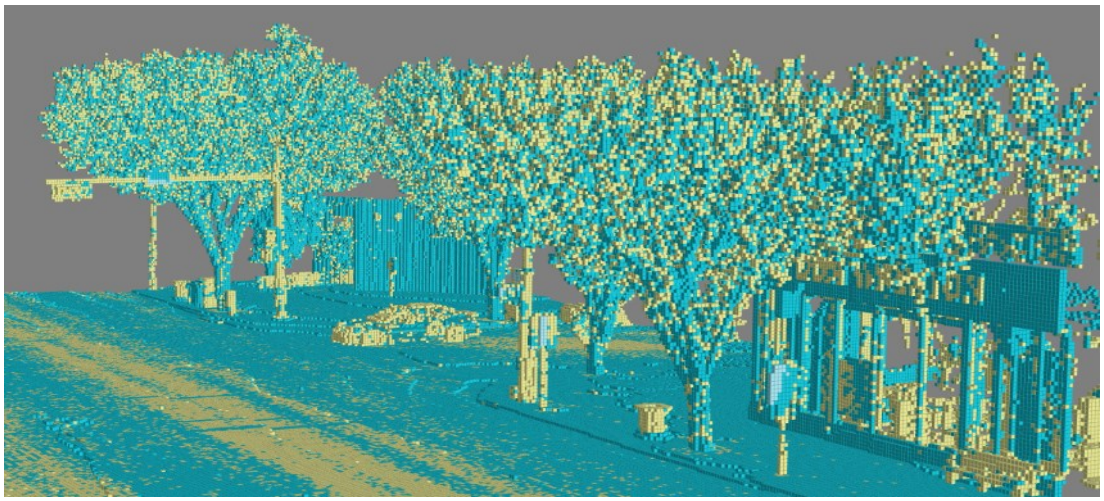

(a) Voxel Size 0.1m

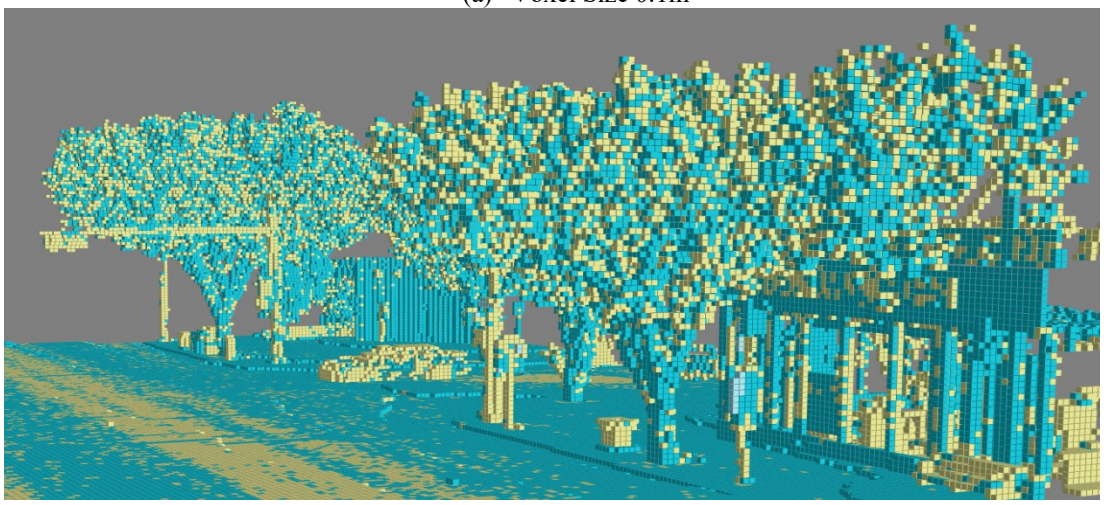

(b) Voxel Size 0.15m

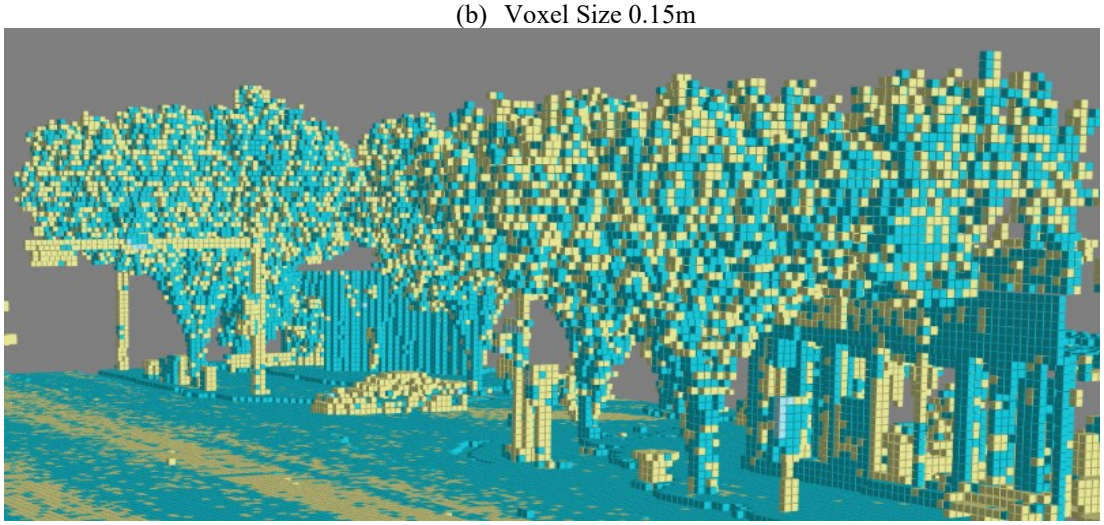

(c) Voxel Size 0.2m

Figure 15 Different Voxel Sizes in Space

3.4.5 Define Observer Point and Visual Field Parameters

When the vehicle trajectory is extracted and the point cloud data voxelized, the next step is to define the observer point. The method allows the user to select a discrete point on the vehicle trajectory along the road from which the visual field is generated. The algorithm produces the trajectory of the vehicle, as shown in Figure 16**,** from which the observer point can be selected. The trajectory points are created from a set of observer points; each point has a unique index *I= (i, i+1, i+2….m)*, which is traced in parallel to the intersection leg. The observer points generated are based on the initial LAS file segmented and prepared to load the point cloud data in MATLAB.

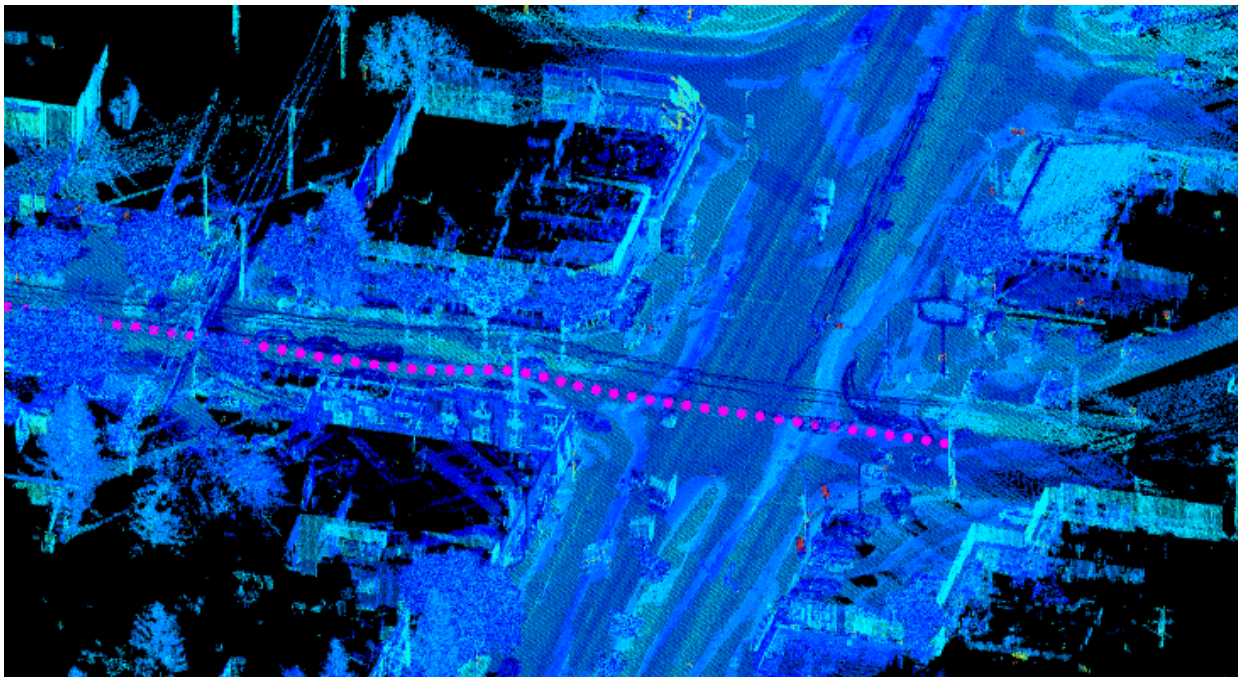

Figure 16 Discrete Point on The Vehicle Trajectory

The horizontal and vertical angle parameters with their corresponding resolutions are vital in simulating the driver's peripheral view to explore the obstacles within the sight triangle and conduct a visibility analysis within the sight distance of the intersection. In this thesis, the horizontal and vertical angles are considered to be 180° and 10°, respectively. A field of vision of 140° is the minimum visual field viewing angle required for a driver's license in most states in the US for a person with two functioning eyes [48]. The peripheral view offers information on larger targets and motion cues, and knowledge of dynamic targets. Figure 17 shows the visual field viewing angle, constructed around the vertical axis through the field of peripheral view forming an angle of ± 90°. The 180° visual field around the *z*-axis is considered to ensure that the whole

field of view is scanned to detect all occlusions impacting the driver's field of vision and causing a visibility problem.

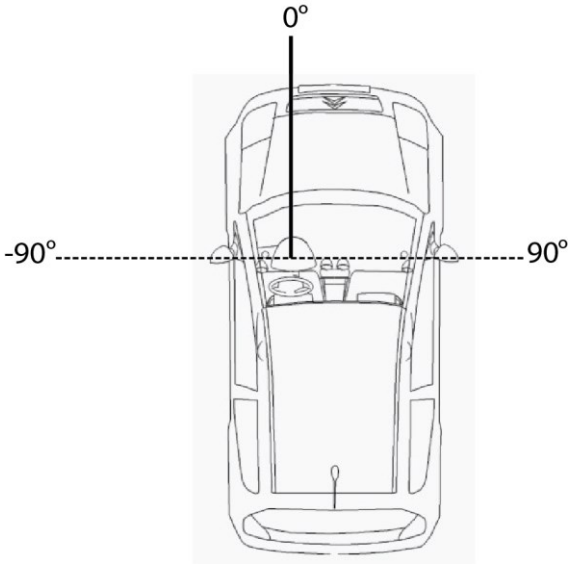

Figure 17 Driver peripheral vision

The sight triangle on both legs of the intersection is defined according to AASHTO guidelines, which vary according to the type of intersection control sign, design speed, and time gap acceptance. As explained in the previous section 2.3, these areas should be clear from any objects that potentially block the driver's sightlines. The aim is to compute every combination of vertical and horizontal angles with their corresponding resolution. The left sight triangle is needed for right-turn maneuvers onto the major road to observe conflicting vehicles approaching from the left and potential occlusions. However, when the driver intends to complete a crossing or left maneuver, the sightline triangles to both left and right need to be assessed to accommodate the turning or crossing maneuver.

The maximum offset distance (scan distance) is the crucial parameter. Defining this parameter accurately for each intersection is vital in estimating the blockage percentage. The offset distance of the sightlines must always be beyond the sight triangle. When no obstacles intersect with the extended sightlines from the pre-defined observer point within the intersection sight triangle, the driver has a clear view from this viewing angle. However, when an obstacle is detected within the sight triangle area, the sightlines are cut short, unable to explore other obstacles, and the driver cannot see beyond that location. Therefore, it is important that the sightline distance be inputted to

cover the entire sight triangle to estimate the blockage percentage accurately when performing the visibility analysis.

Another important parameter is the target offset, which identifies the number of observers points the user should target following the observer point that was initially identified. In other words, how many observers points ahead of the scan need to consider. The method uses the vector between the start and the target to select the scan direction vector. Therefore, the user should select the number where the trajectory point follows a uniform line exactly parallel to the road axis to obtain a precise sight triangle that will be covered by the sightlines representing the visual field. It should be noted that the long leg of the triangle is always perpendicular to the offset vector. Thus, the target offset number must be selected to represent a possible sight triangle matching the road geometry, where the visual field would also be extended to cover the sight triangle area. The target offset must select the number of points along the vehicle trajectory that follows an almost straight line. However, when the trajectory is not uniformly aligned, trials using different target offsets need to be entered to obtain the ideal number that most closely represents actual site conditions.

The target offset parameter is also important in reflecting the appropriate elevation level in the *z*-axis of the visibility analysis, accounting for the road pavement's surface variation. The method extends the vector for the pre-defined observer point and following observer points. To illustrate, let O be the observer point, which simulates the driver's location. The P and Q are the following observers, each a certain level from the ground depending on the road surface but with a constant height of 1.08m as defined in AASHTO for passenger vehicles. As shown in Figure 18, the trajectory vector representing elevation in the analysis is the average of the two trajectory vectors OP and PQ, which is QO represented in the red line. The algorithm forms one of the most powerful features of this algorithm, providing a high level of information to enable the detection of all occlusions within the sight triangle to a high degree of accuracy. The trajectory vectors are averaged to effectively simulate the driver's eye by accounting for variations in road ground level.

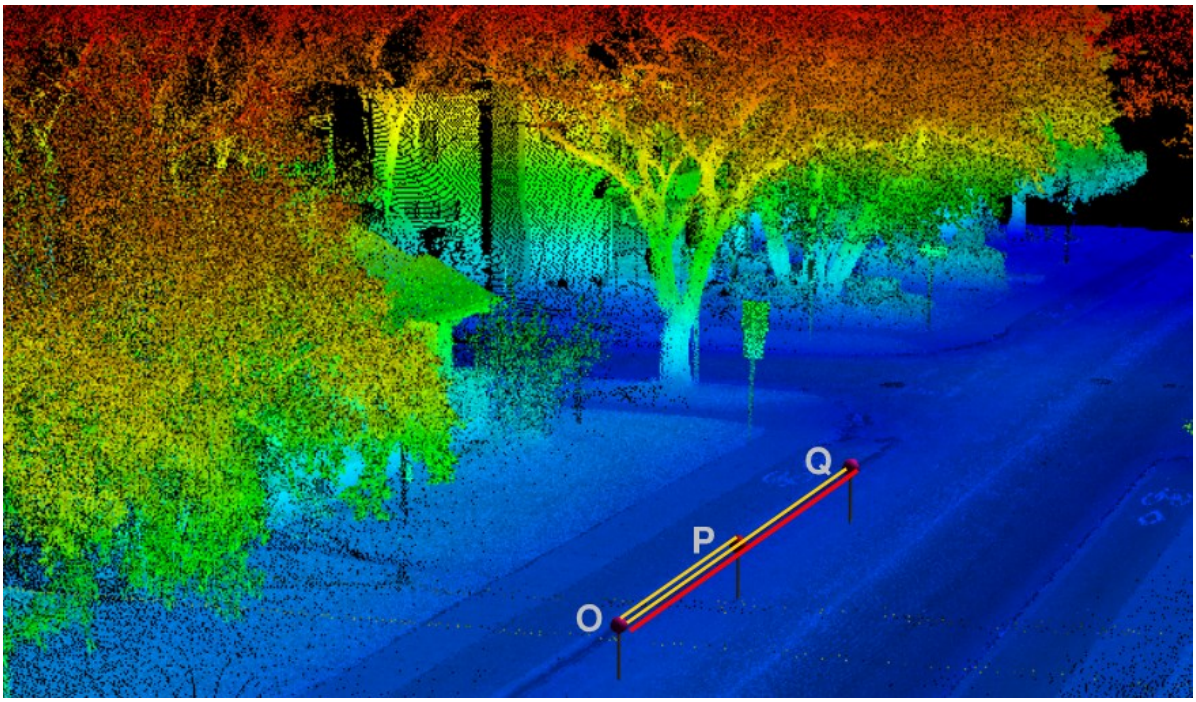

Figure 18 Trajectory Vector

3.4.6 Visual Field Assessment and Visibility Analysis for Blockage Estimation

The mobile LiDAR data consists of closely spaced points in a 3D space, representing the surrounding environment. Since the MLS has a high point cloud density, the sightlines will always detect objects in the space that represent an obstruction. A practical method of extracting such objects blocking the driver's visual field is the voxelization of the point cloud, which is used to discretize the points to occupied or non-occupied voxels. Any occupied voxels indicate an obstruction. This simplification of the visibility analysis is essential in reducing the amount of data and time involved, which also provides a more realistic representation than surface-based models adopted in previous works, accounting for small objects.

This step of the method involves generating a visual field by sampling the line of sight used to detect objects in space from the observer points at a constant resolution angle (interval), as shown in Figure 19. The visual field is spanned by different vertical and horizontal angle pairs defined by the user. The point cloud in space is represented by voxels, each of which may be occupied or non-occupied. Bresenham's algorithm is used to identify occupied voxels. The algorithm is provided by the MATLAB library and used to compute the coordinates between the observer point and points in space representing the voxel's edge. These points all lie on the possible sightline for one pair of horizontal and vertical angles. In other words, the straight line formulated connects the

defined observer and target points. These points were selected to closely approximate a straight line between two points.

In order to find the occupied voxels that represent an obstruction in space, the algorithm checks the coordinates of these voxels. It recognizes the coordinates of occupied voxels as an obstacle in the driver's field of vision, while other points are not further analyzed. Thus, when the sight line hits an occupied voxel at any given intersection, the driver cannot see beyond this location.

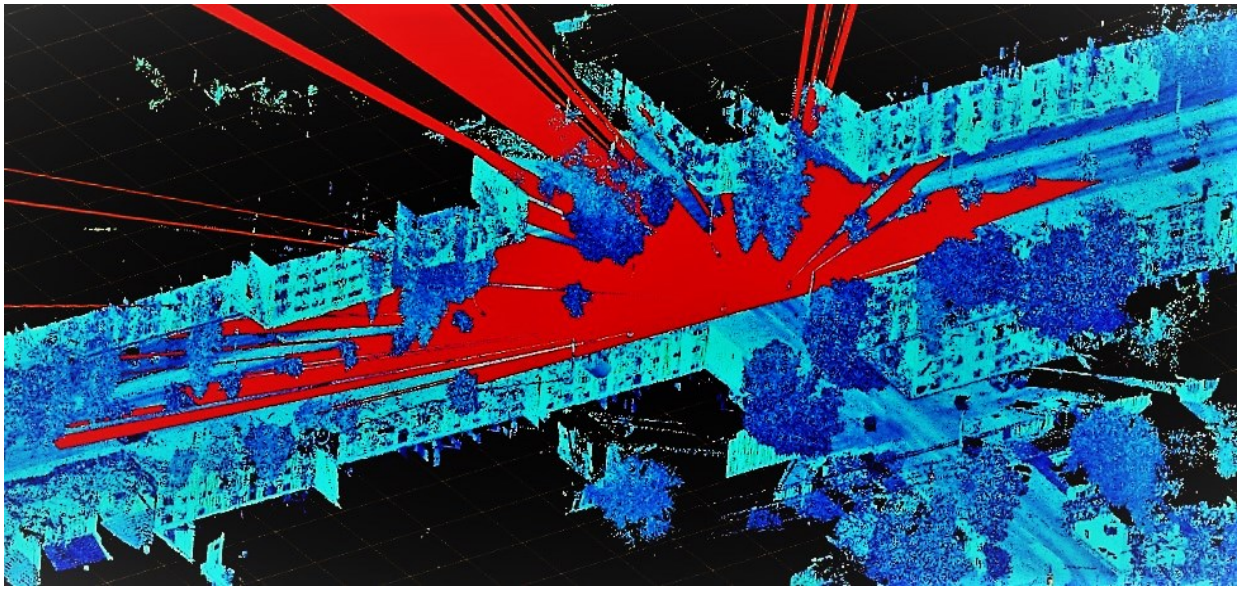

Figure 19 Simulated field at an urban intersection

The method records the distance for each sightline generated within the sight triangle from the pre-defined observer points, whether the sightlines were blocked by voxels or travel through non-occupied voxels. The distances recorded are essential in estimating the blockage percentage within the intersection sight distance. The blockage percentage is estimated by comparing the total offset distance within the sight triangle to the angular triangle area. The method also converts all points representing obstructions to a LAS file to enable the obstacle to be viewed from the driver's perspective, a powerful tool of the proposed algorithm that makes it unique. It should be noted that the vertical angle is always considered at 0° in the visibility analysis and estimation of the blockage percentage.

3.5 Dynamic Visual Field and Driving Speed

To understand the impact of speed on the driver's visual field, it is essential to determine the distance of the observer point from the intersection. This provides information about the vehicle

speed when approaching the intersection, especially when the intersection is yield-controlled, and the driver does not necessarily have to stop to cross the major road or complete certain maneuvers. Thus, having high-quality information about the visual field and the rate of blockage at various observer locations that simulate the driver's eye, where each point has a different speed and visual characteristics, is crucial for the intersection visibility assessment. Driving at a low speed when approaching an intersection allows more time to process information and increases peripheral vision, giving more time for an appropriate response.

This study is always considering that the driver makes a left turn at the intersection to assess the sight triangles from the right and left to spot the coming vehicle on the major road from both sides. In line with the AASHTO Green Book guidelines, the length of the sight triangle leg along the minor road from the edge of the intersection to the decision point is approximately 23.2m. This assumes that drivers making a left turn without stopping will slow to a turning speed of 16 km/h, requiring approximately 3.5 seconds to travel from the decision point to the intersection. Thus, the deceleration rate can be determined from the initial speed at which the driver starts to brake to 16km/h at the intersection, given the known distance and time. For instance, if the minor road speed limit of 50 km/h, the deceleration rate is equivalent to 3.73 m/s^2 for any such road. Thus, the speed at any location between the decision point and the edge of the intersection can be calculated.

Given the vehicle's operating speed approaching an intersection, the viewing angle of the driver's visual field can be estimated at any desired point between the decision point and the edge of the intersection. The literature illustrates that speed is inversely proportional to the visual field viewing angle. The following Table 5 depicts the viewing angle of the visual field at each speed. The greater the speed, the smaller the visual field. For instance, at 50km/h, a driver's visual field allows a range of approximately 90° [15]. When vehicles are moving at high speed, the brain receives more visual information. However, the brain can only process a certain amount of information within a specific time, so, at high speed, it eliminates significant information within the field of vision, potentially contributing to the occurrence of a collision.

Table 5 Vehicle speed and visual field viewing angle [15]

Speed (km/h)	Horizontal Angle View
40	100
70	65
100	40

A dynamic simulation of the driver's view while approaching the intersection is essential to study the impact of vehicle speed on the driver's visual field at the intersection. The driver's sightlines must cover the sight triangle to scan all objects in the sight triangle area and ensure that no obstacles block the driver's vision so that they can complete a certain maneuver safely. By studying the relationship of speed with the driver's view angle, the following equation provides the angle of the driver's view at a given speed

$$y = 185.89\, e^{-0.015x} \tag{11}$$

where y is the horizontal viewing angle, and x is the driver's speed.

Once the driver's viewing angle is known, the previous method will be applied to assess the visibility and the intersection scene from different observer points. The output will show the field of view and whether it will cover the sight triangle area at the intersection the location of any obstructions. The following Figure 20 demonstrates the impact of speed on the visual field and how it may restrict the driver's vision.

By utilizing the MLS data and using the proposed method, as explained in the previous section 3.4, a visualization of the intersection at different speeds is possible, providing a realistic representation of the visual field. The algorithm extracts the obstacles from the driver's perspective at designated observer points close to the intersection at a specific speed by exporting the point cloud that represents an obstruction to the driver's visual field to a LAS file. This allows us to view the intersection and assess its visibility in a real-world situation through the accurate projection of a virtual intersection environment.

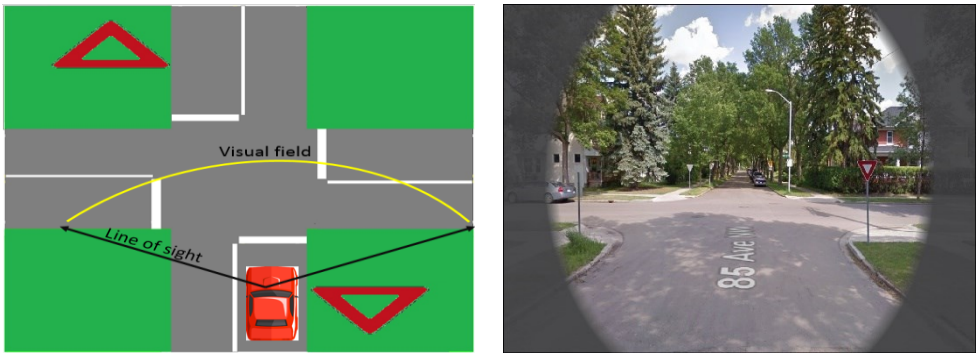

(a) Field of View and visibility at 20 km/h speed

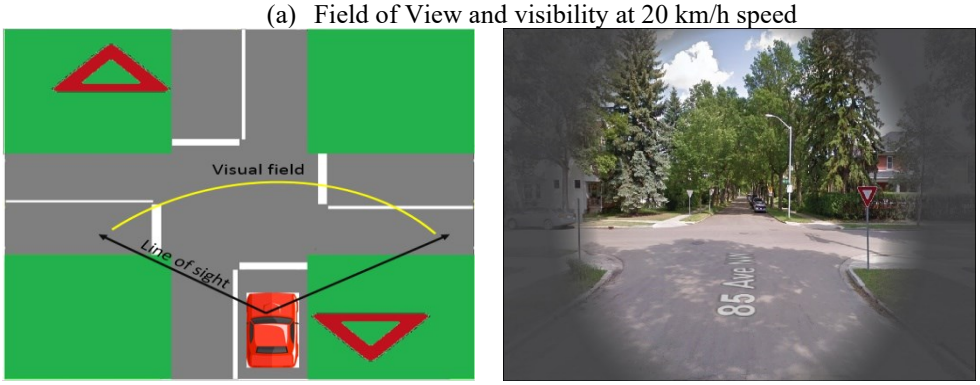

(b) Field of View and visibility at 30 km/h speed

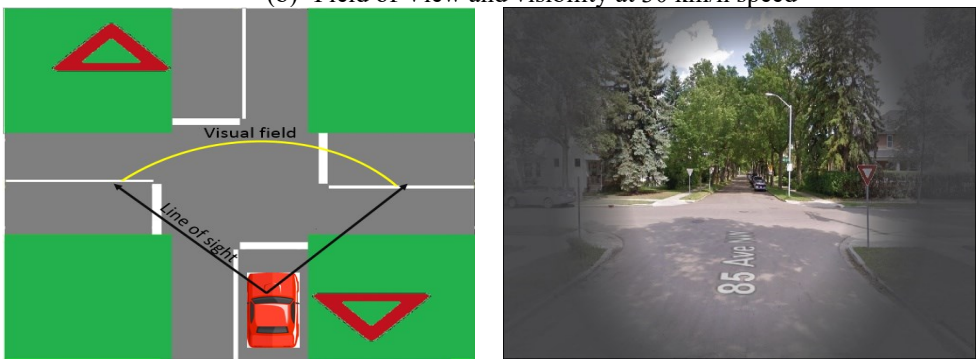

(c) Field of View and visibility at 40 km/h speed

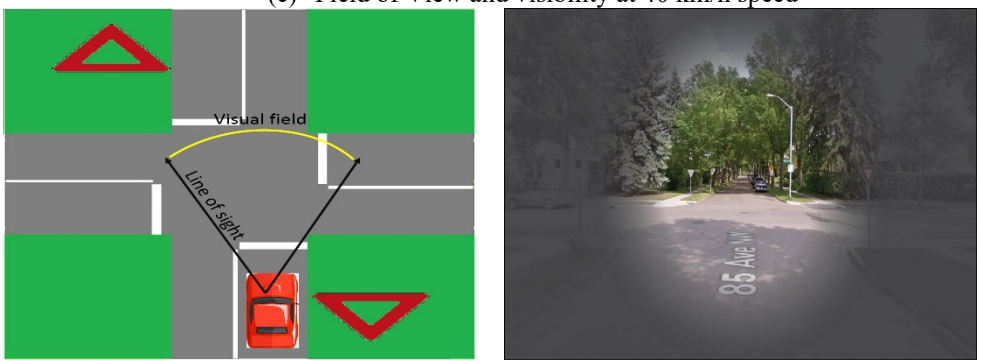

(d) Field of View and visibility at 50 km/h speed

Figure 20 The impact of the visual field in driver's field of vision

3.6 Safety Assessment

3.6.1 Background

There are fundamental principles that must be taken into consideration when conducting any statistical safety analysis. First is the variation in collision frequency, which means that collisions are random events that naturally fluctuate over time at any given site. Second, the RTM means that when roads experience high collision frequency in a specific period are likely to have fewer collisions in the following period even if no measures are taken due to random fluctuations in the number of collisions [107]. Thus, it is essential to distinguish between the influence of the different factors impacting road safety throughout the time and the countermeasure used to treat the collision occurrence. It is important to select the ideal statistical distribution and method to conduct a robust statistical analysis of collision data. In this thesis, the interest is to find the collision-prone intersections and relate a measure of their visibility to historical collision records. Therefore, adopting a technique that accounts for these observations is essential to obtain a reliable.

The research on road safety has shown how the design parameters could significantly impact collision occurrence. The sight distance design element, which is the thesis focus, are likely to exhibit a quantitative effect on road safety. The heterogeneity of previous studies on safety analysis in connection with the sight distance design element needs to be addressed. The literature shows that the relationship between visibility issues and collision occurrence at intersections is limited. To fill this gap, remote sensing technology was used to link the visibility assessment outcome and with the collision proportion for a specific collision pattern. The following sections provide an overview of the techniques used to identify the collision-prone intersection and estimate the relationship between the driver's visibility and collision occurrence at intersections.

3.6.2 Method of Sample Moments

The method of sample moments is used to identify the intersection with an overrepresentation of a particular collision pattern. The methods identify collision-prone locations for a specific collision type by establishing a reference group of similar locations and estimating the mean and variance of the reference population. For instance, intersections with stop and yield control signs at minor roads within the same area were considered for the collision analysis. The collision proportion is the ratio for the number of collisions that occurred due to the visibility issue to the total number of

collisions at the intersection. The site is considered a collision-prone location if the particular collision pattern is overrepresented in the total number of collisions. This method assumes that a relatively large population can be assembled; the mean and variance are related to the expected and variance of the collision frequency. The following procedure is similar to the Bayesian analysis of previous studies [52, 108].

To investigate the location that exhibits overrepresentation of collision pattern, suppose that p is a long-term proportion for all collisions that occur at a specific location and involves a particular feature. For each location given, the binomial distribution is the probability given for the collision occurrence value of this collision pattern as follow [109]:

$$P\left(x_i = x \mid n_i, \widetilde{p_i} = p\right) = \frac{n_i!}{x_i!\,(n_i - x_i)!}\, p^x (1-p)^{n-x} \qquad (0 \le x \le n) \qquad (12)$$

where n_i is defined as the total collision number at location i during a specific time; x_i is the collision number of a specific collision pattern under investigation at location i from the n_i collisions; $\tilde{P}_i$ is the ratio of specific collision pattern x_i to n_i as a random variable; $\bar{P}$ is the mean value for $\tilde{P}_i$; $f(p)$ is the prior distribution with function p in the reference group.

The binomial distribution treats the collision frequency at specific locations as an independent random variable. It can be modeled by a series of Bernoulli trials, which will have one outcome out of two possible outcomes. Thus, the collision proportion of a particular collision pattern is estimated using the binomial distribution [110]. It is also used to investigate the cumulative probability of getting a particular collision pattern to find whether there is a deviation from the random statistical process of collision frequency.

As explained in the previous section, the first step of the method is to establish a reference group. The group should have locations with similar characteristics and should be selected appropriately to have an accurate result. The location type, environment, roadway function, traffic control sign, and any other factor related to the collision pattern are the criteria that must be used to select the reference group. In this thesis, intersections from an urban environment perspective with similar functions, where most intersections have a stop or yield control sign within the same area, are considered the reference group for the collision analysis.

In the next step, the collision proportion (p_i) of each collision pattern (x_i) at the location of the total number of collisions (n_i) needs to be calculated. The collision proportion (p_i) must be computed for each intersection within the group. The Beta distribution is assumed to be the prior distribution for p among the desired reference group [111]. The conventional form of the prior distribution to use in conjunction with binomial distribution in eq (12) for observations of Beta distribution as follows

$$f(p) = \frac{p^{\alpha-1}(1-p)^{\beta-1}}{b(\alpha,\beta)} \qquad (0 < p < 1) \tag{13}$$

where α and β are prior distribution constant parameters. $b(\alpha,\beta)$ is the value of the Beta function at α and β given by

$$b(\alpha,\beta) = \frac{\Gamma(\alpha)\Gamma(\beta)}{\Gamma(\alpha+\beta)} \tag{14}$$

The mean and variance are estimated according to the characteristic of Beta distribution:

$$E\,(p) = \frac{\alpha}{\alpha+\beta} \tag{15}$$

$$Var\,(p) = \frac{\alpha\beta}{(\alpha+\beta)^2(\alpha+\beta+1)} \tag{16}$$

where the parameters α and β of the Beta priors distribution must be a positive value [52].

By equating the variance and mean in Eqs. (15) & (16) to the variance s^2 and sample mean $\bar{p}$, the Beta distribution parameters α and β can be estimated using the method of sample moment.

The mean and variance for m locations is given by

$$\bar{p} = \frac{1}{m}\left(\sum_{i=1}^{m}\frac{x_i}{n_i}\right) \tag{17}$$

$$s^2 = \frac{1}{m-1}\left[\sum_{i=1}^{m}\left(\frac{{x_i}^2 - x_i}{{n_i}^2 - n_i}\right) - \frac{1}{m}\left(\sum_{i=1}^{m}\frac{x_i}{n_i}\right)^2\right] \tag{18}$$

$f(p|x_i, n_i)$ the posterior distribution, can be with the location-specific observation (x_i,n_i). When the parameters α and β are updated to a Beta prior distribution with binomial observations, they bear a natural interpretation, which implies that

$$f(p|x_i, n_i) = \frac{\Gamma(\alpha_i + \beta_i)}{\Gamma(\alpha_i)\Gamma(\beta_i)} p^{\alpha_i - 1} (1-p)^{\beta_i - 1} \quad (19)$$

As a result the new posterior distribution is also a Beta distribution with parameters [112]

$$a_i = \alpha + x_i \quad (20)$$

$$\beta_i = \beta + n_i - x_i \quad (21)$$

A location considered to have an overrepresentation of a specific collision pattern if the probability of collision proportion p_i exceeds the reference group mean $\bar{p}$ is significant. Hence, the case is as follows:

$$\left[1 - \int_0^{\bar{p}} \frac{\Gamma(\alpha + \beta + n_i)}{\Gamma(\alpha + x)\Gamma(\beta + n - x)} p^{\alpha + x - 1} (1-p)^{\beta + n - x - 1} \quad d_p\right] \geq \delta \quad (22)$$

where δ is the significant level and location i identified as collision-prone at the $(1-\delta)$ confidence level.

3.6.3 Beta-Binomial (BB) Collision Regression Model

Previous research proposed a wide array of models to link collision data to several independent variables representing road features and characteristics. The most significant model to investigate specific collision patterns, which can identify the locations with an overrepresentation of a particular collision pattern, is the BB model. Eq (12) shows the basic structure of the BB. Following the previous derivation, the BB function can also be written by the log-likelihood as a function of $\bar{p}$. The $\bar{p}$ can be linked with variable, X that represent the road attributes and characteristics via the logit link [113]:

$$\bar{p} = \frac{1}{1 + exp(-XB)} \quad (23)$$

where $Y = XB$ is the simplest safety performance function with coefficient B [113]. The maximum likelihood estimation (MLE) is used to estimate the coefficient B by applying it across the BB

distribution log-likelihood function. In this thesis, SAS, a computational software program, was used to get the MLE of the function

The BB model accounts for collision data with a small sample size and the low sample mean that due to the large instability. Also, it overcomes the overdispersion data issue, producing a model with extra variability. The extra variability is due to the probability of Beta distribution independent event, *p,* that believed to be capable of modeling a wider range of collision data [113]. Following the derivation and application of the Bayesian theorem in section (3.6.2), the following Eq24 demonstrate the extra variability of BB distribution [113]

$$Var(x) = E[Var(x|p)] + Var[E(x|p)] \tag{24}$$

$$= E\,[np(1-p)] + Var(np)$$

$$= n[E(p) - E(p^2)] + n^2 Var(p)$$

$$= n\,\bar{p}(1 - \bar{p}) + n(n-1)Var(p)$$

Eq 24 demonstrate that the $Var(x)$ is associated with Binomial distribution. however, $Var(p)$ is according to the characteristic of the Beta distribution.

The eventual model must be tested to check whether it complies with the following requirements. First, the coefficients of each variable must be statistically significant. The *p*-value for each variable tests the null hypothesis. According to the confidence level selected, a low *p*-value indicate the null hypothesis should be rejected and removed from the model. It is worth noting that multicollinearity is a statistical phenomenon among variables when two or more explanatory variables are highly linearly related and thus distort the model output. In other words, when two variables, for instance, exhibit a strong correlation, one of them must be removed from the model. The percentage of all possible samples that can be anticipated to include the true population parameter is referred to as a confidence level. In the traffic safety analysis, the confidence level should not be less than 95% to have reliable results. Another important factor is the goodness of fit measures, used to assess the model's quality through an adequate statistical test. In the BB model, the Chi-square test utilizing Pearson $\chi 2$ statistics. For each predicted value y_i a real value μ_i is associated according to the following general expression. Lastly, the sign of the coefficients must explain the impact on collision proportion.

$$\chi 2 = \sum_{i=1}^{n} \frac{(y_i - \mu_i)^2}{\mu_i} \tag{25}$$

The Pearson $\chi 2$ is asymptotically $\chi 2$ distributed with n-p degree of freedom where p is the number of the model variables. When the $\chi 2$ statistic has a low value close to zero or high value, it indicates the model has poor prediction performance.

4 RESULTS AND DISCUSSION

4.1 Automated Visibility-Based Assessment

This section presents and discusses the results of the intersection sight-distance assessment and visibility analysis. The percentage blockage of driver's sightlines at intersections was assessed and computed using MLS by extracting the obstructions using a novel algorithm described in section 3.4. The visibility analysis at the intersection was conducted considering different traffic control signs and transportation modes. The figures in the following sections show the simulated outcomes of the proposed method, visualizing the driver's field of vision based on pre-defined observer point locations. They also present 2D visibility maps and show the angle of vision where obstructions cause driver visibility problems. The 3D visualization of the driver's visual field provides a clear image to facilitate an understanding of the obstacles to the driver's vision and the quantification of these object positions.

Moreover, the results compare visibility for different transportation modes by studying the outcome and rate of blockage for a passenger vehicle and a heavy truck, each with a different observer height. In this thesis, the passenger vehicle height was simulated at 1.08m, while the height of the heavy truck was assumed to be 2.33m, based on AASHTO guidelines standards [9]. This differentiated elevation analysis provides differing representations of road objects, landscape, and furniture, producing a realistic outcome that is essential in improving visibility for all road users.

4.1.1 Yield Sign-Controlled Intersections

When approaching an intersection controlled by a yield sign, the driver requires a certain distance to observe a potential conflicting vehicle and to slow or stop before colliding within the intersection. As explained in the previous section 1.1.2, it can be challenging to maintain these distances in urban areas, especially for yield-controlled intersections, which need a large area free from obstructions. The yield-controlled intersection analysis was performed to compute the blockage percentage within the sight triangle according to AASHTO requirements. This study assumed that a driver approaches the intersection to complete a left turn maneuver without stopping and needs to assess both left and right sight triangles. Therefore, the driver's decision point begins at 25m from the center of the lane for the vehicle approaching from the left, and this

is the location when the driver starts to brake. Since the majority of intersections is two-way—with one lane in each direction—the short leg distance of the sight triangle is 28.5m for the vehicle approaching from the right.

The driver's eye location is considered at the decision point to simulate the driver's 3D visual field. This section of the analysis identifies the blockage percentage for intersections with a yield sign. The vehicle type considered is a passenger car with an observer height of 1.08m, and this height is adopted as the elevation level in the analysis. However, the distance of the long leg of the sight triangle is calculated as illustrated in Table 2, based on the posted speed on the major road and gap time acceptance. The driver's visual field in the horizontal and vertical viewing angles was defined with constant values of 180° and 10°, respectively. Table 6 shows examples of intersection attributes for intersections within the study area: yield-sign-controlled intersections.

Table 6 Yield sign-controlled intersections attributes

Sight Triangle				Short Leg (m)		Long Leg (m)
Intersection	**Major Speed (km/h)**	**Minor Speed (km/h)**	**Approach**	**Left Triangle**	**Right Triangle**	**Left & Right Triangles**
85 Ave & 101 St	30	30	East			67
85 Ave & 100 St	30	30	East	25	28.5	67
84 Ave & 97 St	50	50	North			111

The proposed method performs the visibility analysis by exploring obstructions within the sight triangle area recommended by AASHTO. The blockage percentage is then calculated based on the intersection scene from the driver's perspective. The method also generates a visual field map of the intersection in 3D and *xy*-planes, showing where the sightlines hit with obstacles.

The proposed method offers a fast, automated simulation that detects obstructions blocking the driver's vision in any given scene to provide information about visibility in real-world situations for potential road safety improvements. Table 7 depicts the blockage percentage for both the left and right triangles in different intersections within the study area. The results show that, for yield-controlled intersections, the blockage percentage ranges from 54% to 83%. The high blockage percentage means that many sightlines within the visual field met with obstacles, indicating the presence of a road obstruction within the sight triangle area. An additional factor is the significant length of the sight triangle legs on both minor and major roads. For instance, the observation point on a minor road, representing the driver's location at the decision point, is located far from the intersection. Moreover, the gap acceptance time required for the yield sign is slightly high, and the

distance of the long leg of the sight triangle depends on this parameter. This results in a large sight triangle area which is the factor that yields to increase the blockage.

Table 7 Blockage Percentage of yield sign intersections

Intersection Location	Approach Location	Posted Speed km/h		Blockage Percentage	
		Major Road	Minor Road	Left Triangle	Right Triangle
84 Ave & 97 St	North	50	50	72%	66%
84 Ave & 101 St	East	50	50	71%	73%
84 Ave & 107 St	East	50	50	65%	67%
85 Ave & 100 St	East	30	30	63%	71%
85 Ave & 101 St	East	30	30	67%	65%
85 Ave & 107 St	West	50	50	74%	72%
86 Ave & 98 St	West	50	50	83%	83%
87 Ave & 100 St	East	50	50	79%	65%
87 Ave & 105 St	East	50	50	69%	54%
89 Ave 98 St	East	50	50	58%	70%

Figure 21, 22, and 23 show 2D visibility maps for various intersections. The sight triangle in green represents the area that should be clear from road obstacles and visible to the driver, according to AASHTO standards. The solid yellow circle is the driver's location on the intersecting road. The visual field is shown in red as a set of ray cast sightlines that travel a distance defined by the user unless they intersect with an obstacle. As can be clearly seen from the figures, some sightlines at particular viewing angles were restricted and did not extend to find further obstacles. In other words, the driver cannot see further objects beyond this distance which would block the sightlines at viewing angles. These figures demonstrate the impact of objects such as buildings, road structures, or bushes at an urban intersection on the driver's ability to observe conflicting vehicles, thus significantly contributing to road collisions. Figure 24 shows the obstacle in red detected virtually in 3D.

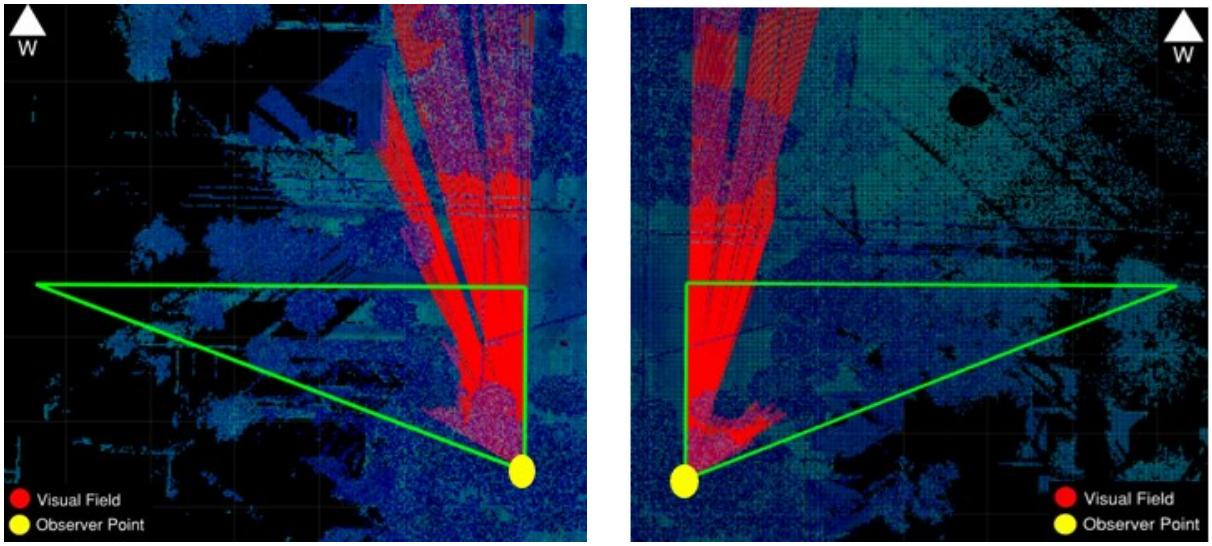

(a) 63% blockage (b) 71% blockage

Figure 21 Visibility Map (Intersection 85 Ave and 100 St)

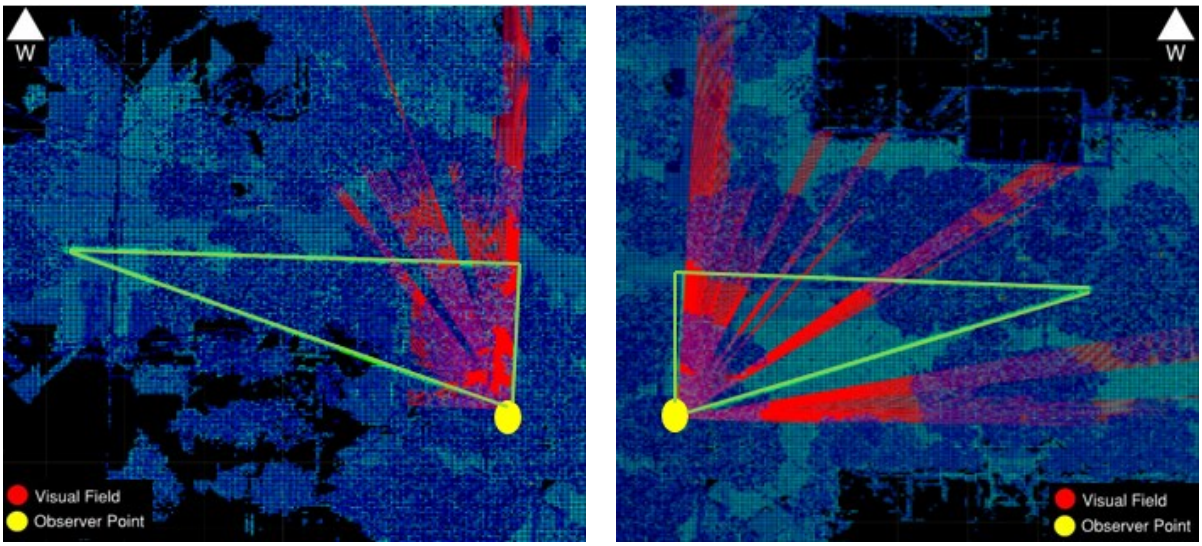

(a) 67% blockage (b) 65% blockage

Figure 22 Visibility Map (Intersection 85 Ave and 101 St)

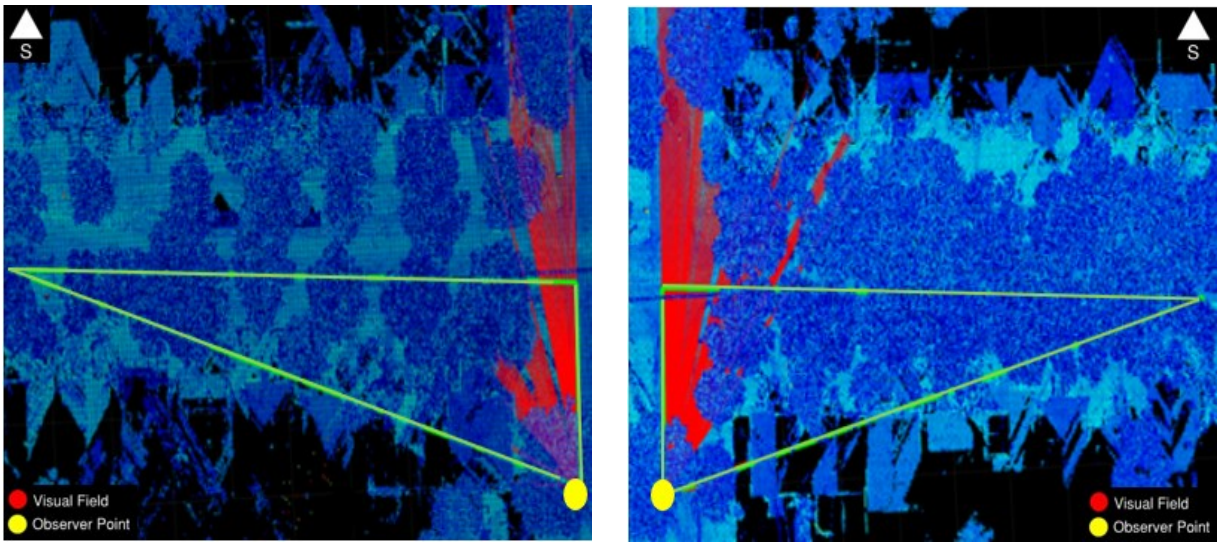

72% blockage 66% blockage

Figure 23 Visibility Map (Intersection 84 Ave and 97 St)

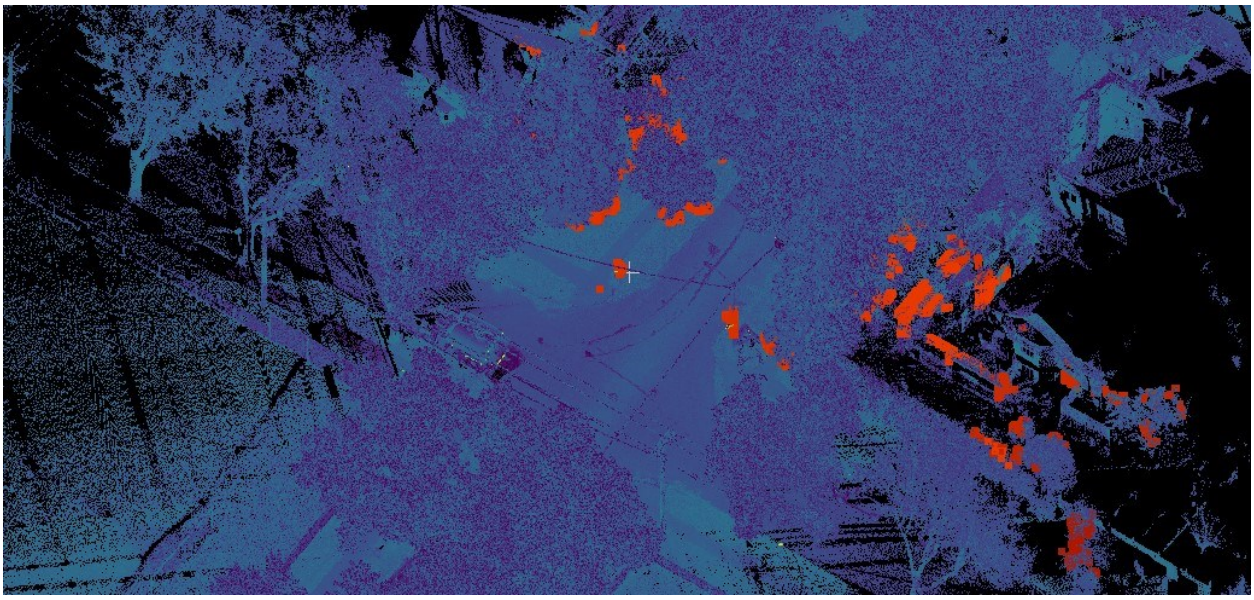

Figure 24 Obstructions in 3D Scene (Intersection 85 Ave and 100 St)

Figure 25, 26, and 27 show the available visible distance plots for the intersections of 85 Ave and 100 St; 85 Ave and 101 St; and 84 Ave and 97 St, respectively. The *x*-axis represents the viewing angle at a specific observation point at the intersection—the decision point—and the *y*-axis represents the available visible distance at that particular observation point. The dashed line drawn across the plots in Figure 25, 26, and 27represent the minimum sight distance at each viewing angle required by the AASHTO guidelines.

At the intersection of 85 Ave & 100 St, Figure 25 shows that the sightline representing the driver's field of vision has its maximum distance at a viewing angle between -2° and 3°. The visual field angles towards the right of the plot are positive; those to the left are negative. When comparing the visual field distance and the minimum sight distance, it can be seen that the minimum distance required is met between viewing angles of -22° to -28°, and -18° to 17°; otherwise, the available sight distance is limited.

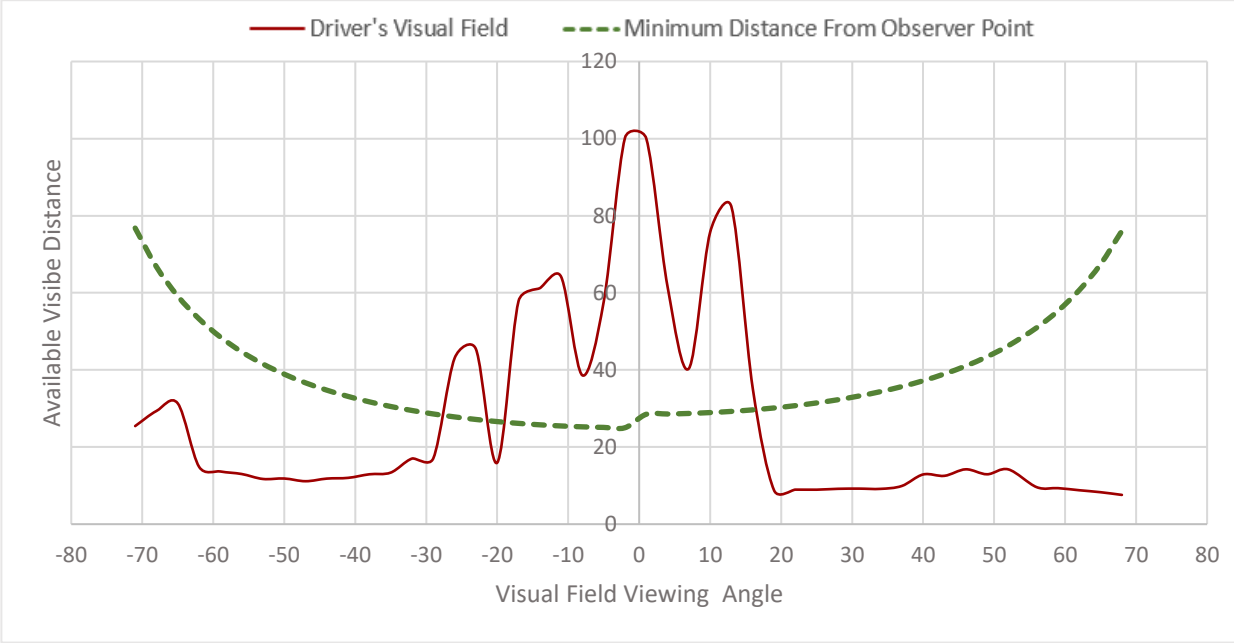

Figure 25 Available Visible Distance (Intersection 85 Ave and 100 St)

At the intersection of 85 Ave and 101 St, as shown in Figure 26, the driver's visual field distance is at its maximum between the viewing angles of -2° and 3°. The figure illustrates that the available visible distance was satisfied when comparing the visual field distance and minimum sight distance between viewing angles of -29° to -21°, -15° to 22°, and 46° to 50°; otherwise, the drivers' sightlines intersect with the road obstructions.

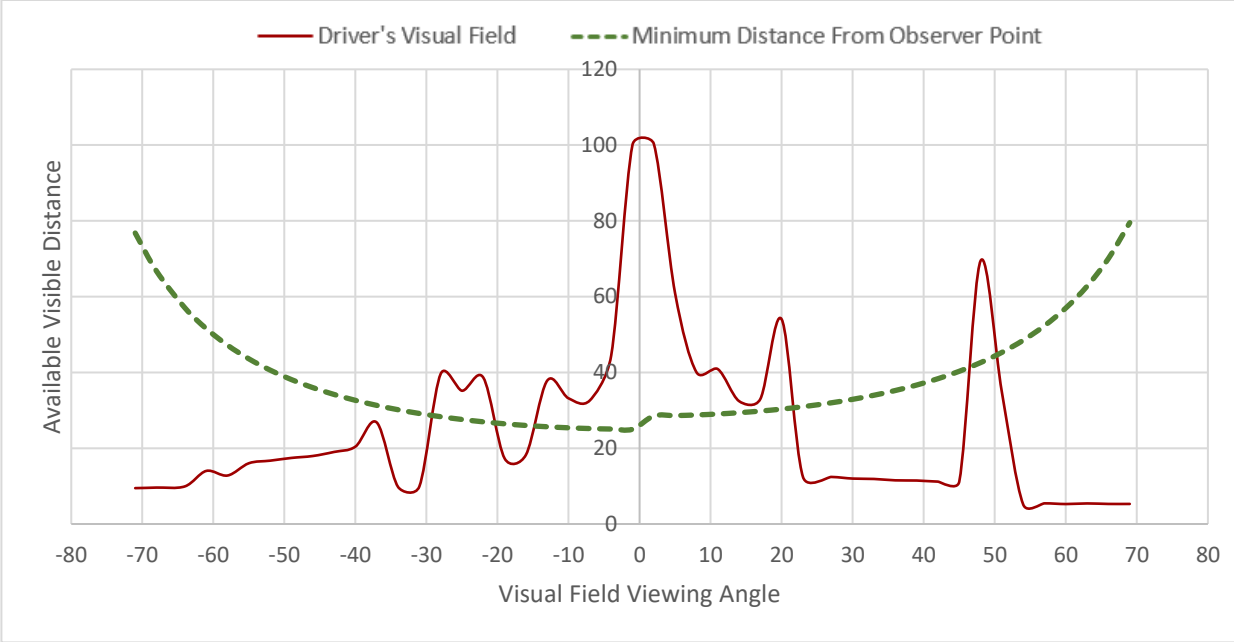

Figure 26 Available visible Distance (intersection 85 Ave & 101 St)

At the intersection of 84 Ave and 97 St, Figure 27 shows that the maximum sightline distance is achieved within the viewing angle range from 0° to 4°. When comparing the visual field distance and minimum sight distance, the plot clearly shows that the minimum distance required was met between viewing angles of -23° to -18°, -15° to 17°, 20° to 32° and 36° to 39°; otherwise, the available visible distance is limited.

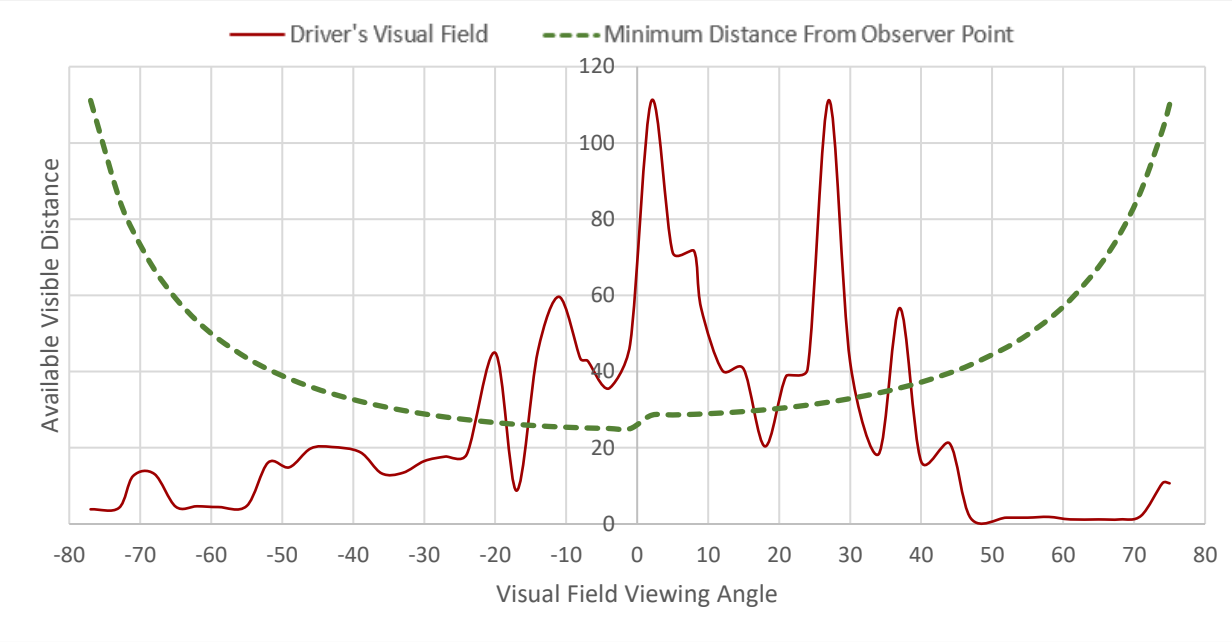

Figure 27 Available Visible distance (intersection 84 Ave & 97 St)

The plots show that the driver's visual field distance fluctuates across different viewing angles at the intersections. Although the plots exhibit similar trends, the variation in the visual field distance across viewing angles explains the difference in the intersection scene from the driver's perspective in a real-life situation. The visual field offset distance trend decreases significantly as the viewing angle increases and does not meet the minimum required sight distance, demonstrating the high blockage percentage in a yield-controlled intersection.

4.1.2 Stop Sign-Controlled Intersection

When approaching the stop-controlled intersection, the driver needs sufficient distance to stop, and observe a potential conflicting vehicle and then depart once any such vehicles are cleared. The main difference to the yield sign is that the driver must stop. The driver's eye location is relatively close to the intersection and requires a smaller sight triangle clear from obstruction.

As in the yield-controlled intersections, visibility analysis was conducted to calculate the blockage percentage within the sight triangle. It is assumed that the driver carries out a left turn maneuver but must stop to view the vehicle approaching the intersection. Nevertheless, the driver's decision point begins at some point between 4.4m and 5.4m from the major road's intersection edge, given the vehicle stop location behind the stop line and the distance of the driver's eye from the front of the vehicle. The vehicle type is again considered a passenger vehicle, which assumes the same

elevation level as previously. However, the gap time acceptance is 0.5 seconds less than for yield-controlled intersections, resulting in a shorter leg distance of the sight triangle as indicated in the AASHTO guide. Table 8 shows the intersection attributes for various stop-controlled intersections within the study area.

Table 8 Stop controlled sign intersections attributes

Sight Triangle				Short Leg (m)		Long Leg (m)
Intersection	Major Speed (km/h)	Minor Speed (km/h)	Approach	Left Triangle	Right Triangle	Left & Right Triangles
86 Ave & 101 St	30	30	West			63
84 Ave & 105 St	50	50	East	7.2	10.5	105
84 Ave & 106 St	50	50	East			105

The blockage percentage is determined at each intersection by a rapid simulation of real-life automotive situations. Table 9 shows the blockage percentage for both the left and right triangles at different intersections. The results show that the blockage percentage ranges from 6% to 56%, which is lower than for yield-controlled intersections. The reason is that the observer point is very close to the intersection, resulting in fewer obstacles as the driver can look directly at the major road to view oncoming vehicles.

Table 9 Blockage Percentage of stop sign intersections

Intersection Location	Approach Location	Posted Speed km/h		Blockage Percentage	
		Major Road	Minor Road	Left Triangle	Right Triangle
82 Ave & 96 St	North	50	50	30%	47%
82 Ave & 97 St	North	50	50	32%	32%
82 Ave & 98 St	North	50	50	18%	33%
82 Ave & 100 St	North	50	50	43%	56%
82 Ave & 106 St	North	50	50	18%	25%
82 Ave & 107 St	North	50	50	31%	35%
84 Ave & 99 St	East	50	50	24%	49%
84 Ave & 105 St	East	50	30	27%	40%
84 Ave & 106 St	East	50	30	13%	12%
86 Ave & 100 St	South	30	30	65%	53%
87 Ave & 98 St	South	50	50	46%	44%
87 Ave & 106 St	East	50	50	6%	12%
89 Ave & 99 St	West	50	50	39%	39%
90 Ave & 99 St	West	50	50	17%	12%
91 Ave & 99 St	East	50	50	42%	42%

Figure 28, 29, and 30 show the visual field generated from the decision point positions within the sight triangle area. As can be seen, some sightlines at viewing angles found no continuity; these

lines hit an obstacle. The area covered by red cast rays in the sight triangle is greater than for the yield sign, demonstrating a lower blockage rate. It should be noted that the distance for both sight triangle legs is smaller than for yield-controlled intersections because the observation point is close to the intersection, and the lower gap-acceptance time shortens the distance required at major roads, leading to a smaller area. These factors combine to result in a lower blockage rate at stop-controlled intersections.

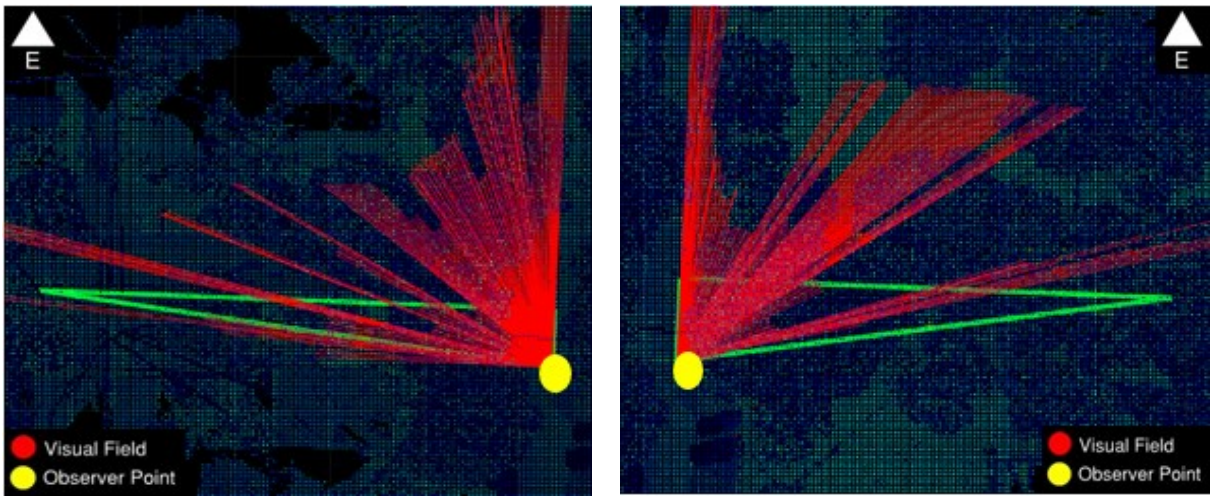

(a) 33% Blockage (b) 33% Blockage

Figure 28 Visibility Map (Intersection 86 Ave and 101 St)

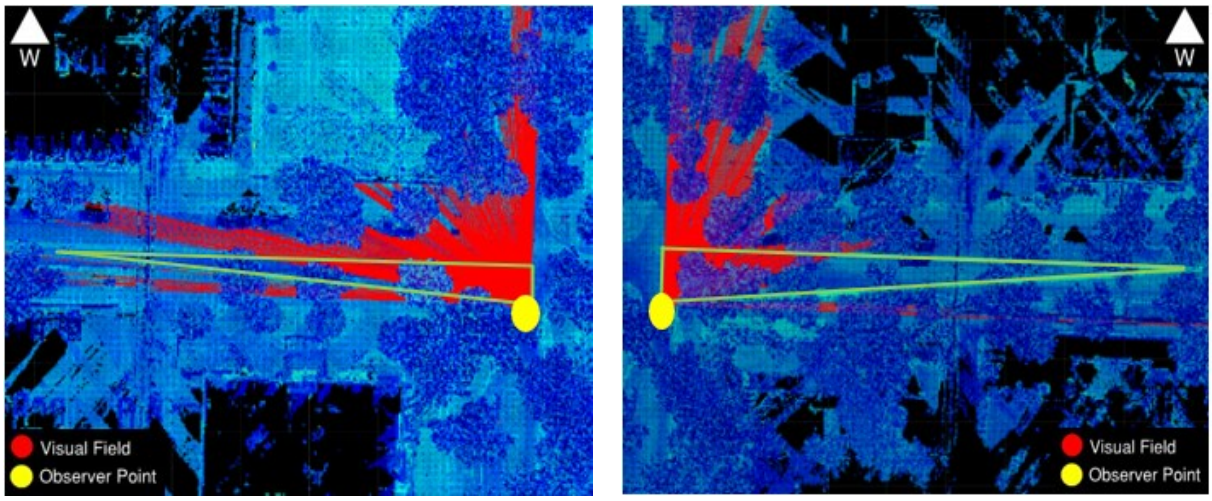

(a) 27% Blockage (b) 40% Blockage

Figure 29 Visibility Map (Intersection 84 Ave and 105 St)

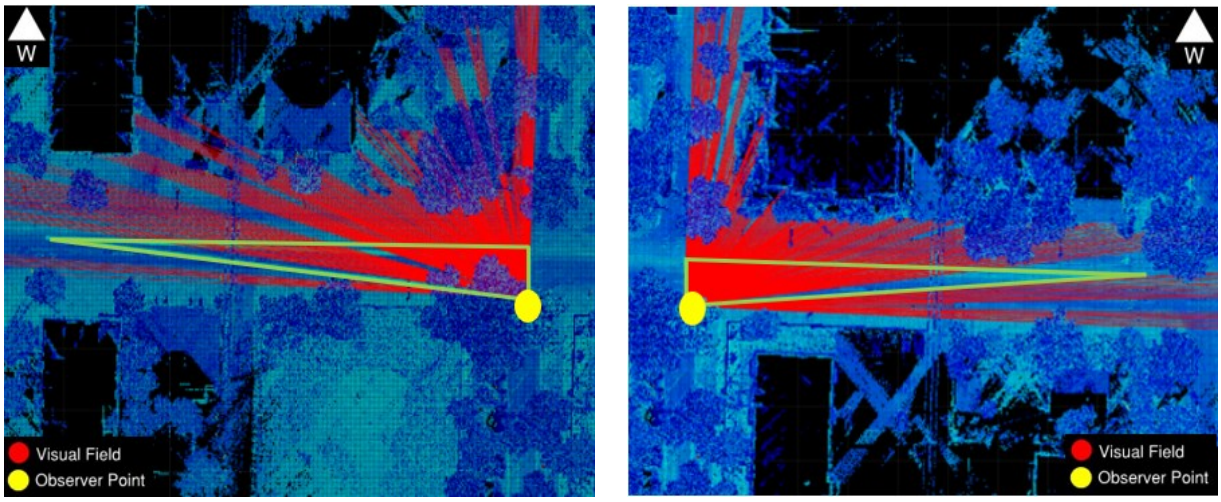

(a) 13% Blockage (b) 12% Blockage

Figure 30 Visibility Map (Intersection 84 Ave and 106 St)

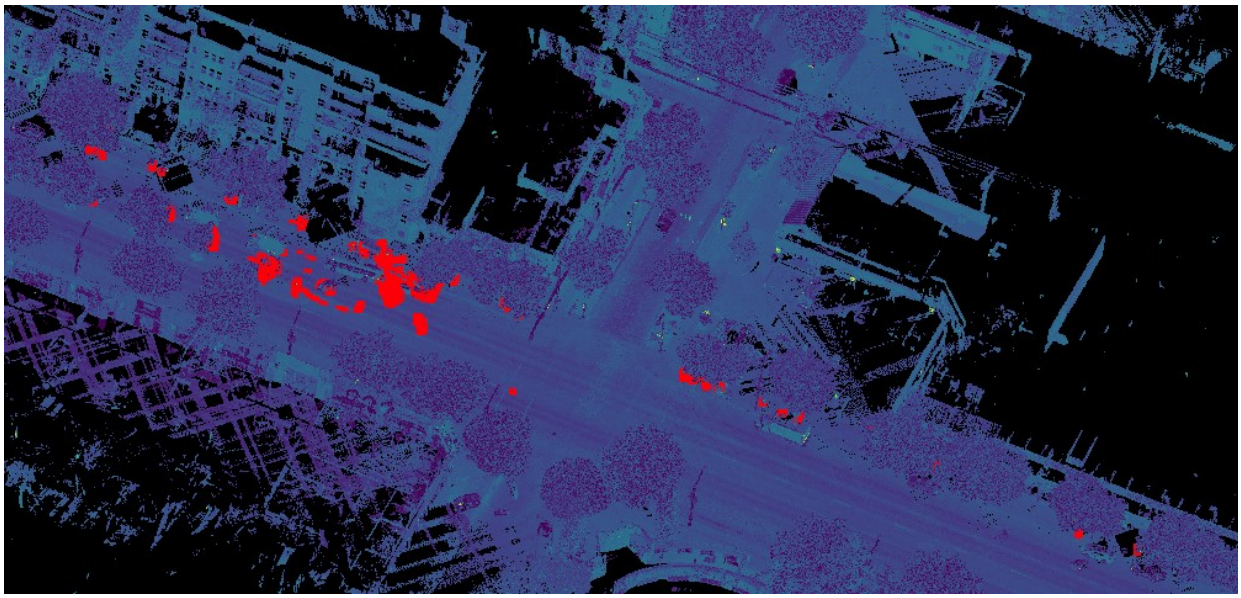

Figure 31 Obstructions in 3D Scene (Intersection 82 Ave and 107 St)

To find the location of the obstruction from the driver's perspective, viewing angles with limited available sight distance need to be identified. Figure 32, 33, and 34 show the estimated available visible distance at the intersections of 86 Ave and 101 St, 84 Ave and 105 St, and 84 Ave and 106 St, respectively. As clearly shown in the plots, the drivers' ability to view oncoming vehicles on a major road in order to carry out certain maneuvers is undoubtedly wider in stop-controlled intersections. The plots show that a large proportion of viewing angles met the minimum intersection sight-distance requirements.

At the intersection of 86 Ave and 101 St, Figure 32 shows that the driver's visual field extends further than the minimum required sight distance, with unobstructed vision found in the range from -79° to -76°, -65° to 60°, -53° to 58°, and 71° to 75°. In other words, the driver has adequate sight distance to observe conflicting vehicles at these viewing angles. The proportion where the sight distance is limited is less when compared to yield-controlled intersections, demonstrating a lower blockage rate.

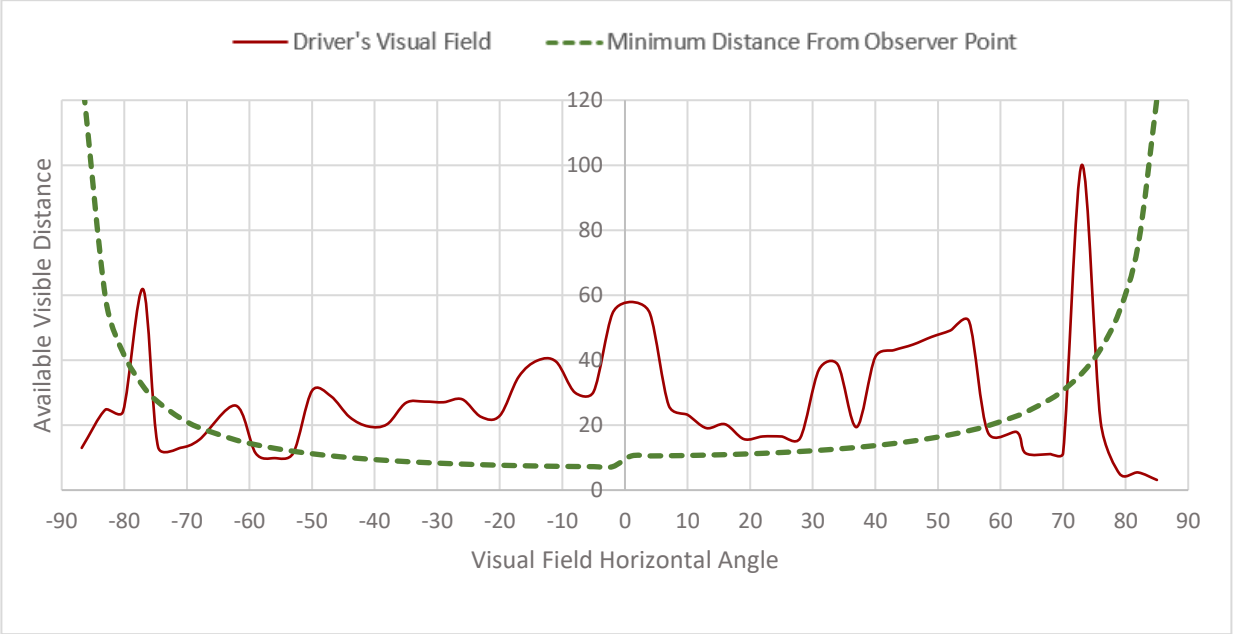

Figure 32 Available visible Distance (intersection 86 Ave and 101 St)

At the intersection of 84 Ave and 105 St, Figure 33 shows that the required intersection sight distance was satisfied at viewing angles from -81° to 73° when comparing the driver's visual field offset distance to the minimum sight distance required. At 84 Ave and 106 St, Figure 34 illustrates that the sightlines were satisfied between viewing angle from -79° to 73° and from 80° to 85°. The results demonstrate high levels of visibility at stop-controlled intersections, which explain the lower blockage percentage.

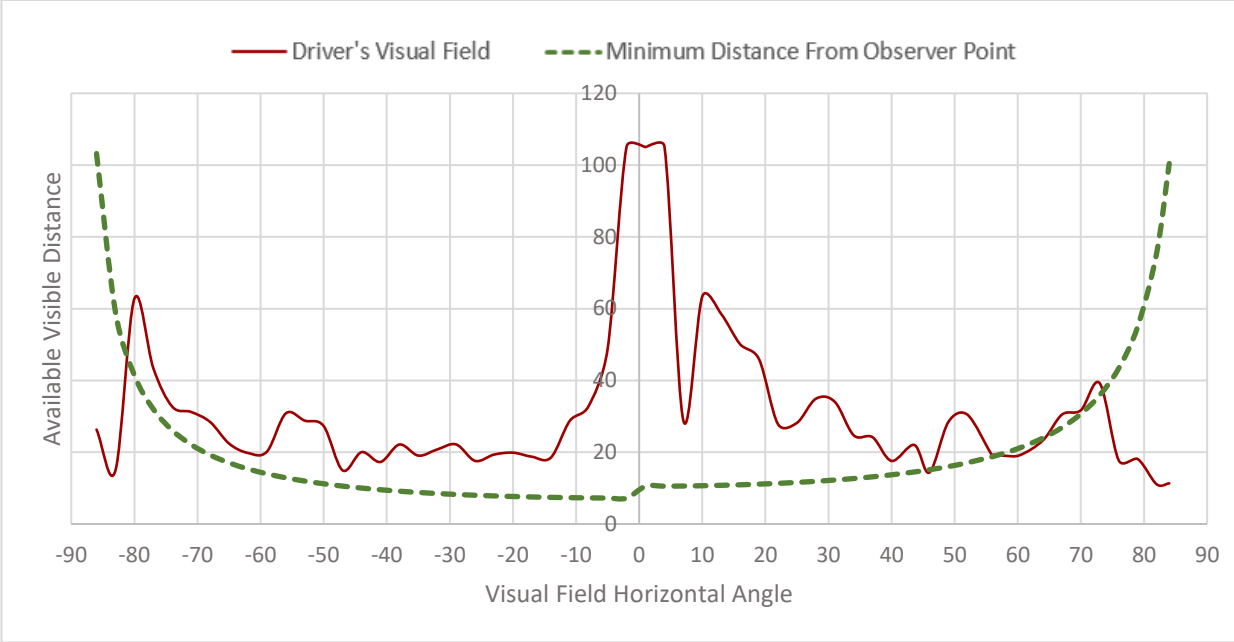

Figure 33 Available Visible Distance (Intersection 84 Ave & 105 St)

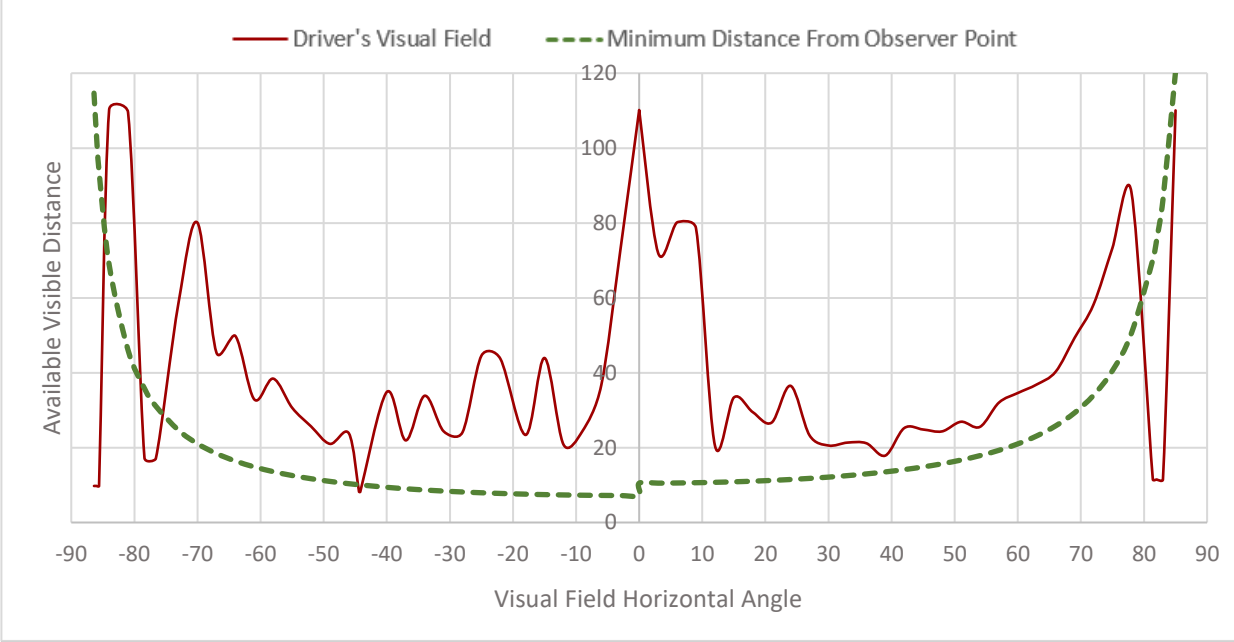

Figure 34 Available Visible Distance (Intersection 84 Ave and 106 St)

The method clearly shows the locations with poor visibility, quantified by the number of sightlines failing to meet the minimum required sight distance. This is a practical and rapid approach to quantifying obstructions and potential hazards that consistently restrict driver visibility from the driver's perspective.

In fact, the trend of the plots above illustrates the accuracy of the proposed method. For yield-controlled intersections, when the driver starts to observe conflicting vehicles on the major road, the results show that the driver can see ahead; however, as the viewing angle increases, the driver's ability to see decreases due to the presence of obstacles that block the driver's vision and thus yield a high blockage percentage. In contrast, stop-controlled intersections require the driver to stop close to the edge of the major road, giving the driver clear vision over a wide viewing angle. The contrast is illustrated in the plots that show poor visibility over wide viewing angles when the sightlines are further from the major road.

4.1.3 Impact of Transportation Mode on Visibility Analysis

In the previous sections, intersection sight distance assessments to evaluate visibility and estimate blockage percentages were based on a passenger vehicle with a lower observer height than a heavy truck. In order to assess the impact of intersection visibility on heavy truck drivers and determine the blockage percentage, visibility analyses were conducted using the same observer point locations. The principal differences compared to a passenger vehicle are the height of the observer and the time gap acceptance, which is two seconds longer for a truck. When moving onto a roadway, a truck always has a lower speed than a passenger vehicle and needs more time to enter the major road and carry out certain maneuvers. Since the long leg distance of the sight distance triangle is determined by the speed posted on the major roadway and the time gap acceptance, the sight triangle clear from obstruction required by a truck is larger than that required by a passenger vehicle.

Table 10 shows samples of intersection and sight triangle attributes for both yields- and stop-controlled intersections from the observer height of a heavy truck. When comparing the area of the sight triangles and the intersection sight distance in Table 10 with Table 6 and Table 8, it can be noticed that for passenger vehicles, when the intersection is yield controlled sign intersection, the long leg of the sight triangle is 67 meters; however, it is 84 meters for trucks. The same applies to the stop-controlled sign intersection which the distance for passenger vehicle and truck is 105m and 139m, respectively. This demonstrates the change in the sight triangle area using a different mode of transportation, which each has a different observer height.

Table 10 Intersection and Sight Triangle Attributes

Intersection	Sight Triangle				Short Leg (m)		Long Leg (m)
	Major Speed (km/h)	Minor Speed (km/h)	Sign	Approach	Left Triangle	Right Triangle	Left & Right Triangles
85 Ave & 101	30	30	Yield	East	25	28.5	84
84 Ave & 105	50	50	Stop	East	7.2	10.5	139

When a heavy truck approaches a yield-controlled intersection, the visibility map in Figure 35 shows that the blockage percentages for the left and right sight triangles are 70% and 77%, respectively. However, for a passenger vehicle, the equivalent figures were found to be 67% and 65%, respectively. Thus, drivers of heavy trucks approaching yield-controlled intersections in an urban environment experience slightly more blockage than passenger vehicles due to the increased impact of vegetation, cantilever tree branches, and other road features blocking sightlines.

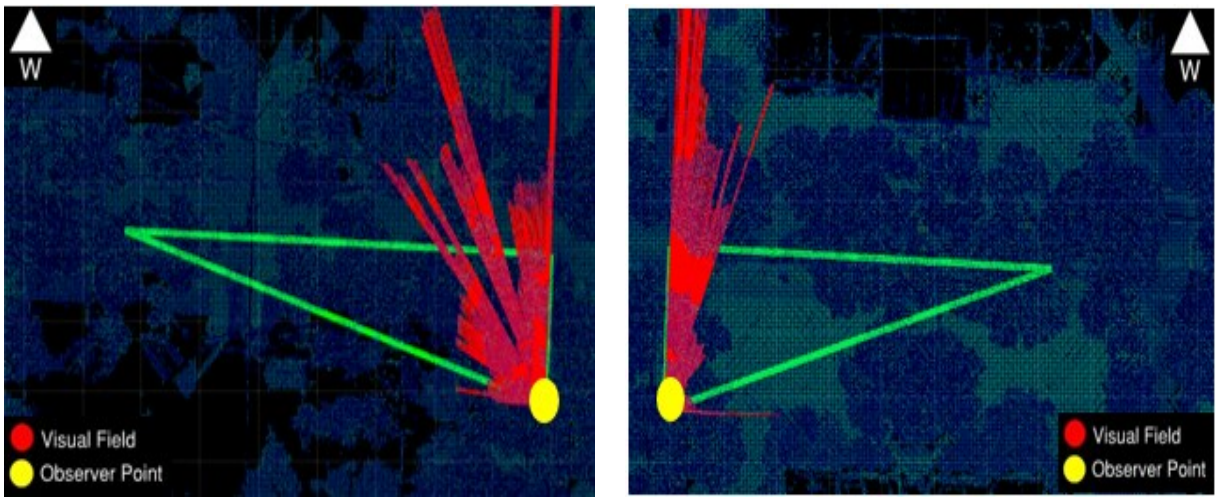

(a) 70% blockage (b) 77% blockage

Figure 35 Visibility Map (Intersection 85 Ave and 101 St)

In contrast, at stop-controlled intersections, where heavy trucks are required to stop before departing, Figure 36 shows that the sightlines cover a large proportion of the sight triangle, with blockage percentages for the left and right sight triangles only 20% and 26%, respectively. In this case, the heavy truck has more available visible distance than the passenger car because the driver of the truck at the intersection has higher sightlines, allowing them a clearer view of the scene and enabling them to see oncoming vehicles on the major road.

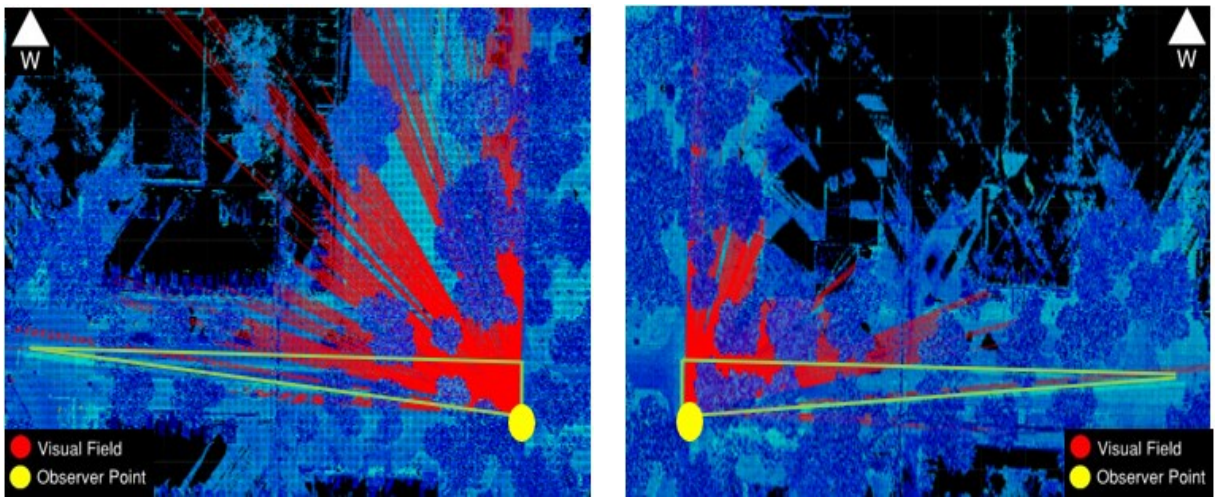

(a) 20% Blockage (b) 26% Blockage

Figure 36 Visibility Map (Intersection 84 Ave and 105 St)

This section conducted intersection sight distance assessments to consider the impact of observer height on visibility. The findings show that this factor contributes to variation in the block percentage. When the intersection is yield-controlled, more attention should be given to heavy trucks; however, the focus should be on passenger vehicles at stop-controlled intersections when assessing potential improvements to address visibility problems in an intersection's safety performance.

4.2 Impacts of Voxel Size on the Extraction Results

It is vital to study the impact of voxel size in the information extracted from the visibility analysis and intersection sight distance assessment. Therefore, the algorithm was used to determine the offset distance in the simulated driver's visual field at different voxel sizes. Voxel size is a sensitive parameter and an essential step of the algorithm that may influence the calculation of blockage percentages since different voxel sizes result in different visual field distances and therefore impact the quality of the information derived from the visibility assessments. As an illustration, the yield- and stop-controlled intersections at 85 Ave and 101 St, and 84 Ave and 105 St respectively were analyzed at different voxel sizes to demonstrate the impact of voxel size on the assessment. The plots in Figure 37, 38, 39, and 40 show the distance that the driver can see at various viewing angles and considering different voxel sizes. The plots show that each intersection, irrespective of voxel size, shows similar trends and exhibits only a slight variation in offset distance.

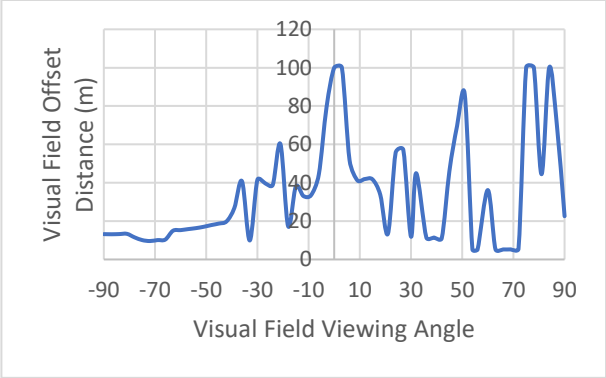

(a) 0.1 m Voxel Size

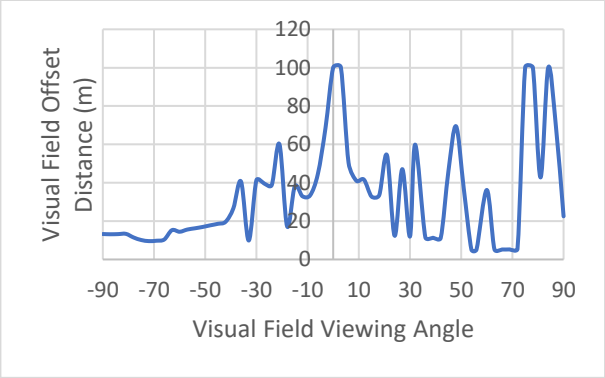

(b) 0.15 m Voxel Size

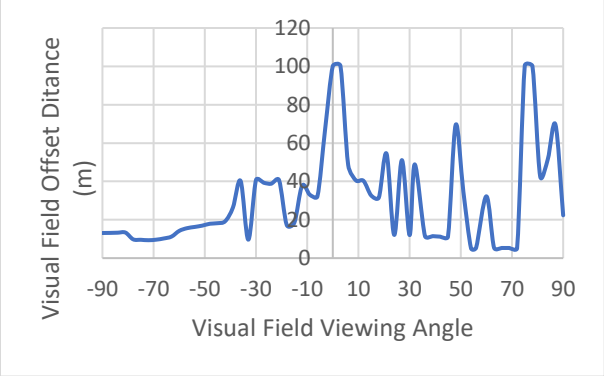

(c) 0.20 m Voxel Size

Figure 37 Available Visible Distance Estimated at Different Voxel Size (Intersection 85 Ave and 101 St)

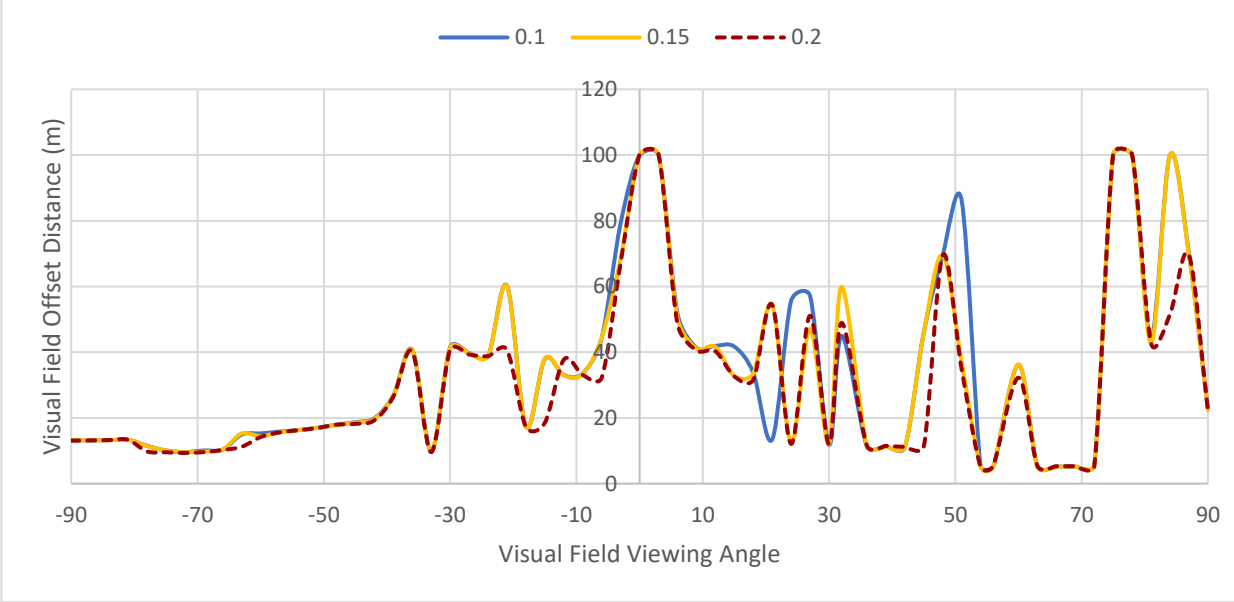

Figure 38 Available Visible Distance Multi-voxel size (Intersection 85 Ave and 101 St)

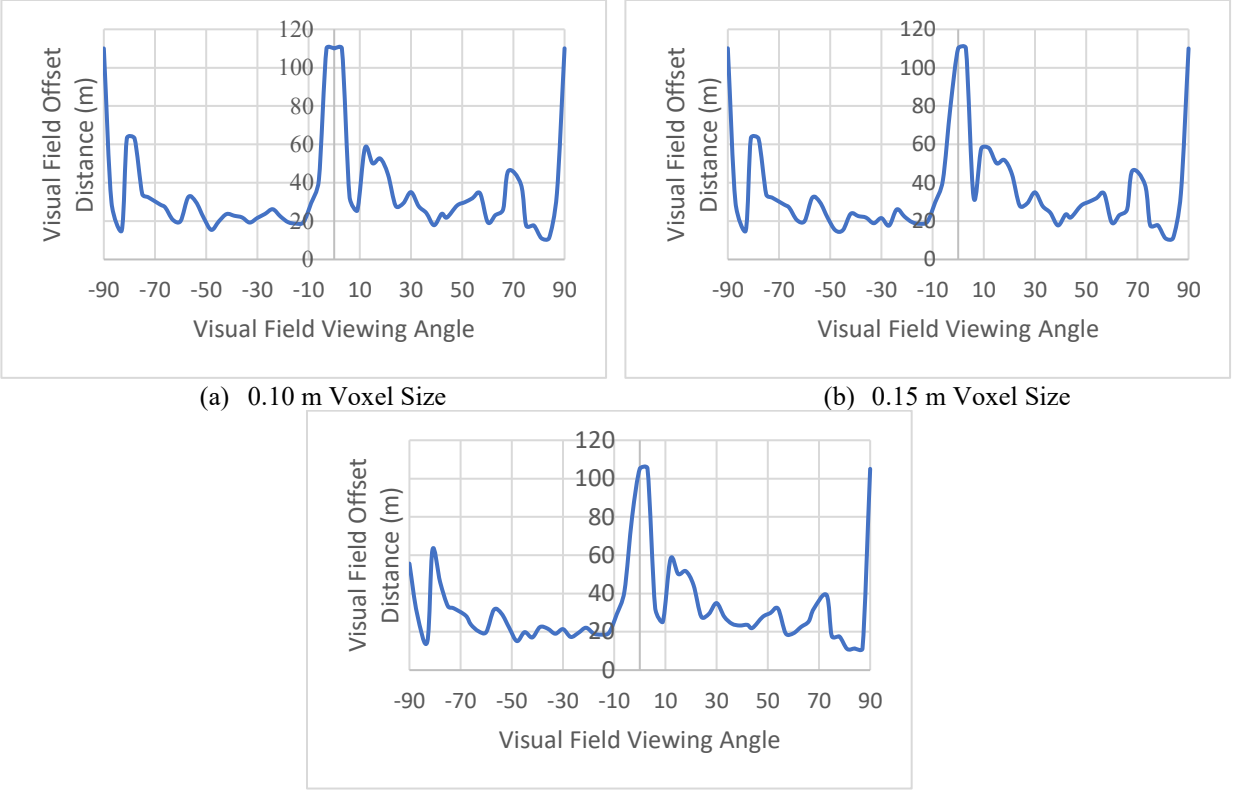

(a) 0.10 m Voxel Size

(b) 0.15 m Voxel Size

(c) 0.20 m Voxel Size

Figure 39 Available Visible Distance Estimated at Different Voxel Size (Intersection 84 Ave and 105 St)

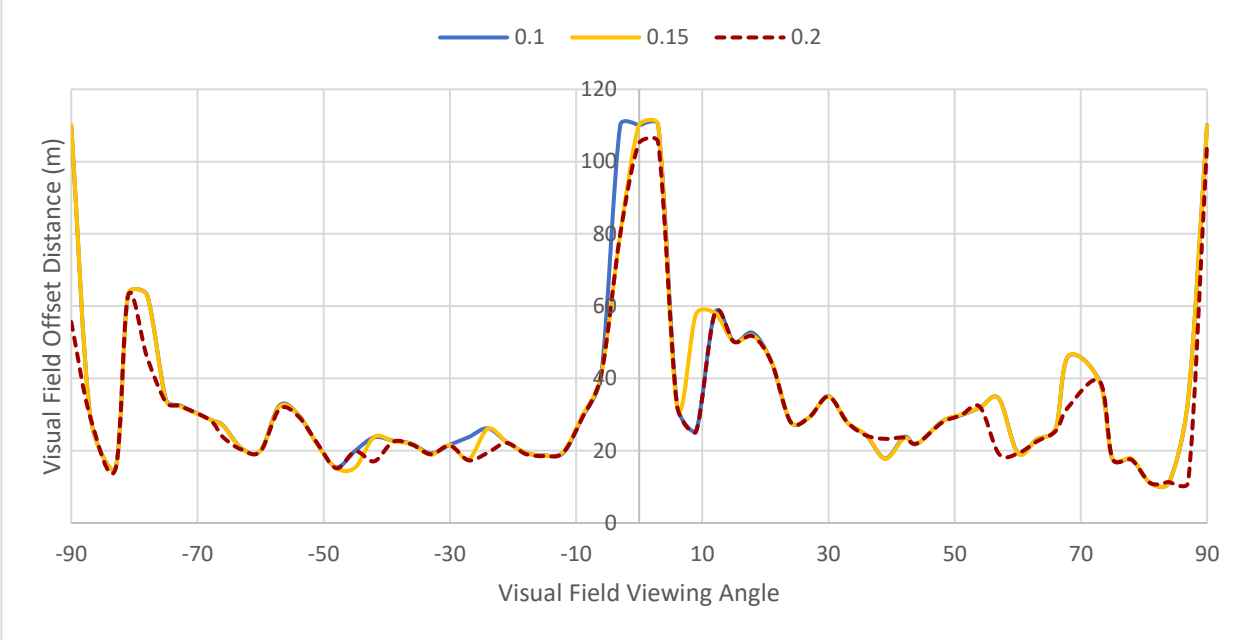

Figure 40 Available Visible Distance Multi-voxel size (Intersection 84 Ave and 105 St)

Although the plots show the estimated sightline distances at different voxel sizes to be very similar, this variation in distance needs to be quantified. To understand the impact of voxel size and address

these variations in the visibility assessment, the difference in each sightline of the visual field at a defined observer point with a different viewing angle was compared to the estimated sightlines at a voxel size of 0.2m. A 0.2m size was chosen because the blockage percentage was estimated using this specific voxel size in the visibility assessment. The plots in Figure 41 for both intersections show the average difference in sightline distance, measured in meters, at different voxel sizes.

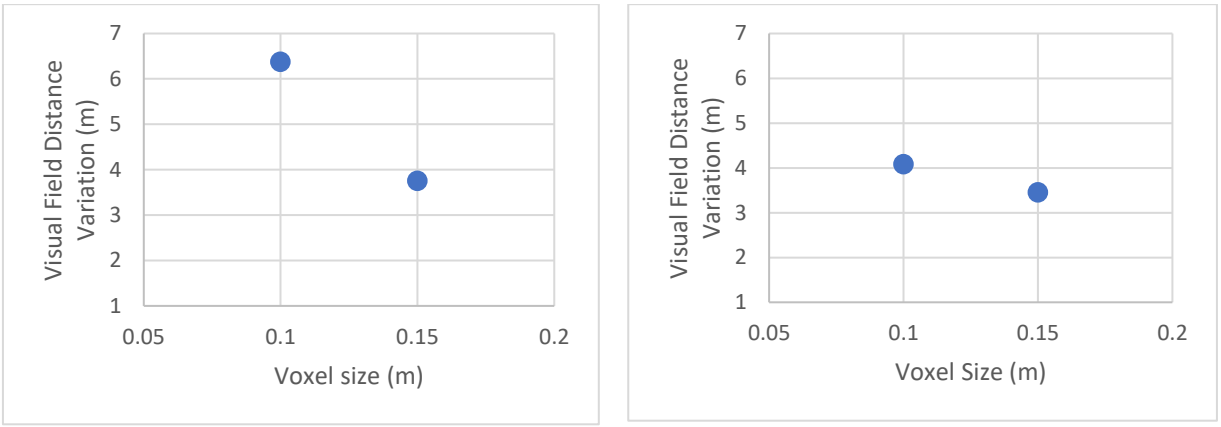

Intersection 85 Ave and 101 St

Intersection 84 Ave and 105 St

Figure 41 Average Difference in Estimated Visual Field Distance Compared to 20 cm voxel size

The variation in the estimated distances demonstrates that reducing the voxel size results in a slight increase in visual field offset distance and provides a greater field of view. The increase varies depending on the voxel size used in the analysis; however, the estimated average increase ranges from 3.75m to 6.38m for 85 Ave and 101 St and from 3.45m to 4.09m for 84 Ave and 105 St. Moreover, the plots show a boost when voxel size decreases, which is a highly intuitive outcome and correlates with expectation. To explain, reducing the voxel size from 0.2m to 0.1m results in eight times as many voxels. Thus, when the size of the voxel is 0.2m, and it contains one point cloud, this voxel is occupied and represents a road obstacle, and when the sightline hits this voxel, it stops traveling to explore other voxels. A reduced voxel size of 0.1m results in eight voxels of 0.1m, equivalent to one voxel of 0.2m in size. In the same situation, one voxel out of eight will be occupied, while the others will be visible to sightlines to explore the voxel that represents the obstruction.

One of the reasons for the minimal impact of voxel size on the intersection visibility analysis is the fact that sightlines are associated with voxels and not point clouds. Irrespective of voxel size, the proposed algorithm functions by extracting the obstacle objects represented in space as voxel

grids. The voxel contains several point clouds, and one point is sufficient to make a voxel represent an obstruction. In other words, as long as the voxel is occupied, regardless of the number of point clouds it contains, it is sufficient to stop the sightlines from exploring other voxels. Thus, the impact of voxel size may not be significant. The results illustrate that the impact of voxel size in the application of the intersection sight distance was less pronounced when the voxel size ranged from 0.1m to 0.2m.

In fact, the impact of the change of voxel size on the performance of the intersection assessment tool was minimal. Other transportation applications, however, may be highly sensitive to voxel size, which may impact the accuracy of the information extracted. The outcome of this sensitivity analysis demonstrates that the use of a finer voxel size is not always necessary. In other words, the research shows that the algorithm for the extraction of obstacles within intersection sight distance remains effective when using slightly larger voxels with no significant effect on the quality of the information obtained. The use of a smaller voxel size would significantly increase the processing time for extraction, especially when working with the high point density of MLS, which may be costly, as explained in the previous section 3.4.4. In this case study, the density of the point cloud is used to assess intersection visibility and estimate the blockage percentage ranges from 43.6 million to 76.4 million. The observations in this section are valuable for any municipalities or transportation agencies with budgetary limitations that require high-performance machines and equipment to process large amounts of complex data.

4.3 Dynamic Visual Field and Driving Speed

This section investigates the impact of driving speed on the driver's field of vision when approaching an intersection. It also studies the area covered by the driver field of vision within the sight triangle from various observer points to assess the sight triangle's visibility. The analysis tests the visibility for a driving vehicle at an intersection by generating a visual field from the decision point to the turning point close to the intersection edge where the driver completes a certain maneuver. For example, the intersection of 84 Ave and 106 St is yield-controlled and has been assessed to evaluate the driver's visual field at different observer points. The first point was the decision point recommended by AASHTO, 25m from the center of the major road for a vehicle approaching from the left. The speed at that point was 50km/h, assumed from the posted speed on the intersecting road when the driver starts to break. The second observer point was 10m from the

decision point toward the intersection. Given a deceleration rate of 3.73 m/s^2, the speed at the second point was assumed to be 40 km/h. The third and fourth observer points were at distances of 16.5 and 21.5m from the decision point and had driving speeds of 30 and 20km/h, respectively. As the speed and the observer point locations are available, the visual field viewing angle can be determined to perform the visibility analysis. Figure 42 shows the visual field at various observer points, each with a different viewing angle according to the vehicle speed; these decreases when approaching an intersection to check for conflicting vehicles.

As seen from Figure 42, the distance along the long leg of the sight triangle depends on the design speed of the major intersection and the gap time acceptance, both of which are constant. Therefore, the distance along the major road is constant at all observer points; however, the short leg varies depending on where the observer point is located. Thus, as the vehicle approaches the intersection, the sight triangle area becomes smaller, allowing the driver to view the area clearly. The analysis shows that the driver has a wider field of view when approaching the intersection. When the vehicle decelerates, the driver can observe more visual information and provide sufficient time for the driver to react. In other words, when the driver approaches the intersection, the opportunity to spot vehicles in the major road increases as the sight triangle decreases. As a result, a vehicle approaching the intersection has greater peripheral vision close to the intersection, increasing the probability of spotting oncoming vehicles on the major road.

The assessment has considered a viewing angle of 180° in the previous sections, utilizing the driver's full peripherical vision. However, in this section, the impact of speed on the visual field is considered in order to account for the human visual limitations. When the driver is at the decision point, the short leg distance is considerable. As shown in Figure 42 (d), at a vehicle speed of 50 km/h, a large proportion of the sight triangle area is not covered when simulating the visual field. This means that the driver may not be able to spot the coming vehicle on the major road—even if there is no obstruction exists—as the viewing angle is limited to 90°.

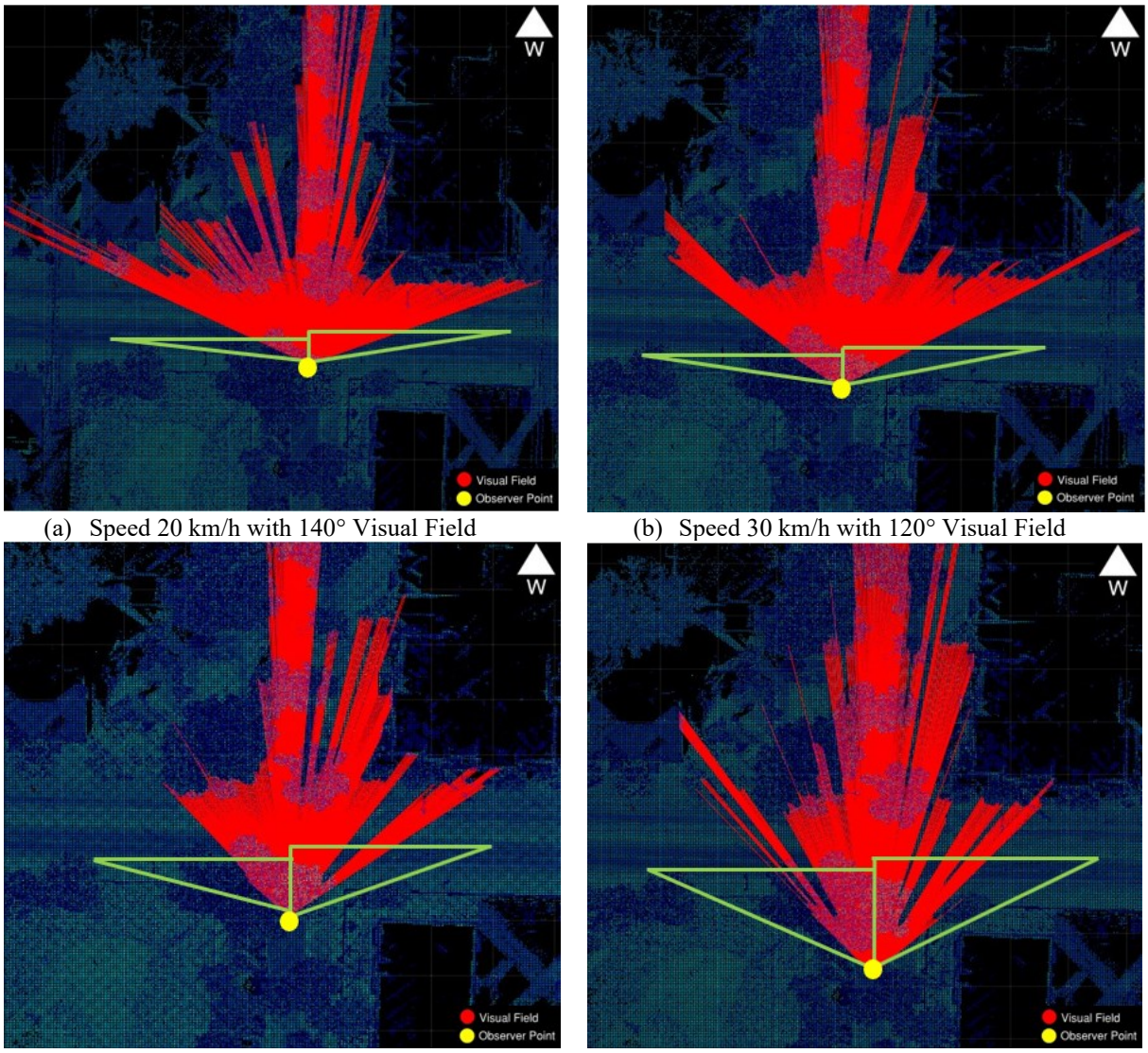

(a) Speed 20 km/h with 140° Visual Field (b) Speed 30 km/h with 120° Visual Field

(c) Speed 40 km/h with 100° Visual Field (d) Speed 50 km/h with 90° Visual Field

Figure 42 Visual Field for Different Speed

While the vehicle is moving, the driver has limited ability to process visual information and react. Speed is inversely proportional to the driver's visual field at intersecting roads. However, the AASHTO recommended distance that determines the sight triangle area is primarily dependent on the speed on the major road, which has no relation to the design speed at the intersecting road and does not take into consideration the impact of speed on the driver's peripheral vision, and instead it solely focused on the deceleration rate and time gap acceptance to enter the intersection. This leads to a visibility problem that impacts intersection safety and demonstrates the importance of accounting for human visual limitations, one of the Vision Zero principles for achieving safe mobility.

To sum up, the sight triangle area defined by the AASHTO guide is very conservative and could also be costly and challenging to maintain in an urban environment. Even if this area is maintained, it may not significantly improve intersection visibility in urban areas due to human visual limitations. Optimizing sight distance design at the intersection by studying the impact of operating speed is essential in enhancing road safety and improving intersection visibility.

4.4 Safety-Based Assessment

4.4.1 Method of Sample Moments

The method of sample moments has been used to identify those intersections with an overrepresentation of collisions that occurred due to poor visibility. An intersection is considered to have an overrepresentation of a particular collision pattern if the probability that its pattern ratio significantly exceeds the reference group average. The method was used and applied at intersections in urban areas using collision data from 2009 to 2019. The collisions caused by visibility problems were identified as a collision pattern. The collision pattern was considered as a violation of stop and yield signs. The expected mean was then computed to rank the intersections, with intersections with a high expected mean value requiring urgent attention for safety improvements. Adopting a 0.05 significance level, beta distribution was used to identify collision-prone sites.

When specific collision patterns are overrepresented, there is a high probability that the pattern will be investigated if a collision occurs. Thus, the overrepresentation assessment method can be represented by a higher than usual rate of occurrence of a specific pattern compared to the number of collisions. Table 11 shows a list of intersections ranked according to the expected mean where "YES" in the collision-prone intersection column indicates an intersection with an overrepresentation of collision pattern, together with the blockage rate for each intersection resulting from the visibility assessment.

Table 11 Collision Analysis Result

Intersection Name	Blockage Rate	Expected Mean	Collision Prone Intersection
87 Ave & 105 St	1.24	0.94	YES
85 Ave & 107 St	1.46	0.94	YES
86 Ave & 100 St	1.19	0.90	YES
87 Ave & 100 St	1.44	0.90	YES
86 Ave & 98 St	1.66	0.87	YES
84 Ave & 97 St	1.38	0.79	YES
84 Ave & 107 St	1.31	0.79	YES
89 Ave 98 St	1.28	0.79	NO
85 Ave & 100 St	1.34	0.71	NO
84 Ave & 101 St	1.44	0.69	NO
85 Ave & 101 St	1.32	0.62	NO
87 Ave & 98 St	0.91	0.62	NO
87 Ave & 106 St	0.18	0.51	NO
84 Ave & 100 St	1.48	0.41	NO
84 Ave & 106 St	0.25	0.41	NO
84 Ave & 105 St	0.67	0.37	NO
82 Ave & 107 St	0.67	0.30	NO
82 Ave & 98 St	0.51	0.23	NO
82 Ave & 106 St	0.43	0.23	NO
91 Ave & 99 St	0.85	0.22	NO
82 Ave & 97 St	0.64	0.21	NO
82 Ave & 96 St	0.78	0.21	NO
90 Ave & 99 St	0.30	0.19	NO
84 Ave & 99 St	0.73	0.16	NO
89 Ave & 99 St	0.78	0.09	NO
82 Ave & 100 St	0.99	0.08	NO

As shown in Table 11, seven of the 26 intersections were found to be hazardous intersections and were considered collision prone. In other words, 27% of intersections exhibited an overrepresentation of collisions caused by visibility problems. The collision analysis shows that, when the intersections are ranked according to the EB mean, the five top-ranked intersections were found to be collision-prone. It should be noted that the intersections considered hazardous experience over 80% of visibility-related collisions. The analysis also found that all collision-prone intersections were controlled by yield signs. As indicated in the previous section, they exhibit high blockage percentages due to limited available sight distance. This means that locations with restricted sightlines due to road features and objects at intersections were at increased risk of collisions.

The principal advantage of using the empirical Bayes in the identification process is to account for bias at locations with a low collision frequency. The collision frequency for a particular intersection is inversely proportional to the variance of the estimated ratio of the collision pattern to the total number of collisions [52]. In other words, locations with a low collision frequency will have high RTM bias. For instance, the intersection of 85 Ave and 100 St has a total of eight collisions, six of which (i.e., a ratio of 0.75) were caused by visibility issues. This may very likely be due to chance alone and does not mean that the location should be considered collision prone. In other words, a location with a low number of collisions of which a high proportion falls into one collision pattern is not necessarily a collision-prone intersection.

4.4.2 Beta-Binomial (BB) Regression Model

This method examines the collision record and visibility problems through regression modeling and aims to study the relationship between the proportion of collisions falling within the visibility issue collision pattern and the blockage percentage. Since the study focused on investigating specific collision patterns, BB distribution was proposed to develop a collision model to link the collision proportion and blockage percentage.

In the first step, the collision proportion was calculated for each intersection, according to the given data, and set as a dependent variable (CP). Since the study investigates the impact of poor visibility, this blockage rate was regarded as the independent variable (B). The computational software program SAS was used to develop a collision model [114]. The BB model coefficients were computed using a finite mixture of univariate distributions in SAS: "The FMM Procedure".

Referring to the model output as shown in Table 12 and Table 13, coefficient B was statistically significant since the P_r value is lower than the 0.05 significance level, reflecting a 95% confidence level. For the goodness of fit model assessment, Maximum Log-Likelihood Estimation (MLE) was used. Pearson's chi-squared measure, shown in the model as the "Pearson Statistic" must be compared with the tabulated chi-squared distribution. Since one coefficient is considered in the model and has 26 site observations, the degree of freedom (DF) is equal to 25. Therefore, the tabulated chi-squared distribution value is equal to 14.611, which is greater than the Pearson Statistics output of the regression model. Thus, the model regression coefficients and the goodness of fit are found to be statistically significant.

Table 12 Parameter estimates for BB Model

Effect	Estimate	Standard Error	z-value	$P_r>\|z\|$
Intercept	-2.5822	1.2487	-2.07	0.0387
B	2.398	1.123	2.14	0.0327

Table 13 Goodness of fit estimation value

Fit statistics	-2 log-likelihood	Pearson Statistics
Value	23.5001	8.0387

The results of the BB model indicate that the collision proportion of the visibility issue collision pattern increases as the blockage rate increases. As a result, the safety assessment finds that locations with restricted sightlines due to road obstacles at intersections were at increased risk of collisions; thus, limited available visible distance contributed to collision occurrences. Therefore, identifying a design deficiency—such as limited sight distance at an intersection—and linking it with the collision record to generate a function that explains the relationship with collision occurrence would significantly encourage traffic safety professionals to choose cost-effective countermeasure to improve visibility at such intersections.

5 CONCLUSIONS

5.1 Summary

In this thesis, 3D LiDAR technology was used in the analysis of an intersection sight distance application to address visibility issues at yield- and stop-controlled intersections. Sight distance is an essential design element in intersection infrastructure and is critical for safe urban mobility. The first part of the thesis proposed a method to develop a novel, fully automated algorithm to facilitate visibility assessment by extracting the vehicle trajectory and simplifying the data into voxels representing the real-life environment. The algorithm's flexibility allows the user to consider various factors, including transportation mode, speed, different viewing angles, the traffic sign controlling the intersecting roadway, and the speed on the major roadway. In field-based assessments, the results may be overestimated and do not accurately represent the actual situation.

The use of LiDAR in this new method provides information with a high level of accuracy on a broad scale. It computes the blockage percentage at each intersection from each viewpoint according to pre-defined parameters inputted by the user. The calculation is based on identifying the location of obstacles that block the simulated drivers' visual field. This analytical approach will significantly assist transportation agencies in optimizing this design element and will improve intersection visibility by enhancing drivers' field of vision. It also provides information about intersection infrastructure on an unprecedented scale for potential improvement and maintenance purposes.

The sensitivity of the impact of voxel size has not previously been investigated in LiDAR transportation applications. Previous studies have selected the voxel size according to the LiDAR scanning characteristics, but the size may not be ideal for conducting the analysis in that particular application and, thus, produces an error in estimating the available sight distance. In this thesis, the impact of different voxel sizes was investigated, and the findings show that this is minimal on the visibility assessment of the intersection. This dramatically helps transportation agencies with a limited budget to conduct analyses using LiDAR, as a high-performance computer processer is not, therefore, needed. However, the voxel size may be sensitive in other transportation applications and significantly impact the assessment's output.

The impact of speed on the driver's visual field is significant in the intersection sight distance assessment. Driving at low speed when approaching an intersection provides sufficient time for the driver to analyze the visual information received and react accordingly to complete certain maneuvers safely. However, when driving at a higher speed, the visual field viewing angle is reduced and cannot cover the sight triangle that should be clear from obstruction. It is likely that the driver is unable to see conflicting vehicles and, thus, collisions are more likely to occur. This applies particularly to yield-controlled intersections where the driver is not necessarily required to stop. Thus, the intersection sight distance design should be maintained to account for human visual limitations and the capability to drive safely.

The second part of this thesis focused on conducting a statistical analysis to study the relationship between collision occurrence and limited available sight distance at intersections. Bayesian analysis was used to quantify the safety impacts of the intersection associated with poor visibility to enhance road safety. The first stage of the analysis used the method of sample moments to find collision-prone intersections with an overrepresentation of collisions with poor visibility. Then, a collision model was developed using BB distribution to find the relationship links between the collision proportion due to limited intersection visibility and blockage percentage. The outcome shows that intersections with restricted sight distance due to road obstacles at intersections had an increased risk of collisions. This information will significantly help in prioritizing intersections for potential treatment. There is, however, a lack of research linking the results of the method proposed using LiDAR-based analysis to identify inadequate sight distance with the occurrence of collisions, and such research is essential in assessing this relationship to rank hazardous sites and select cost-effective countermeasures.

5.2 Research Contributions

As already highlighted in previous sections, the method proposed in this thesis would significantly help transportation and safety professionals to conduct intersection sight distance assessments and visibility analyses in the urban infrastructure efficiently, without the burden of manual techniques. Traditional processes are tedious and require a substantial on-site resource to carry out field surveying work, including equipment and tools that may affect the traffic operation and lead to unsafe situations that impact the road user.

The new method applies MLS in the area of interest and acquires the collision records to perform the analysis. The technique efficiency supports agencies in the transportation field to assess intersection sight distance design elements and identify hazardous intersections where visibility should be optimized. It also provides high-quality information about the intersection characteristics and the location of obstacles. Having such information on a large scale helps assets and maintenance management teams adopt policies and make decisions to improve road safety by improving the field of vision at urban intersections, significantly and cost-effectively decreasing the occurrence of collisions.

The research also provides insights into voxel size sensitivity and its impact on the quality of information. Voxel size is a sensitive parameter, especially when working with the high point density of MLS. Selecting the ideal voxel size is critical in obtaining accurate extraction information. To address this, a sensitivity analysis was conducted using various voxel sizes. While voxel size does not significantly impact the result of this sight distance application, it may be very sensitive in other transportation applications to extract different geometric road features. These findings help agencies with a limited budget to work with this kind of dataset without the need to invest in a powerful computing server.

The research also demonstrates the importance of driving speed and its impact on the driver's visualization of information. It is vital to investigate the driving behavior of road users and the human capabilities that impact the driver's vision. This will help agencies evaluate road performance by optimizing intersections and accounting for human limitations by setting a consistent plan and building a sustainable road infrastructure aimed at safe mobility. A further potential strategy could be reducing the speed at collision-prone intersections to increase the driver's peripheral vision. It is believed that the dynamic visual field for drivers approaching intersections has never previously been assessed, one of the emerging topics that make this research appealing.

5.3 Limitations and Future Work

This research can be expanded in many ways to improve safe urban mobility through, for example, accounting for more complex situations by improving the accuracy of the algorithm developed and considering additional human factors and their impact on the driver's visual field and viewing angle.

In this research, the intersection sight distance assessment and visibility analysis were conducted at at-grade intersections. Although the proposed method accounts for pavement surface-level variation, additional challenges may arise when the intersection is located at separated grades or when the driver approaches the intersection at near-horizontal alignment. In this case, identifying the elevation of the analysis may require additional vehicle trajectory calculations as each observer point has different levels, and the number of target offset must be carefully selected to simulate the real environment and situation.

MLS has a significantly high point cloud density. The voxelization process adopted to discretize the point cloud and generate ray-casting lines representing the high-resolution visual field is extremely expensive due to the computational time required, especially when the application requires a high resolution. Moreover, the selection of an inappropriate voxel size leads to minor inaccuracies in detecting obstacles, especially when combined with the ray-casting approach. Such limitations could be avoided using a point-based isovist method, which is naturally distributed in 3D in space and can be analyzed in the *xy*-plane, along horizontal and vertical sections.

Road users are a crucial element in the transportation system. Previous research has found that road users' contribution to road collisions is significantly higher than in other transportation systems, so understanding the factors contributing to collisions is fundamental to improving road safety. One important factor impacting drivers' vision is age. Previous studies, especially in the medical field, have studied the relationship between the reduction of the visual field, age, and driving behavior. The outcomes of these studies need to be integrated into LiDAR transportation applications such as the intersection sight distance assessment. The visual field reduction affects the driver's viewing angle and therefore requires greater attention within the sight triangle area. Also, an analysis of collisions involving senior drivers needs to be evaluated to ascertain whether they contribute to the collisions as a result of poor vision at the intersection.

Although this research focuses on conducting intersection sight distance assessment to optimize the field of vision of the driver, it can be enhanced for application in the AV environments. One such recent application is the use of point clouds to simulate AVs' movement in virtual reality using twin scans of the existing environment and assess readiness for the deployment of future technologies in a shared environment between active modes of transportation and automated vehicles.

REFERENCES

[1] PIARC, "Road Safety Manual " 2003.

[2] Federal Highway Administration, "The National Intersection Safety Problem," 2009.

[3] The City of Edmonton, "Motor Vehicle Collisions Report," 2017.

[4] X. Wang, M. Abdel-Aty, and P. A. Brady, "Crash Estimation at Signalized Intersections: Significant Factors and Temporal Effect," *Transportation Research Record,* vol. 1953, no. 1, pp. 10-20, 2006/01/01 2006.

[5] J. A. Bonneson and K. Zimmerman, "Identifying Intersections with Potential for Red Light–Related Safety Improvement," *Transportation Research Record,* vol. 1953, no. 1, pp. 128-136, 2006/01/01 2006.

[6] M. Poch and F. Mannering, "Negative Binomial Analysis of Intersection-Accident Frequencies," *Journal of Transportation Engineering,* vol. 122, no. 2, pp. 105-113, 1996/03/01 1996.

[7] P. T. Savolainen and A. P. Tarko, "Safety Impacts at Intersections on Curved Segments," *Transportation Research Record,* vol. 1908, no. 1, pp. 130-140, 2005/01/01 2005.

[8] J. T. Hanna, T. E. Flynn, and W. L. Tyler, "Characteristics of intersection accidents in rural municipalities," (in en), *Transportation research record,* vol. 601, pp. 79-82, / 1976.

[9] American Association of State Highway and Transportation Officials (AASHTO), *A Policy on Geometric Design of Highways and Streets*, 7th ed. 2018.

[10] Alberta Transportation, "Highway Geometric Design Guide," 1999.

[11] Transportation Association of Canada (TAC), "Geometric Design Guide for Canadian Roads," 1999.

[12] D. F. Preusser, A. F. Williams, S. A. Ferguson, R. G. Ulmer, and H. B. Weinstein, "Fatal crash risk for older drivers at intersections," *Accident Analysis & Prevention,* vol. 30, no. 2, pp. 151-159, 1998/03/01/ 1998.

[13] S. A. Gargoum, M. H. Tawfeek, K. El-Basyouny, and J. C. Koch, "Available sight distance on existing highways: Meeting stopping sight distance requirements of an aging population," (in eng), no. 1879-2057 (Electronic).

[14] AAA Organization, "Sharpness of vision and changing Focus."

[15] U.S. Department of Transportation - Federal Highway Administration, "Guidelines For The Visual Impact Assessment Of Highway Projects," 2015.

[16] Vision Zero LA, "Elimination Traffic deaths in Los Angeles by 2025," 2015.

[17] J. Glennon, "Effect of sight distance on highway safety," 1987.

[18] M. Liu, G. Lu, and Y. Li, *The Impact Analysis of Intersection Sight Distance on Vehicle Speed*. 2010, pp. 295-304.

[19] K. Ismail and T. Sayed, "New Algorithm for Calculating 3D Available Sight Distance," *Journal of Transportation Engineering,* vol. 133, no. 10, pp. 572-581, 2007/10/01 2007.

[20] Y. Hassan, S. Easa, and A. Halim, "Sight distance on horizontal alignments with continuous lateral obstructions," *Transportation Research Record Journal of the Transportation Research Board,* vol. 1500, pp. 31-42, 07/01 1995.

[21] A. J. Khattak, S. Hallmark, and R. Souleyrette, "Application of Light Detection and Ranging Technology to Highway Safety," *Transportation Research Record,* vol. 1836, no. 1, pp. 7-15, 2003/01/01 2003.

[22] M. Castro, L. Iglesias, J. A. Sánchez, and L. Ambrosio, "Sight distance analysis of highways using GIS tools," *Transportation Research Part C: Emerging Technologies,* vol. 19, no. 6, pp. 997-1005, 2011/12/01/ 2011.

[23] M. Castro, S. Lopez-Cuervo, M. Paréns-González, and C. de Santos-Berbel, "LIDAR-based roadway and roadside modelling for sight distance studies," *Survey Review,* vol. 48, no. 350, pp. 309-315, 2016/09/02 2016.

[24] L. McKinley, "Sight Distance Standards and Deviations for Highway Approaches," *Oregon Department Of Transportation,* 2013.

[25] D. W. Harwood, J. M. Mason, R. E. Brydia, M. T. Pietrucha, and G. L. Gittings, "NCHRP Report 383: Intersection Sight Distance," *TRB, National Research Council, Washington, D.C.,* 1996.

[26] J. Lovell David, "Automated Calculation of Sight Distance from Horizontal Geometry," *Journal of Transportation Engineering,* vol. 125, no. 4, pp. 297-304, 1999/07/01 1999.

[27] J. Lovell David, J.-C. Jong, and C. Chang Peter, "Improvements to Sight Distance Algorithm," *Journal of Transportation Engineering,* vol. 127, no. 4, pp. 283-288, 2001/08/01 2001.

[28] D. G. Kim and D. J. Lovell, "A Procedure for 3-D Sight Distance Evaluation Using Thin Plate Splines," *4th International Symposium on Highway Geometric Design, TRB, Valencia, Spain,* 2010.

[29] M. K. Jha, G. A. K. Karri, and W. Kuhn, "New Three-Dimensional Highway Design Methodology for Sight Distance Measurement," *Transportation Research Record,* vol. 2262, no. 1, pp. 74-82, 2011/01/01 2011.

[30] G. Nehate and M. Rys, "3D Calculation of Stopping-Sight Distance from GPS Data," *Journal of Transportation Engineering,* vol. 132, no. 9, pp. 691-698, 2006/09/01 2006.

[31] M. Castro, A. Anta José, L. Iglesias, and A. Sánchez José, "GIS-Based System for Sight Distance Analysis of Highways," *Journal of Computing in Civil Engineering,* vol. 28, no. 3, p. 04014005, 2014/05/01 2014.

[32] M. Castro, A. Garcia-Espona, and L. Iglesias, "Terrain Model Resolution Effect on Sight Distance on Roads," *Periodica Polytechnica Civil Engineering,* vol. 59, no. 2, pp. 165-172, 01/01 2015.

[33] J. Khattak Aemal and H. Shamayleh, "Highway Safety Assessment through Geographic Information System-Based Data Visualization," *Journal of Computing in Civil Engineering,* vol. 19, no. 4, pp. 407-411, 2005/10/01 2005.

[34] Y. Tsai, Q. Yang, and Y. Wu, "Use of Light Detection and Ranging Data to Identify and Quantify Intersection Obstruction and Its Severity," *Transportation Research Record,* vol. 2241, no. 1, pp. 99-108, 2011/01/01 2011.

[35] M. Bassani, N. Grasso, M. J. I.-I. A. o. t. P. Piras, Remote Sensing, and S. I. Sciences, "3D GIS Based Evaluation Of The Available Sight Distance To Assess Safety Of Urban Roads," pp. 137-143, 2015.

[36] S. Gargoum, K. El-Basyouny, and J. Sabbagh, "Assessing Stopping and Passing Sight Distance on Highways Using Mobile LiDAR Data," *Journal of Computing in Civil Engineering,* vol. 32, no. 4, p. 04018025, 2018/07/01 2018.

[37] M. Bassani, N. Grasso, M. Piras, and L. Catani, "Estimating the Available Sight Distance in the Urban Environment by GIS and Numerical Computing Codes," *ISPRS International Journal of Geo-Information,* vol. 8, no. 2, 2019.

[38] C. de Santos-Berbel, M. Castro, S. L.-C. Medina, and M. Paréns-González, "Sight Distance Studies on Roads: Influence of Digital Elevation Models and Roadside Elements," *Procedia - Social and Behavioral Sciences,* vol. 160, pp. 449-458, 2014/12/19/ 2014.

[39] M. C. Malpica, C. d. S. Berbel, and L. I. Martínez, "A comprehensive methodology for the analysis of highway sight distance," 2017.

[40] J. Jung, M. J. Olsen, D. S. Hurwitz, A. G. Kashani, and K. Buker, "3D virtual intersection sight distance analysis using lidar data," *Transportation Research Part C: Emerging Technologies,* vol. 86, pp. 563-579, 2018/01/01/ 2018.

[41] Y. Ma, Y. Zheng, J. Cheng, and S. Easa, "Real-Time Visualization Method for Estimating 3D Highway Sight Distance Using LiDAR Data," *Journal of Transportation Engineering, Part A: Systems,* vol. 145, no. 4, p. 04019006, 2019/04/01 2019.

[42] A. Shalkamy, K. El-Basyouny, and H. Y. Xu, "Voxel-Based Methodology for Automated 3D Sight Distance Assessment on Highways using Mobile Light Detection and Ranging Data," *Transportation Research Record,* vol. 2674, no. 5, pp. 587-599, 2020/05/01 2020.

[43] S. A. Gargoum and L. Karsten, "Virtual assessment of sight distance limitations using LiDAR technology: Automated obstruction detection and classification," *Automation in Construction,* vol. 125, p. 103579, 2021/05/01/ 2021.

[44] S. Hagstrom, "Voxel-Based LIDAR Analysis and Applications," 2014.

[45] U. Pyysalo, "VIEWSHED ANALYSIS AND VISUALIZATION OF LANDSCAPE VOXEL MODELS," 2009.

[46] C. Cabo, C. Ordóñez, S. Garcia-Cortes, and J. Martínez-Sánchez, "An algorithm for automatic detection of pole-like street furniture objects from Mobile Laser Scanner point

clouds," *ISPRS Journal of Photogrammetry and Remote Sensing,* vol. 87, pp. 47–56, 01/31 2014.

[47] D. Jo, S. Lee, and Y. Lee, *The Effect of Driving Speed on Driver's Visual Attention: Experimental Investigation*. 2014, pp. 174-182.

[48] V. D. Bhise, *Ergonomics in the Automotive Design Process*. Boca Raton: CRC Press, Taylor & Francis, 2012.

[49] W. Yuan, Z. Liu, and R. Fu, "Predicting Drivers' Eyes-Off-Road Duration in Different Driving Scenarios," *Discrete Dynamics in Nature and Society,* vol. 2018, p. 3481628, 2018/11/01 2018.

[50] J. Higle and J. M. Witkowski, "Bayesian identification of hazardous locations," 1988.

[51] U. Brüde and J. Larsson, "The use of prediction models for eliminating effects due to regression-to-the-mean in road accident data," *Accident Analysis & Prevention,* vol. 20, no. 4, pp. 299-310, 1988/08/01/ 1988.

[52] T. Sayed, F. Navin, and W. Abdelwahab, "A countermeasure-based approach for identifying and treating accident prone locations," *Canadian Journal of Civil Engineering,* vol. 24, pp. 683-691, 02/06 2011.

[53] M. J. Maher and I. Summersgill, "A comprehensive methodology for the fitting of predictive accident models," *Accident Analysis & Prevention,* vol. 28, no. 3, pp. 281-296, 1996/05/01/ 1996.

[54] D. Lord, S. P. Washington, and J. N. Ivan, "Poisson, Poisson-gamma and zero-inflated regression models of motor vehicle crashes: balancing statistical fit and theory," *Accident Analysis & Prevention,* vol. 37, no. 1, pp. 35-46, 2005/01/01/ 2005.

[55] J. K. Lindsey, "Response surfaces for overdispersion in the study of the conditions for fish eggs hatching," (in eng), no. 0006-341X (Print).

[56] P. d. Leur and T. Sayed, "Development of a Road Safety Risk Index," *Transportation Research Record,* vol. 1784, no. 1, pp. 33-42, 2002/01/01 2002.

[57] A. Heine, "Integrated Evaluation Of Rural Road Networks," *Prace Naukowe Politechniki Warszawskiej. Transport, 96,211-222,* 2013.

[58] V. F. Babkov, "Road Conditions and Traffic Safety," *Transportation Research Board,* 1975.

[59] K. Deng, H. Zhang, and Y. Huang, "Safety Analysis on Road Sight Distance," in *2008 International Conference on Intelligent Computation Technology and Automation (ICICTA)*, 2008, vol. 2, pp. 461-465.

[60] P. L. Olson, D. E. Cleveland, P. S. Fancher, L. P. Kostyniuk, and L. W. Schneider, " Parameters Affecting Stopping Sight Distance," *National Cooperative Highway Research Program Report 270, National Research Council, Washington, D.C. ,* 1984.

[61] W. J. Sparks, "The Influence of highway characteristics on accident rates," *Public Works, 99(3), 101-103,* 1968.

[62] T. Urbanik II, W. Hinshaw, and D. B. Fambro, "Safety Effects of Limited Sight Distance on Crest Vertical Curves " *Transportation Research Record No. 1208,* 1989.

[63] T. M. Coburn, "The Relation Between Accidents And Layout On Rural Roads," *1st Australian Road Research Board (ARRB) Conference,* pp. 502-509, 1962.

[64] D. Fambro *et al.*, "Stopping Sight Distance Considerations At Crest Vertical Curves On Rural Two-Lane Highways In Texas. Final Report," 1989.

[65] K. Fitzpatrick, D. Fambro, and A. Stoddard, "Safety Effects of Limited Stopping Sight Distance on Crest Vertical Curves," *Transportation Research Record,* vol. 1701, pp. 17-24, 01/01 2000.

[66] K. González-Gómez and M. Castro, "Analysis of sight distances at urban intersections from a vulnerable users' approach: A case study," *Transportation Research Procedia,* vol. 45, pp. 226-233, 2020/01/01/ 2020.

[67] W. Cheung, "LiDAR remote sensing and applications, by Pinliang Dong and Qi Chen, Boca Raton, CRC Press, 2018, 200 pp., US$94.95 (paperback), ISBN 9781138747241," *Annals of GIS,* vol. 24, no. 3, pp. 223-224, 2018/07/03 2018.

[68] E. P. Baltsavias, "Airborne laser scanning: basic relations and formulas," *ISPRS Journal of Photogrammetry and Remote Sensing,* vol. 54, no. 2, pp. 199-214, 1999/07/01/ 1999.

[69] O. M. Williams K, Roe GV, Glennie C, "Synthesis of Transportation Applications of Mobile LIDAR," *remote sensing 5,* pp. no. 9: 4652-4692, 2013.

[70] S. Gargoum and K. El-Basyouny, "Effects of LiDAR Point Density on Extraction of Traffic Signs: A Sensitivity Study," vol. 2673, no. 1, pp. 41-51, 2019.

[71] C. G. Duffell and D. M. Rudrum, "Remote Sensing Techniques for Highway Earthworks Assessment," in *Site Characterization and Modeling*, 2005, pp. 1-13.

[72] M. J. Olsen, G. Roe, C. Glennie, F. Persi, M. Reedy, D. Hurwitz, K. Williams, H. Tuss, and a. M. K. A. Squellati, "NCHRP 15-44 Guidelines for the Use of Mobile LiDAR in Transportation Applications, 2013," *http://onlinepubs.trb.org/onlinepubs/nchrp/docs/nchrp15-44_finalguidelines.pdf,* 2013.

[73] D. J. Findley and K. M. Tsai, "Infrastructure Investment Protection with LiDAR," *North Carolina Department of Transportation https://pdfs.semanticscholar.org/4aec/cdff9791509251cf02db962ffd339bbbecb7.pdf*.

[74] M. Jalayer, J. Gong, H. Zhou, and M. Grinter, "Evaluation of Remote Sensing Technologies for Collecting Roadside Feature Data to Support Highway Safety Manual Implementation," *Journal of Transportation Safety & Security,* vol. 7, no. 4, pp. 345-357, 2015/10/02 2015.

[75] S. Gargoum, K. El-Basyouny, J. Sabbagh, and K. Froese, "Automated Highway Sign Extraction Using Lidar Data," *Transportation Research Record,* vol. 2643, no. 1, pp. 1-8, 2017/01/01 2017.

[76] M. Soilán, B. Riveiro, J. Martínez-Sánchez, and P. Arias, "Traffic sign detection in MLS acquired point clouds for geometric and image-based semantic inventory," *ISPRS Journal of Photogrammetry and Remote Sensing,* vol. 114, pp. 92-101, 2016/04/01/ 2016.

[77] B. Riveiro, L. Díaz-Vilariño, B. Conde-Carnero, M. Soilán, and P. Arias, "Automatic Segmentation and Shape-Based Classification of Retro-Reflective Traffic Signs from Mobile LiDAR Data," *IEEE Journal of Selected Topics in Applied Earth Observations and Remote Sensing,* vol. 9, no. 1, pp. 295-303, 2016.

[78] M. Gouda and K. El-Basyouny, "“A Deep Learning Algorithm to Extract Traffic Signs from Point Cloud Dat," *Transportation Research Board 99th Annual Meeting, Washington, D.C,* 2020.

[79] A. Adam and C. Ioannidis, "Automatic road sign detecion and classification based on support vector machines and HOG descriptos," *ISPRS Annals of Photogrammetry, Remote Sensing and Spatial Information Sciences,* vol. II-5, pp. 1-7, 05/01 2014.

[80] W. Kuo and C. Lin, "Two-Stage Road Sign Detection and Recognition," in *2007 IEEE International Conference on Multimedia and Expo*, 2007, pp. 1427-1430.

[81] H. S. Lee and K. Kim, "Simultaneous Traffic Sign Detection and Boundary Estimation Using Convolutional Neural Network," *IEEE Transactions on Intelligent Transportation Systems,* vol. 19, no. 5, pp. 1652-1663, 2018.

[82] F. Zaklouta and B. Stanciulescu, "Real-Time Traffic-Sign Recognition Using Tree Classifiers," *IEEE Transactions on Intelligent Transportation Systems,* vol. 13, no. 4, pp. 1507-1514, 2012.

[83] Y. Zhu, C. Zhang, D. Zhou, X. Wang, X. Bai, and W. Liu, "Traffic sign detection and recognition using fully convolutional network guided proposals," *Neurocomputing,* vol. 214, pp. 758-766, 2016/11/19/ 2016.

[84] L. Karsten, S. Gargoum, M. Saleh, and K. El-Basyouny, "Automated Framework to Audit Traffic Signs Using Remote Sensing Data," *Journal of Infrastructure Systems,* vol. 27, no. 3, p. 04021014, 2021/09/01 2021.

[85] K. R. S. Kodagoda, W. S. Wijesoma, and A. P. Balasuriya, "CuTE: curb tracking and estimation," *IEEE Transactions on Control Systems Technology,* vol. 14, no. 5, pp. 951-957, 2006.

[86] P. Kumar, C. P. McElhinney, P. Lewis, and T. McCarthy, "Automated road markings extraction from mobile laser scanning data," *International Journal of Applied Earth Observation and Geoinformation,* vol. 32, pp. 125-137, 2014/10/01/ 2014.

[87] S. Gargoum, K. El-Basyouny, and J. Sabbagh, "Automated Extraction of Horizontal Curve Attributes using LiDAR Data," *Transportation Research Record,* vol. 2672, no. 39, pp. 98-106, 2018/12/01 2018.

[88] W. Zhang, "LIDAR-based road and road-edge detection," in *2010 IEEE Intelligent Vehicles Symposium*, 2010, pp. 845-848.

[89] C.-W. Wu, S.-H. Chio, t3, and ¬, "Road surface modeling from vehicle-borne point cloud by profile analysis," 2012.

[90] S. S. Adlinge, and A. K. Gupta,, "Pavement deterioration and its causes," *International Journal of Innovative Research and Development 2.4 (2013): 437-450*.

[91] K. T. Chang, J. R. Chang, and J. K. Liu, "Detection of Pavement Distresses Using 3D Laser Scanning Technology," *Computing in Civil Engineering (2005),* pp. 1-11.

[92] T. B. J. Coenen and A. Golroo, "A review on automated pavement distress detection methods," *Cogent Engineering,* vol. 4, no. 1, p. 1374822, 2017/01/01 2017.

[93] E.-B. K. Gargoum S., Shalkamy A., and Gouda M., "Feasibility of Extracting Highway Vertical Profiles from LiDAR Data.,," *NRC Research Press,* 2018.

[94] S. Higuera de Frutos and M. Castro, "A Method to Identify and Classify the Vertical Alignment of Existing Roads," *Computer-Aided Civil and Infrastructure Engineering,* vol. 32, no. 11, pp. 952-963, 2017/11/01 2017.

[95] M. Gouda, K. El-Basyouny, and B. Mello, "Automated Extraction and Assessment of Horizontal Curve Attributes and Transition Trajectories using LiDAR Data," *Transportation Association of Canada 2020 conference, Vancouver, Canada.,* 2020.

[96] Y. Tsai, C. Ai, Z. Wang, and E. Pitts, "Mobile Cross-Slope Measurement Method Using Lidar Technology," *Transportation Research Record,* vol. 2367, no. 1, pp. 53-59, 2013/01/01 2013.

[97] R. L. M. Systems, "RIEGL VUX-1HA Datasheet," 2015.

[98] Esri, "Fundamentals aboit LiDAR," *ArcGIS Desktop*.

[99] H. Guan, J. Li, S. Cao, and Y. Yu, "Use of mobile LiDAR in road information inventory: A review," *International Journal of Image and Data Fusion,* vol. 7, pp. 219-242, 07/02 2016.

[100] Statistics Canada, "Population and dwelling counts for census metropolitan areas," 2017.

[101] A. Aijazi, P. Checchin, and L. Trassoudaine, "Segmentation Based Classification of 3D Urban Point Clouds: A Super-Voxel Based Approach with Evaluation," *Remote Sensing, vol. 5, issue 4, pp. 1624-1650,* vol. 5, pp. 1624-1650, 03/01 2013.

[102] C. Cabo, C. Ordoñez, S. García-Cortés, and J. Martínez, "An algorithm for automatic detection of pole-like street furniture objects from Mobile Laser Scanner point clouds," *ISPRS Journal of Photogrammetry and Remote Sensing,* vol. 87, pp. 47-56, 2014/01/01/ 2014.

[103] B. Yang, Z. Dong, G. Zhao, and W. Dai, "Hierarchical extraction of urban objects from mobile laser scanning data," *ISPRS Journal of Photogrammetry and Remote Sensing,* vol. 99, pp. 45-57, 2015/01/01/ 2015.

[104] M. Yadav, B. Lohani, A. K. Singh, and A. Husain, "Identification of pole-like structures from mobile lidar data of complex road environment," *International Journal of Remote Sensing,* vol. 37, no. 20, pp. 4748-4777, 2016/10/17 2016.

[105] J. Wang, R. Lindenbergh, and M. Menenti, "SigVox – A 3D feature matching algorithm for automatic street object recognition in mobile laser scanning point clouds," *ISPRS Journal of Photogrammetry and Remote Sensing,* vol. 128, pp. 111-129, 2017/06/01/ 2017.

[106] S. A. Gargoum, J. C. Koch, and K. El-Basyouny, "A Voxel-Based Method for Automated Detection and Mapping of Light Poles on Rural Highways using LiDAR Data," *Transportation Research Record,* vol. 2672, no. 45, pp. 274-283, 2018/12/01 2018.

[107] F. Galton, "Regression Towards Mediocrity in Hereditary Stature," *The Journal of the Anthropological Institute of Great Britain and Ireland,* vol. 15, pp. 246-263, 1886.

[108] B. G. Heydecker and J. Wu, "Using the information in road accident records," *19th Summer Annual Meeting of PTRC (European Transport Highways and Planning), Sussex, United Kingdom, September 9–13.,* 1991.

[109] S. Garren, R. Smith, and W. Piegorsch, "Bootstrap Goodness-of-Fit Test for the Beta-Binomial Model," *Journal of Applied Statistics,* vol. 28, 11/07 2000.

[110] P. Park and J. Young, "Investigation of a supplementary tool to assist in the prioritization of emphasis areas in North American strategic highway safety plans," *Accident; analysis and prevention,* vol. 45, pp. 392-405, 03/01 2012.

[111] J. S. Maritz and T. Lwin, *Empirical Bayes methods*, 2nd ed. London, United Kingdom: Chapman and Hall, 1989, pp. 88-102.

[112] T. M. Calvin, *Bayesian analysis*. New York: McGraw-Hill Inc., 1990.

[113] J. Tong and D. Lord, "Investigating the application of beta-binomial models in highway safety," 2007.

[114] SAS Institute Inc, "SAS University Edition."